DTIC FILE COPY

AD-A230 603

(1)

DTIC
ELECTE
JAN 07 1991
S B D

ADAPTIVE FILTERING AND SMOOTHING FOR TRACKING A HYPERSONIC AIRCRAFT FROM A SPACE PLATFORM

Kenneth A Gotski
Captain, USAF

AFIT/GA/ENY/90D-6

DEPARTMENT OF THE AIR FORCE
AIR UNIVERSITY
AIR FORCE INSTITUTE OF TECHNOLOGY

Wright-Patterson Air Force Base, Ohio

DISTRIBUTION STATEMENT A
Approved for public release;
Distribution Unlimited

AFIT/GA/ENY/90D-6

(1)

ADAPTIVE FILTERING AND
SMOOTHING FOR TRACKING A HYPERSONIC
AIRCRAFT FROM A SPACE PLATFORM

Kenneth A Gotski
Captain, USAF

AFIT/GA/ENY/90D-6

Approved for public release; distribution unlimited

DTIC
ELECTE
JAN 07 1991
S B D

AFIT/GA/ENY/90D-6

ADAPTIVE FILTERING AND SMOOTHING FOR TRACKING A HYPERSONIC AIRCRAFT FROM A SPACE PLATFORM

THESIS

Presented to the Faculty of the School of Engineering
of the Air Force Institute of Technology
Air University
In Partial Fulfillment of the
Requirements for the Degree of
Masters of Science in Astronautical Engineering

Kenneth A. Gotski, B.S.
Captain, USAF

December 1990

Approved for public release; distribution unlimited

Acknowledgements

I am thankful to Capt Ziegler whose prior efforts gave rise to this thesis topic. My wife deserves my greatest thanks, as any wife should. I am especially grateful to Dr. P. Maybeck who first taught me about linear stochastic filters and to my advisor, Dr. W. Wiesel, who reminded me that the world is often nonlinear. Finally, I thank the many people in AFIT Computer Services who endured my numerous questions and requests.

Accession For		
NTIS GRA&I	☑	
DTIC TAB	☐	
Unannounced	☐	
Justification		
By		
Distribution/		
Availability Codes		
Dist	Avail and/or Special	
A-1		

QUALITY INSPECTED 4

Table of Contents

Page

List of Figures

Figure Page

Figure		Page
A.5.	a_I Covariance and Error, 1 G, 1 Second Data Data Interval, Six State Filter	A-4
A.6.	a_T Covariance and Error, 1 G, 1 Second Data Interval, Six State Filter	A-4
A.7.	Longitude Covariance and Error, 1 G, 10 Second Data Interval, Six State Filter	A-5
A.8.	Latitude Covariance and Error, 1 G, 10 Second Data Interval, Six State Filter	A-5
A.9.	Heading Covariance and Error, 1 G, 10 Second Data Interval, Six State Filter	A-6
A.10.	Velocity Covariance and Error, 1 G, 10 Second Data Interval, Six State Filter	A-6
A.11.	a_I Covariance and Error, 1 G, 10 Second Data Data Interval, Six State Filter	A-7
A.12.	a_T Covariance and Error, 1 G, 10 Second Data Interval, Six State Filter	A-7
A.13.	Longitude Covariance and Error, 1 G, 1 Second Data Interval, Probability Weighting Adaptation	A-8
A.14.	Latitude Covariance and Error, 1 G, 1 Second Data Interval, Probability Weighting Adaptation	A-8
A.15.	Heading Covariance and Error, 1 G, 1 Second Data Interval, Probability Weighting Adaptation	A-9
A.16.	Velocity Covariance and Error, 1 G, 1 Second Data Interval, Probability Weighting Adaptation	A-9
A.17.	a_I Covariance and Error, 1 G, 1 Second Data Interval, Probability Weighting Adaptation .	A-10
A.18.	a_T Covariance and Error, 1 G, 1 Second Data Interval, Probability Weighting Adaptation .	A-10
A.19.	Longitude Covariance and Error, 1 G, 10 Second Data Interval, Probability Weighting Adaptation	A-11
A.20.	Latitude Covariance and Error, 1 G, 10 Second Data Interval, Probability Weighting Adaptation	A-11

List of Tables

Abstract

This study took a previously developed six state Kalman filter (designed for space-based tracking of a hypersonic transatmospheric vehicle), tuned it, and performed a Monte Carlo analysis. Three multiple model adaptive filters were then developed, with sub-filters designed for quiescent periods and periods with apparent acceleration. Next, a smoother was developed using the six state filter as the forward filter and a form of that same filter as the backward filter. The smoother and all of the above filters were compared for their ability to most accurately estimate the transatmospheric vehicle's state, with special emphasis on the acceleration states. This emphasis was motivated by a desire to evaluate the Kalman filter's usefulness as a real-time intelligence gathering tool. From the data generated, it was concluded that neither the adaptive filters nor the smoother improved upon the performance of the six state Kalman filter.

ADAPTIVE FILTERING AND SMOOTHING FOR TRACKING A HYPERSONIC AIRCRAFT FROM A SPACE PLATFORM

I. Introduction

The transatmospheric vehicle (TAV) is envisioned as an air-breathing, horizontal take off, hypersonic craft capable of using aircraft-style flight to ascend to and descend from orbit. The TAV is seen as the next step in the evolution of surface-to-orbit travel.

The infrared signature from air friction on the TAV, as well as the signature from its necessarily hot and powerful engines, should be a brilliant point source even when viewed from geosynchronous orbit. Thus the very nature of the TAV, its hypersonic speed, will readily betray its position to virtually any orbital, infrared-sensing platform. That same speed would render conventional aircraft tracking useless. A tracking algorithm using data from orbital sensors would allow continuous tracking in the event of telemetry loss, in the case of enemy/non-broadcasting TAVs, and when, for national security reasons, the TAV does not wish to advertise its position through its transponder.

Objectives

This thesis refines a previously developed TAV tracking algorithm (Ziegler), and builds upon that work. The primary objective is to estimate the TAV's position, heading, velocity, and acceleration with minimal errors. A secondary

objective is to compare the performance characteristics of a basic Kalman filter, three different multiple-model adaptive Kalman filters, and a smoother, when applied to the problem of estimating TAV state.

Approach

To properly develop the above filters, this thesis will model TAV dynamics, as well as data collection and processing. Ziegler's six state Kalman filter will be refined and subjected to a Monte Carlo analysis to allow accurate filter tuning. Next, a reduced order, four state filter will be designed with the intention of better modeling periods without accelerations, and this filter will be integrated with the six state filter as the two sub-filters in various multiple-model adaptive filter algorithms. Finally, a smoother will be evaluated as an off-line alternative for estimating the TAV's state.

Overview

A geosynchronous infrared sensor of known accuracy will supply position data to the various filters. The sensor data will be preprocessed into longitude and latitude, and the filters will utilize these position "measurements" to estimate the TAV's state.

The TAV is assumed to be a brilliant, "...isotropically radiating point source operating in the outer fringes of an atmosphere surrounding a perfectly spherical and rotating

earth." (6:1-3) This thesis will ignore the altitude state because $\bar{r}_{TAV_{orbital}} \approx \bar{r}_{earth}$ when observed from a geostationary orbit.

II. Vehicle Dynamics (6:2-1 through 2-10)

A dynamics truth model is essential in properly evaluating Kalman filter performance. The truth model states must be compared to the filter's estimates to be sure the filter is properly estimating those states. For this thesis, a truth model that ignores altitude is believed to be adequate since the radius of a low earth orbit is so close in magnitude to the earth's radius. This section derives the equations of motion for the transatmospheric vehicle under the above assumption.

State Variables

Six state variables have been chosen to represent the TAV's overall state. Earth longitude, λ, is defined positive east of the Greenwich Meridian, and negative westward. Earth latitude, δ, is defined as positive north of the equator, and negative southward. Heading, h, is the clockwise angle from the true north direction to the current direction of travel. Velocity is the speed along the current direction of travel (and, by definition, there's no component of velocity out of the direction of travel). Intrack acceleration, a_I, is the rate of change in speed along the direction of travel. Transverse acceleration, a_T, is the rate of change in velocity along the line out the left wing of the TAV (perpendicular to the current direction of travel).

$$(\bar{a}_I/|\bar{a}_I|) \times (\bar{a}_T/|\bar{a}_T|) = (\text{local zenith}) \tag{2.1}$$

Equations of Motion

To find velocity, basic dynamics states

$$V = \omega \cdot r \tag{2.2}$$

where r is the radius and ω is the angular rate. From this the TAV velocity can be stated

$$\mathbf{V}_{TAV} = \begin{pmatrix} V_\lambda \\ V_\delta \end{pmatrix} = \begin{pmatrix} \omega_\lambda \\ \omega_\delta \end{pmatrix} \begin{pmatrix} R_e \cdot \cos \delta \\ R_e \end{pmatrix} \tag{2.3}$$

where ω_λ is the angular rate of change in the longitudinal direction, and ω_δ is the angular rate of change in the latitudinal direction. Over a sufficiently small period of time, this spherical geometry problem about the earth can be approximated by planar geometry

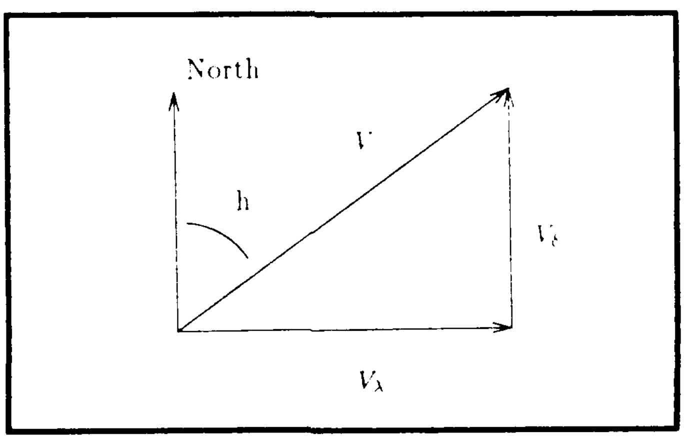

Figure 2.1 Planar Representation of TAV Motion

Call this small period of time dt and Equation (2.3) becomes

$$\overline{V}_{TAV} = \begin{pmatrix} V_\lambda \\ V_\delta \end{pmatrix} = \begin{pmatrix} V_{TAV}\cdot\sin h \\ V_{TAV}\cdot\cos h \end{pmatrix} = \begin{pmatrix} (d\lambda/dt)\cdot R_e\cdot\cos\delta \\ (d\delta/dt)\cdot R_e \end{pmatrix} \quad (2.4)$$

Solving for $\dot{\lambda}$ and $\dot{\delta}$

$$\begin{pmatrix} \dot{\lambda} \\ \dot{\delta} \end{pmatrix} = (1/R_e)\cdot\begin{pmatrix} V_{TAV}\cdot\sin h\ /\cos\delta \\ V_{TAV}\cdot\cos h \end{pmatrix} \quad (2.5)$$

Correcting for the earth's rotation

$$\begin{pmatrix} \dot{\lambda} \\ \dot{\delta} \end{pmatrix} = \begin{pmatrix} (V_{TAV}\cdot\sin h)/(R_e\cdot\cos\delta) - \omega_e \\ (V_{TAV}\cdot\cos h)/R_e \end{pmatrix} \quad (2.6)$$

To find $\dot{h}$ and $\dot{V}$, define the ENZ frame such that

$\hat{E}$ = local eastward direction at TAV location

$\hat{N}$ = local northward direction at TAV location

$\hat{Z} = \hat{E} \times \hat{N}$ (6:2-6)

and the b-frame (body frame) such that

$\hat{B}_1 = \overline{a}_I/|\overline{a}_I|$

$\hat{B}_2 = \overline{a}_T/|\overline{a}_T|$

$\hat{B}_3 = \hat{B}_1 \times \hat{B}_2$ (6:2-6)

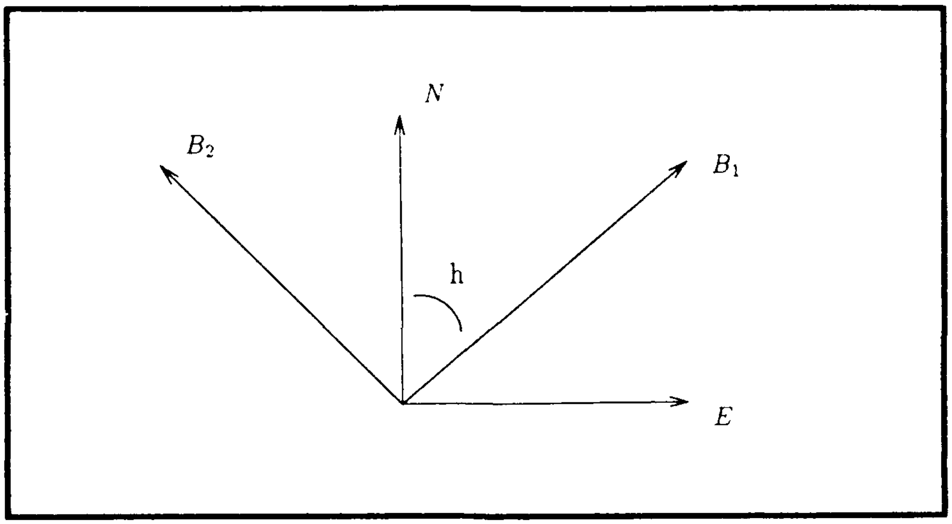

Figure 2.2. TAV Coordinate Frames (6:2-6)

$$\hat{E} = \sin h\ \hat{B}_1 - \cos h\ \hat{B}_2 \tag{2.7a}$$

$$\hat{N} = \cos h\ \hat{B}_1 + \sin h\ \hat{B}_2 \tag{2.7b}$$

$$\hat{Z} = \hat{B}_3 \tag{2.7c}$$

Inertial acceleration, as a function of inertial velocity, expressed in the body frame is

$$\bar{A}^b = \frac{d^b}{dt}(\bar{V}) + \bar{\omega}^{bi} \times \bar{V}^b \tag{2.8a}$$

$$= \frac{d^b}{dt}(V\ \hat{B}_1) + \bar{\omega}^{bi} \times \bar{V}^b \tag{2.8b}$$

$$= \dot{V}\ \hat{B}_1 + \bar{\omega}^{bi} \times (V\ \hat{B}_1) \tag{2.8c}$$

with

$$\bar{\omega}^{bi} = \bar{\omega}^{b,ENZ} + \bar{\omega}^{ENZ,i} \tag{2.9}$$

where

$$\bar{\omega}^{bi} = \text{angular rotation of the body frame with respect to the inertial frame}$$

$$\bar{\omega}^{b,ENZ} = \text{angular rotation of body frame with respect to ENZ-frame}$$

$$\bar{\omega}^{ENZ,i} = \text{angular rotation of ENZ frame with respect to inertial frame}$$

From Figure 2.2

$$\bar{\omega}^{b,ENZ} = -\dot{h}\,\hat{B}_3 \qquad (2.10)$$

Since the ENZ-frame motion is dependent upon TAV and earth motion,

$$\bar{\omega}^{ENZ,i} = \bar{\omega}_e + \bar{\omega}_{TAV} \qquad (2.11a)$$

$$= \bar{\omega}_e + \dot{\bar{\lambda}} + \dot{\bar{\delta}} \qquad (2.11b)$$

$$= \bar{\omega}_e + \dot{\lambda}\cdot\cos\delta\,\hat{N} - \dot{\delta}\,\hat{E} + \dot{\lambda}\cdot\sin\delta\,\hat{Z} \qquad (2.11c)$$

where

$$\bar{\omega}_e = \omega_e\cdot\cos\delta\,\hat{N} + \omega_e\cdot\sin\delta\,\hat{Z} \qquad (2.11d)$$

Expressed in the body frame this becomes

$$\begin{aligned}\bar{\omega}^{ENZ,i} = &\left(-\dot{\delta}\cdot\sin h + (\dot{\lambda} + \omega_e)\cdot\cos\delta\cdot\cos h\right)\hat{B}_1 \\ &+ \left(\dot{\delta}\cdot\cos h + (\dot{\lambda} + \omega_e)\cdot\cos\delta\cdot\cos h\right)\hat{B}_2 \\ &+ (\dot{\lambda} + \omega_e)\cdot\sin\delta\,\hat{B}_3\end{aligned} \qquad (2.12)$$

therefore

$$\bar{\omega}^{b,i} = \omega_1\,\hat{B}_1 + \omega_2\,\hat{B}_2 + \omega_3\,\hat{B}_3 \qquad (2.13)$$

where

$$\omega_1 = -\dot{\delta}\cdot\sin h + (\dot{\lambda} + \omega_e)\cdot\cos\delta\cdot\cos h$$

$$\omega_2 = \dot{\delta}\cdot\cos h + (\dot{\lambda} + \omega_e)\cdot\cos\delta\cdot\cos h$$

$$\omega_3 = (\dot{\lambda} + \omega_e)\cdot\sin\delta - \dot{h}$$

Substituting Equation (2.13) into Equation (2.8) gives

$$\bar{A} = \dot{V}\,\hat{B}_1 + \begin{vmatrix} \hat{B}_1 & \hat{B}_2 & \hat{B}_3 \\ \omega_1 & \omega_2 & \omega_3 \\ V & 0 & 0 \end{vmatrix} \tag{2.14a}$$

where $|\cdot|$ indicates a cross product. This becomes

$$\bar{A} = \dot{V}\,\hat{B}_1 + V\cdot\omega_3\,\hat{B}_2 + V\cdot\omega_2\,\hat{B}_3 \tag{2.14b}$$

Neglecting the $\hat{B}_3$ term in the previously assumed negligible altitude direction gives

$$\bar{A} = \dot{V}\,\hat{B}_1 + V\cdot\left((\dot{\lambda} + \omega_e)\cdot\sin\delta - \dot{h}\right)\hat{B}_2 \tag{2.14c}$$

Now, substituting $\dot{\lambda}$ from Equation (2.6)

$$\bar{A} = \dot{V}\,\hat{B}_1 + \left\{\left(\frac{V_{TAV}^2\cdot\sin h}{R_e\cdot\cos\delta}\right)\cdot\sin\delta - V\cdot\dot{h}\right\}\hat{B}_2 \tag{2.14d}$$

but

$\bar{a}_I = \hat{B}_1$ component of inertial acceleration

$\bar{a}_T = \hat{B}_2$ component of inertial acceleration

therefore

$$a_I = \dot{V} \tag{2.15}$$

$$a_T = \frac{V^2\cdot\sin h\ \cdot\sin\delta}{R_e\cdot\cos\delta} - V\cdot\dot{h} \tag{2.16}$$

Solving these equations for $\dot{V}$ and $\dot{h}$ gives

$$\dot{V} = a_I \tag{2.17}$$

$$\dot{h} = -a_T/V + (V\cdot\sin h\ \cdot\sin\delta\ )/(R_e\cdot\cos\delta) \tag{2.18}$$

Finally, since changes in acceleration have no deterministic model, impulsive changes in acceleration were assumed and the rates of change for acceleration were set to zero.

$$\dot{a}_I = \dot{a}_T = 0 \tag{2.19}$$

Summarizing Equations (2.6), (2.17), (2.18), and (2.19) gives

$$\begin{bmatrix} \dot{\lambda} \\ \dot{\delta} \\ \dot{h} \\ \dot{V} \\ \dot{a}_I \\ \dot{a}_T \end{bmatrix} = \begin{bmatrix} (V \cdot \sin h)/(R_e \cdot \cos \delta) - \omega_e \\ (V \cdot \cos h)/R_e \\ -a_T/R_e + (V \cdot \sin h \cdot \sin \delta)/(R_e \cdot \cos \delta) \\ a_I \\ 0 \\ 0 \end{bmatrix} = \dot{\bar{x}} \quad (2.20)$$

<u>Propagating the Truth Model</u> (6:2-10)

The six equations of motion are first order differential equations of the form $\dot{\bar{x}} = f(\bar{x},t)$. Given the initial conditions, Equation (2.20) can be numerically integrated to give a time history of the truth model states.

For this thesis, the Hamming predictor-corrector method was used as the numerical integrator. "Given initial conditions, the time step size, and the right hand side of the equations of motion, the Hamming algorithm produced detailed time histories for λ, δ, h, V, a_I, and a_T." (6:2-10) For all calculations, units of angles were radians, units of velocity were DU/TU, and units of acceleration were DU/TU^2. One DU is the average equatorial radius of the earth, about 6378.145 kilometers. One TU is approximately 806.8 seconds, resulting in one gravity (G) equaling one DU/TU^2.

III. Sensor (6:3-1 through 3-9)

This chapter deals with the collection and processing of the raw data from the geosynchronous sensor. Ziegler's technique of preprocessing the data has been retained due to its simplifying effect on the Kalman filter algorithms.

Raw Data

The geosynchronous satellite carrying the sensor, by the nature of its orbit, remains at a constant longitude and latitude. For this thesis, the sensor has been placed at 0° longitude and 0° latitude. The thermal emissions of the TAV are located in the sensor's field of view via azimuth (Az) and elevation (El) as shown in Figure 3.1.

Azimuth is the spherical angle from the northward direction to the great circle containing the TAV. Elevation is the angle seen by the sensor from the nadir to the TAV as shown in Figure 3.2. From the geometry, $0 < El < 8.6^\circ$. (6:3-2)

Another component of the raw data is the uncertainty associated with each measurement. No measurement is exact; each one has error due to uncertainties in sensor position, sensor attitude, atmospheric effects, vibrations, etc. (6:3-2) According to the central limit theorem, these error sources, when summed together, become zero-mean, Gaussian

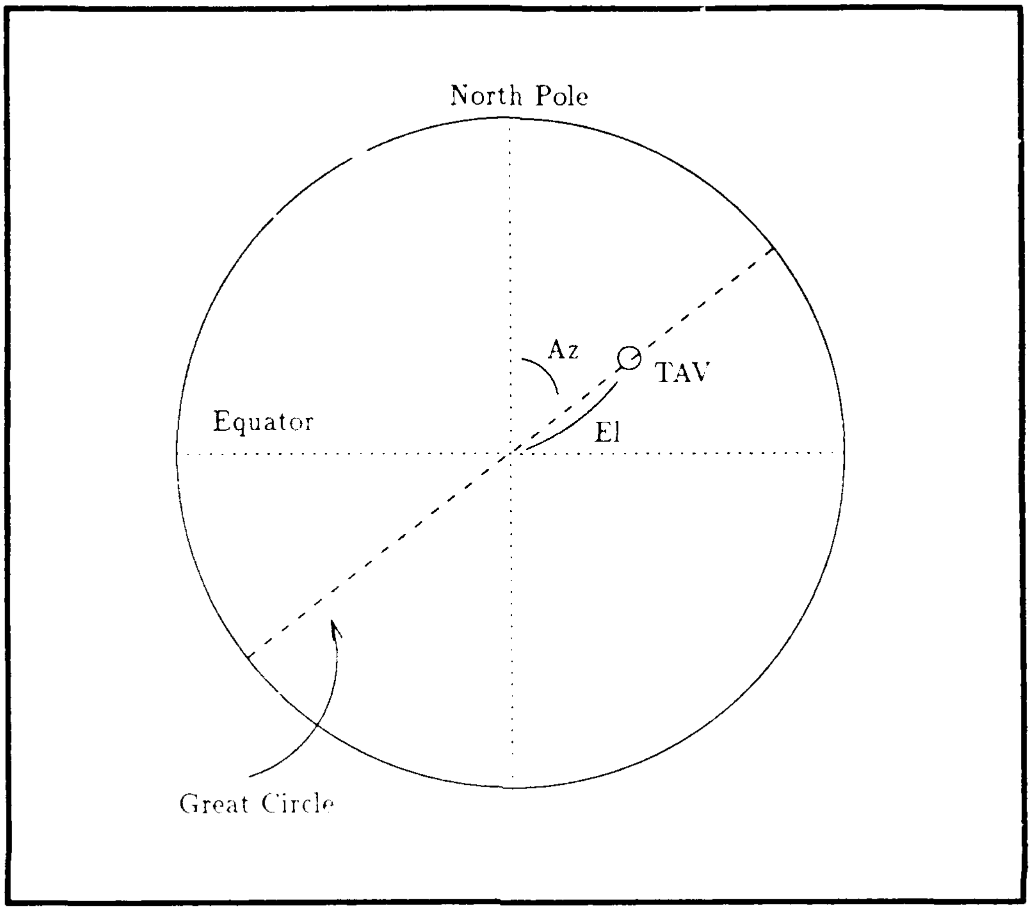

Figure 3.1. Azimuth and Elevation Data Angles (6:3-1)

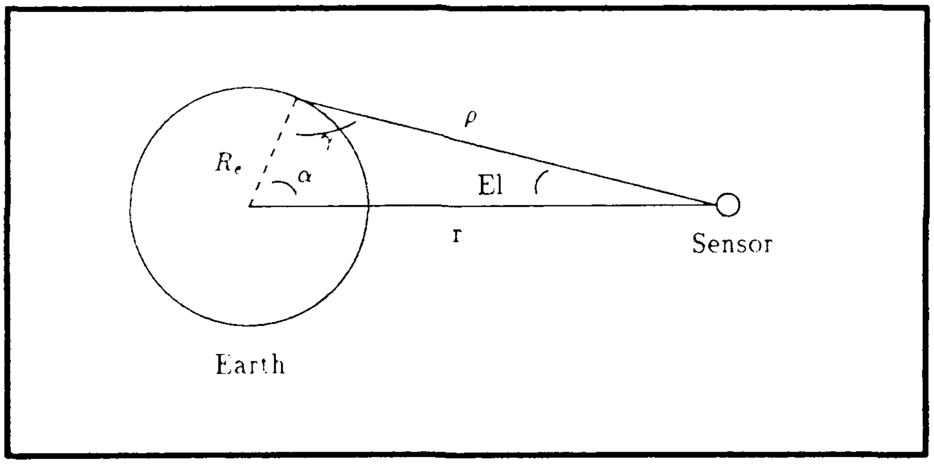

Figure 3.2. Planar View of Elevation

random variables. This thesis will carry forward the standard deviations (σ) of 3.5×10^{-5} radians for azimuth errors and 4.3×10^{-6} radians for elevation errors. (4:3)

Assuming azimuth and elevation errors are statistically independent of each other, the data covariance matrix can be defined as

$$[Q] = \lceil\sigma^2_{Az} \quad \sigma^2_{El}\rfloor = \lceil 1.225\times10^{-9} \quad 1.849\times10^{-11}\rfloor \qquad (3.1)$$

Processed Data

The dynamics equations are, in part, functions of longitude and latitude. A bit of foreknowledge allows the simplification of the observation matrix, [H], in the Kalman filter algorithms presented in later chapters. This simplification of [H] was achieved by converting azimuth and elevation into longitude and latitude. The data covariance, [Q], was also converted. This section derives longitude and latitude in terms of elevation and azimuth as well as the Jacobian for converting [Q].

From Figure 3.2 and the planar law of sines

$$r/\sin\gamma = R_e/\sin El \qquad (3.2)$$

(5:3-4)

where r is the distance from the sensor to the earth's center and R_e is the radius of the earth.

Solving for γ

$$\gamma = \sin^{-1}\left((r\cdot\sin El)/R_e\right) \qquad (3.3)$$

From the geometry, $90^\circ < \gamma < 180^\circ$, since a $\gamma < 90^\circ$ would indicate a TAV located behind the earth, and that would make it unobservable. Solving for α (from Figure 3.2.)

$$\alpha = 180^\circ - (El + \gamma) \tag{3.4}$$

The spherical geometry of this problem is represented in Figure 3.3.

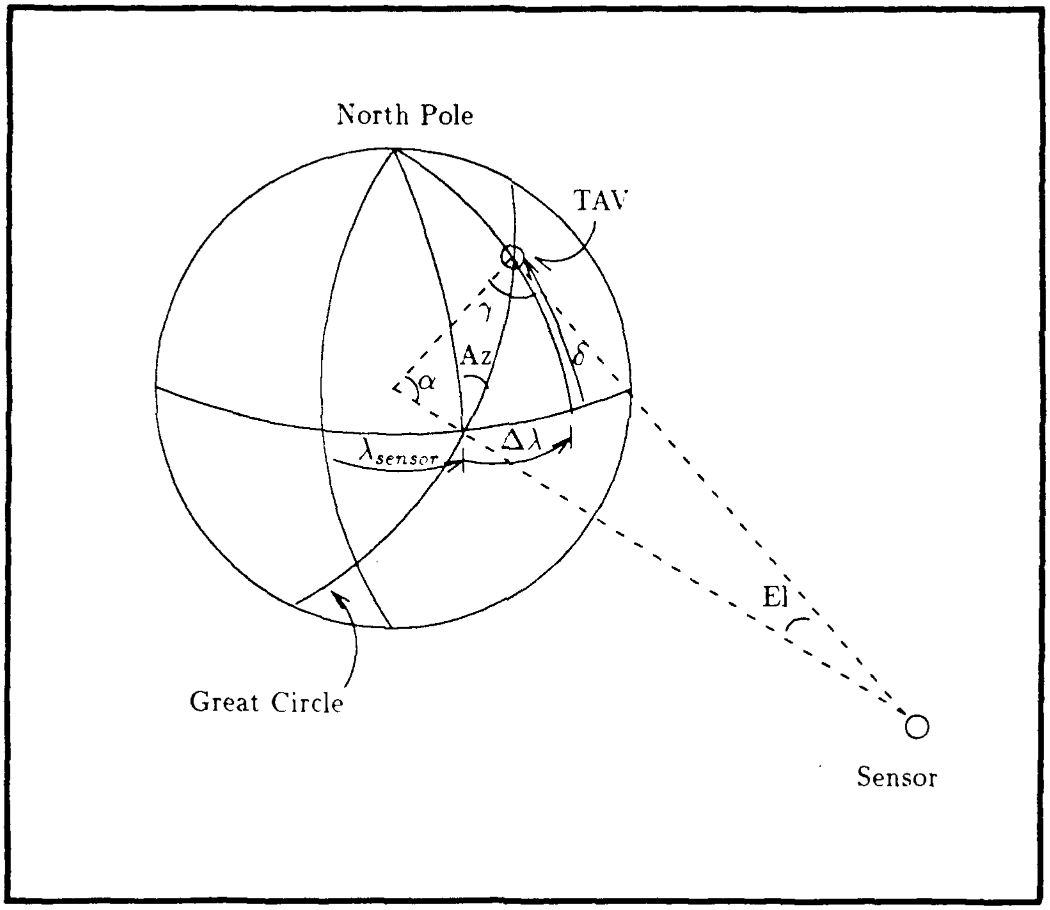

Figure 3.3. Spherical Geometry of TAV Tracking Problem

(6:3-5)

The law of sines for oblique spherical triangles gives

$$(\sin \delta)/\left(\sin(90^\circ - Az\right) = (\sin \alpha)/\sin 90^\circ \tag{3.5}$$

Solving for δ

$$\delta = \sin^{-1}\left(\sin\alpha \cdot \cos Az\right) \tag{3.6}$$

Combining Equations (3.3) and (3.4) with Equation (3.6)

$$\delta = \sin^{-1}\left\{\sin\left[180^\circ - \left(El + \sin^{-1}(r \cdot \sin El \ / \ R_e)\right)\right] \cdot \cos Az\right\} \tag{3.7a}$$

or

$$\delta = \sin^{-1}\left[\sin\left(El + \sin^{-1}(r \cdot \sin El \ / \ R_e)\right) \cdot \cos Az\right] \tag{3.7b}$$

Also from Figure 3.3

$$\lambda = \lambda_{sensor} + \Delta\lambda \tag{3.8}$$

where

λ_{sensor} = sensor longitude

$\Delta\lambda$ = TAV longitude relative to sensor's

From spherical geometry

$$\sin\Delta\lambda = \tan\delta \cdot \cot(90^\circ - Az) \tag{3.9a}$$

or

$$\Delta\lambda = \sin^{-1}\left[\tan\delta \cdot \cot(90^\circ - Az)\right] \tag{3.9b}$$

Substituting Equations (3.7b) and (3.9b) into Equation (3.8)

$$\lambda = \lambda_{sensor} + \sin^{-1}\left\{\tan\left[\sin^{-1}\left(\sin(El + \sin^{-1}[r \cdot \sin El \ /R_e]) \cdot \cos Az\right)\right] \cdot \tan Az\right\} \tag{3.10}$$

Equations (3.7b) and (3.10) define the relation between El, Az and λ, δ. From the geometry, δ and $\Delta\lambda$ are constrained to be between -90° and 90°, so there is no uncertainty as to the quadrant within which either angle resides. Therefore, δ and λ are completely defined.

The transformation from $[Q_{Az,El}]$ to $[Q_{\lambda,\delta}]$ is simply

$$[Q] = [Q_{\lambda,\delta}] = [J][Q_{Az,El}][J]^T \tag{3.11}$$

where

[J] is the system Jacobian

Since Equations (3.7b) and (3.10) are of the form

$$\lambda = f_1(Az, El) \tag{3.12a}$$

$$\delta = f_2(Az, El) \tag{3.12b}$$

then

$$[J] = \begin{bmatrix} \dfrac{\partial f_1}{\partial Az} & \dfrac{\partial f_1}{\partial El} \\ \dfrac{\partial f_2}{\partial Az} & \dfrac{\partial f_2}{\partial El} \end{bmatrix} \tag{3.13}$$

where (6:3-7 through 3-9)

$$\frac{\partial f_1}{\partial Az} = \left\{ 1 - \left[\tan\left(\sin^{-1}\left\{El + \sin^{-1}\left(\frac{r}{R_e}\cdot\sin El\right)\right]\cos Az\right\}\right)\right.$$

$$\left.\cdot\tan Az\right]^2\Big\}^{-1/2} \cdot \left[\sec^2\left(\sin^{-1}\left\{\sin\left[El + \sin^{-1}\left(\frac{r}{R_e}\cdot\sin El\right)\right]\right.\right.\right.$$

$$\left.\left.\cdot\cos Az\right\}\right)\cdot\left(1 - \left\{\sin\left[El + \sin^{-1}\left(\frac{r}{R_e}\cdot\sin El\right)\right]\cos Az\right\}^2\right)^{-1/2}$$

$$\cdot(-\sin Az)\cdot(\tan Az)\cdot\left\{\sin\left[El + \sin^{-1}\left(\frac{r}{R_e}\cdot\sin El\right)\right]\right\}$$

$$\left.\cdot(\sec^2 Az)\cdot\tan\left(\sin^{-1}\left\{\sin\left[El + \sin^{-1}\left(\frac{r}{R_e}\cdot\sin El\right)\right]\cos Az\right\}\right)\right]$$

$$\frac{\partial f_1}{\partial El} = \left\{ 1 - \left[\tan\left(\sin^{-1}\left\{\sin\left[El + \sin^{-1}\left(\frac{r}{R_e}\cdot\sin El\right)\right]\cos Az\right\}\right)\right.\right.$$

$$\left.\left.\cdot\tan Az\right]^2\right\}^{-1/2} \cdot \left[\sec^2\left(\sin^{-1}\left\{\sin\left[El + \sin^{-1}\left(\frac{r}{R_e}\cdot\sin El\right)\right]\right.\right.\right.$$

$$\left.\left.\cdot\text{ccs } Az\right\}\right)\cdot\left(1 - \left\{\sin\left[El + \sin^{-1}\left(\frac{r}{R_e}\cdot\sin El\right)\right]\cdot\cos Az\right\}^2\right)^{-1/2}$$

$$\cdot \cos Az \cdot \cos\left[El + \sin^{-1}\left(\frac{r}{R_e}\cdot \sin El\right)\right]$$

$$\cdot\left\{ 1 + \left[1 - \left(\frac{r}{R_e}\cdot \sin El\right)^2\right]^{-1/2} \cdot \frac{r}{R_e}\cdot \cos El\right\}\tan Az\Bigg]$$

$$\frac{\partial f_2}{\partial Az} = \left(1 - \left\{\sin\left[El + \sin^{-1}\left(\frac{r}{R_e}\cdot \sin El\right)\right]\cdot \cos Az\right\}^2\right)^{-1/2}$$

$$\cdot \sin\left[El + \sin^{-1}\left(\frac{r}{R_e}\cdot \sin El\right)\right]\cdot\left(-\sin Az\right)$$

$$\frac{\partial f_2}{\partial El} = \left(1 - \left\{\sin\left[El + \sin^{-1}\left(\frac{r}{R_e}\cdot \sin El\right)\right]\cdot \cos Az\right\}^2\right)^{-1/2}$$

$$\cdot \cos Az \cdot \cos\left[El + \sin^{-1}\left(\frac{r}{R_e}\cdot \sin El\right)\right]$$

$$\cdot\left\{ 1 + \left[1 - \left(\frac{r}{R_e}\cdot \sin El\right)^2\right]^{-1/2} \cdot \frac{r}{R_e}\cdot \cos El\right\}$$

Equations (3.7b), (3.10), and (3.13) define the necessary numerical tools for converting data and data covariance from Az, El to λ, δ. Their usage is presented in the Kalman filter derivations in Chapters IV and V.

IV. Six State Kalman Filter

The Kalman filter developed by Ziegler has been revised after a careful analysis of its performance when subjected to measurements with zero-mean, Gaussian random variable components. This chapter explains the motivation for a six state Kalman filter, explains design and tuning, and documents the filter's performance.

Motivation

The result of tracking a TAV should be useful information about the current state of the vehicle and apparent intentions in the next few moments. A reasonable amount of data would be the TAV's position, its velocity and heading, and any observable, applied accelerations. The six states of this Kalman filter contain all of the above information in longitude, latitude, velocity, heading, intrack acceleration, and transverse acceleration. This filter will estimate all of these states for every data point.

State Equation

Equation (2.20), in a linear approximation, defines the TAV dynamics.

$$\begin{bmatrix} \lambda_{i+1} \\ \delta_{i+1} \\ h_{i+1} \\ V_{i+1} \\ a_{I_{i+1}} \\ a_{T_{i+1}} \end{bmatrix} = \begin{bmatrix} (V_i \cdot \sin h_i / R_e \cdot \cos \delta_i) - \omega_e \\ (V_i \cdot \cos h_i) / R_e \\ -a_{Ti}/V_i + [V_i \cdot \sin h_i \cdot \sin\delta_i / (R_e \cdot \cos\delta_i)] \\ a_{Ii} \\ 0 \\ 0 \end{bmatrix} \cdot \Delta t + \begin{bmatrix} \lambda_i \\ \delta_i \\ h_i \\ V_i \\ a_{Ii} \\ a_{Ti} \end{bmatrix} \tag{4.1}$$

This equation is the filter's model of TAV flight dynamics for all possible accelerations.

State Transition Matrix

Discrete time propagation of the state vector, $\overline{x}$, in Equation (4.1) is of the form

$$\overline{x}_{i+1}(t) = f[\overline{x}_i(t), \Delta t] \tag{4.2}$$

The state transition matrix is found by taking the gradient

$$[\Phi(t_{i+1}, t_i)] = \nabla_{x_i} \left(f[\overline{x}_i(t), t] \right) \tag{4.3}$$

which, expanded, is

$$[\Phi] = \begin{bmatrix} \frac{\partial\lambda_{i+1}}{\partial\lambda_i} & \frac{\partial\lambda_{i+1}}{\partial\delta_i} & \frac{\partial\lambda_{i+1}}{\partial h_i} & \frac{\partial\lambda_{i+1}}{\partial V_i} & \frac{\partial\lambda_{i+1}}{\partial a_{Ii}} & \frac{\partial\lambda_{i+1}}{\partial a_{Ti}} \\ \frac{\partial\delta_{i+1}}{\partial\lambda_i} & \frac{\partial\delta_{i+1}}{\partial\delta_i} & \frac{\partial\delta_{i+1}}{\partial h_i} & \frac{\partial\delta_{i+1}}{\partial V_i} & \frac{\partial\delta_{i+1}}{\partial a_{Ii}} & \frac{\partial\delta_{i+1}}{\partial a_{Ti}} \\ \frac{\partial h_{i+1}}{\partial\lambda_i} & \frac{\partial h_{i+1}}{\partial\delta_i} & \frac{\partial h_{i+1}}{\partial h_i} & \frac{\partial h_{i+1}}{\partial V_i} & \frac{\partial h_{i+1}}{\partial a_{Ii}} & \frac{\partial h_{i+1}}{\partial a_{Ti}} \\ \frac{\partial V_{i+1}}{\partial\lambda_i} & \frac{\partial V_{i+1}}{\partial\delta_i} & \frac{\partial V_{i+1}}{\partial h_i} & \frac{\partial V_{i+1}}{\partial V_i} & \frac{\partial V_{i+1}}{\partial a_{Ii}} & \frac{\partial V_{i+1}}{\partial a_{Ti}} \\ \frac{\partial a_{Ii+1}}{\partial\lambda_i} & \frac{\partial a_{Ii+1}}{\partial\delta_i} & \frac{\partial a_{Ii+1}}{\partial h_i} & \frac{\partial a_{Ii+1}}{\partial V_i} & \frac{\partial a_{Ii+1}}{\partial a_{Ii}} & \frac{\partial a_{Ii+1}}{\partial a_{Ti}} \\ \frac{\partial a_{Ti+1}}{\partial\lambda_i} & \frac{\partial a_{Ti+1}}{\partial\delta_i} & \frac{\partial a_{Ti+1}}{\partial h_i} & \frac{\partial a_{Ti+1}}{\partial V_i} & \frac{\partial a_{Ti+1}}{\partial a_{Ii}} & \frac{\partial a_{Ti+1}}{\partial a_{Ti}} \end{bmatrix} \quad (4.4)$$

where

$$\frac{\partial\lambda_{i+1}}{\partial\delta_i} = \frac{V_i \cdot \sin h_i \cdot \sin\delta_i}{R_e \cdot \cos^2\delta_i} \cdot \Delta t$$

$$\frac{\partial\lambda_{i+1}}{\partial h_i} = \frac{V_i \cdot \cos h_i}{R_e \cdot \cos\delta_i} \cdot \Delta t$$

$$\frac{\partial\lambda_{i+1}}{\partial V_i} = \frac{\sin h_i}{R_e \cdot \cos\delta_i} \cdot \Delta t$$

$$\frac{\partial\delta_{i+1}}{\partial h_i} = \frac{-V_i \cdot \sin h_i}{R_e} \cdot \Delta t$$

$$\frac{\partial\delta_{i+1}}{\partial V_i} = \frac{\cos h_i}{R_e} \cdot \Delta t$$

$$\frac{\partial h_{i+1}}{\partial\delta_i} = \left(V_i \cdot \sin h_i + \frac{V_i \cdot \sin h_i \cdot \sin^2\delta_i}{\cos^2\delta_i} \right) \cdot \frac{\Delta t}{R_e}$$

$$\frac{\partial h_{i+1}}{\partial h_i} = \frac{V_i \cdot \cos h_i \cdot \sin \delta_i}{R_e \cdot \cos \delta_i} \cdot \Delta t + 1$$

$$\frac{\partial h_{i+1}}{\partial V_i} = \left(\frac{a_{Ti}}{V_i^2} + \frac{\sin h_i \cdot \sin \delta_i}{R_e \cdot \cos \delta_i} \right) \cdot \Delta t$$

$$\frac{\partial h_{i+1}}{\partial a_{Ti}} = \frac{-\ \Delta t}{V_i}$$

$$\frac{\partial V_{i+1}}{\partial a_{Ii}} = \Delta t$$

$$\frac{\partial \lambda_{i+1}}{\partial \lambda_i} = \frac{\partial \delta_{i+1}}{\partial \delta_i} = \frac{\partial V_{i+1}}{\partial V_i} = \frac{\partial a_{Ii+1}}{\partial a_{Ii}} = \frac{\partial a_{Ti+1}}{\partial a_{Ti}} = 1$$

and all other partials are equal to zero.

<u>Measurements</u> (3:44)

Data is assumed to consist of a deterministic portion and a zero-mean, white Gaussian noise, $\overline{v}_i$.

$$\overline{z} = h[\overline{x}(t_i), t_i] + \overline{v}_i \qquad (4.5)$$

where

$$\overline{h}[\overline{x}(t_i), t_i] = \begin{bmatrix} 1 & 0 & 0 & 0 & 0 & 0 \\ 0 & 1 & 0 & 0 & 0 & 0 \end{bmatrix} \cdot \overline{x}$$

and $\overline{v}_i$ has strength

$$[Q] = [J][Q_{az,el}][J]^T$$

with [J] and $[Q_{az,el}]$ defined in Equations (3.13) and (3.1).

[H] is defined as

$$[H] = \frac{\partial \overline{h}[\overline{x}_i(t_i), t_i]}{\partial \overline{x}} = \begin{bmatrix} 1 & 0 & 0 & 0 & 0 & 0 \\ 0 & 1 & 0 & 0 & 0 & 0 \end{bmatrix} \qquad (4.6)$$

State Covariance (3:44)

To allow easy starting of the filter, each state at t = 0 was assumed independent of the other states, and covariance could be assumed to be of the form

$$[P_0] = \lceil \sigma^2_{\lambda} \quad \sigma^2_{\delta} \quad \sigma^2_{h} \quad \sigma^2_{V} \quad \sigma^2_{aI} \quad \sigma^2_{aT} \rfloor \tag{4.7}$$

This allows the entry of six values as opposed to a fully populated 6×6 matrix.

Covariance is propagated via

$$[P_{i+1}] = [\Phi_{i+1,i}][P_i][\Phi_{i+1,i}]^T + [Q_n] \tag{4.8}$$

where $[\Phi_{i+1,i}]$ is defined by Equation (4.4) and $[Q_n]$ is the dynamics noise matrix, which is the strength of the zero mean Gaussian white noise representing the uncertainty in the dynamics model. $[Q_n]$ is assumed to be diagonal.

$$[Q_n] = \lceil Q_{n_\lambda} \quad Q_{n_\delta} \quad Q_{n_h} \quad Q_{n_V} \quad Q_{n_{aI}} \quad Q_{n_{aT}} \rfloor \tag{4.9}$$

The six diagonal elements of $[Q_n]$ will be adjusted through the tuning process.

Filter Algorithm (5:100)

The extended Kalman filter equations are

$$[K(t_i)] = [P(t_i^-)][H]^T\left\{[H][P(t_i^-)][H]^T + [Q]\right\}^{-1} \tag{4.10}$$

$$[P(t_i^+)] = \left\{[I] - [K(t_i)][H]\right\}[P(t_i^-)] \tag{4.11}$$

$$\delta\bar{x}(t_i^+) = \delta\bar{x}(t_i^-) + [K(t_i)]\left\{\bar{r}_z - [H]\delta\bar{x}(t_i^-)\right\} \tag{4.12}$$

where

$[K]$ = Kalman gain matrix

$[P(t_i^-)]$ = state covariance prior to update

$[P(t_i^+)]$ = state covariance after update

$[Q]$ = measurement noise strength

$[I]$ = 6×6 identity matrix

$\delta\bar{x}(t_i^-)$ = prior correction to state estimate

$\delta\bar{x}(t_i^+)$ = new correction to state estimate

$\bar{r}_z$ = data residual

Equation (4.12) is iterated until the correction to each state is less than .001% of the current estimate of that state.

Tuning

All tuning was performed through Monte Carlo analyses. Monte Carlo analysis consisted of a series of fifteen trajectory simulations differing only in the random noise on each measurement. The filter estimated the states through all of these simulations, and the mean and covariance of each state's error were calculated. The dynamics noise strength was adjusted until the square root of the diagonal components of the filter covariance matrix were slightly more than the error magnitude. For example, raising the strength of the dynamics noise would inform the filter that it should trust the dynamics less, and the filter covariance would thus increase via Equation (4.8). This resulted in a filter whose own estimate of it's error (the filter covariance) was slightly pessimistic: it overestimated the size of it's errors. The six state filter was tuned for one second data intervals for the flight profile defined in

Table (IV.1), starting from the initial conditions in Table (IV.2).

Table IV.1. Flight Profile, 1 G Accelerations

Time (sec)	Time (TU)	Maneuver
0 - 60	0 - .074	Constant Speed
61 - 180	.075 - .223	1 G Intrack Acceleration
181 - 300	.224 - .372	Constant Speed
301 - 420	.373 - .521	1 G Transverse Accel.
421 - 480	.522 - .595	Constant Speed

Table IV.2. Central Trajectory Initial Conditions

State	Covariance
λ = 0.0 rads	$P_{\lambda\lambda}$ = 1.25e-5 rads^2
δ = 0.0 rads	$P_{\delta\delta}$ = 1.25e-5 rads^2
h = 0.7854 rads	P_{hh} = 3.e-3 rads^2
V = 0.5 DU/TU	P_{VV} = 3.e-2 (DU/TU^2)^2
a_I = 0.0 DU/TU^2	P_{II} = 3.5e-2 (DU/TU^2)^2
a_T = 0.0 DU/TU^2	P_{TT} = 2.5 (DU/TU^2)^2

The dynamics noise matrix values that presented the best performance are given in Table (IV.3). The square root of the filter covariance and the average state error (from fifteen Monte Carlo runs) for both heading and intrack acceleration are presented in Figures (4.1) and (4.2) for the one second data interval with 1 G accelerations. These plots are representative of the filter's performance in tracking all six states. Note the axis scale factors in the corners of the plot. Also, the distinct peaks on both plots are indicative of the filter's lag in detecting the occurrence of accelerations.

Table IV.3. Dynamics Noise Strengths, Six State Filter, One Second Interval

$Q_{\lambda\lambda}$	= 1.e-14	$(\text{rads})^2$
$Q_{\delta\delta}$	= 2.e-14	$(\text{rads})^2$
Q_{hh}	= 1.e-13	$(\text{rads})^2$
Q_{vv}	= 6.e-11	$(DU/TU)^2$
Q_{II}	= 8.e-3	$(DU/TU^2)^2$
Q_{TT}	= 4.5e-3	$(DU/TU^2)^2$

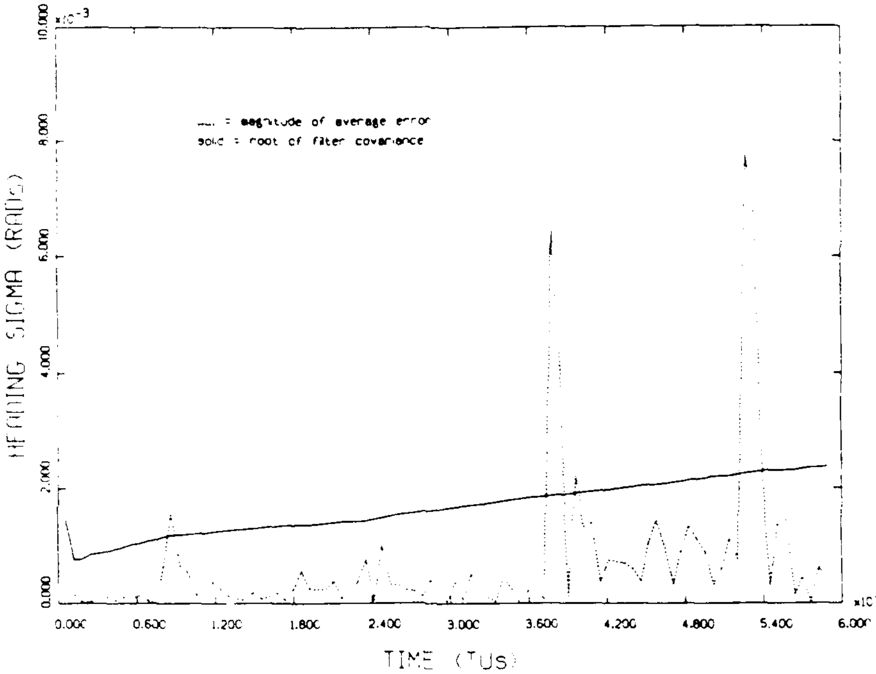

Figure 4.1. Heading Covariance and Error, 1 G, 1 Second Data Interval, Six State Filter

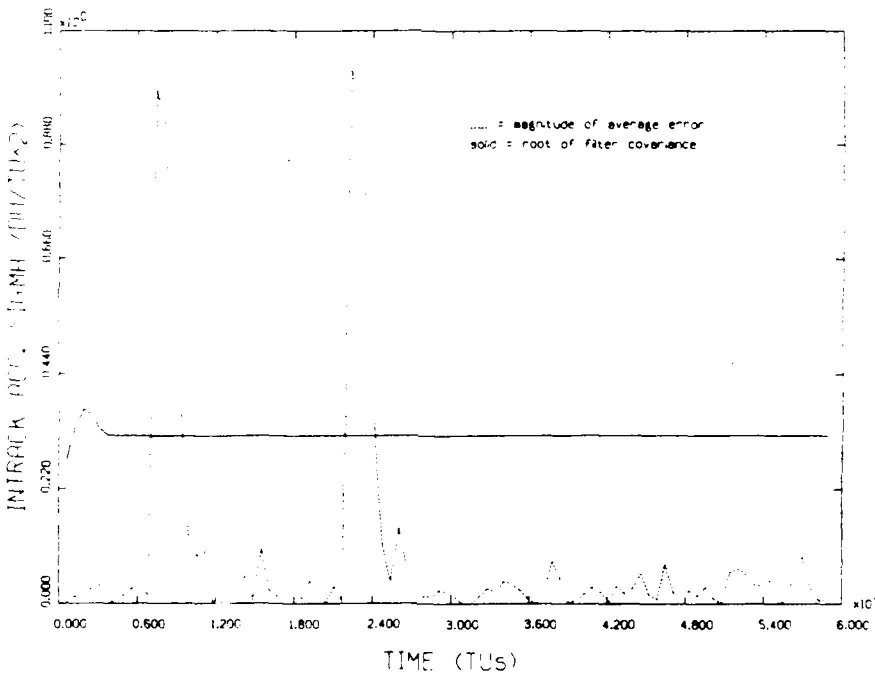

Figure 4.2. a_I Covariance and Error, 1 G, 1 Second Data Interval, Six State Filter

The gradual rise in both heading covariance and heading error appeared to indicate an unstable filter where error increases with time. A trajectory which flew backwards towards the initial conditions showed reverse trends in filter performance, indicating that filter performance is a function of the distance from the sensor's projection upon the earth's surface. The earth's curvature apparently degrades the filter's performance.

Intrack acceleration error spiked at the beginning and end of the 1 G maneuver. The narrowness of those spikes indicate that the filter rapidly recognized the presence of the maneuver.

The variation of state errors among the fifteen Monte Carlo runs also indicate filter performance. Figures (4.3) and (4.4) show that average heading and intrack acceleration errors remained close to a mean of zero except when maneuvers started or ended. The $\pm 1\ \sigma$ curves represent the amount that errors varied among the Monte Carlo runs. The relative tightness of the $\pm 1\ \sigma$ curves indicate that the six state Kalman filter consistently estimated TAV states throughout all the Monte Carlo runs.

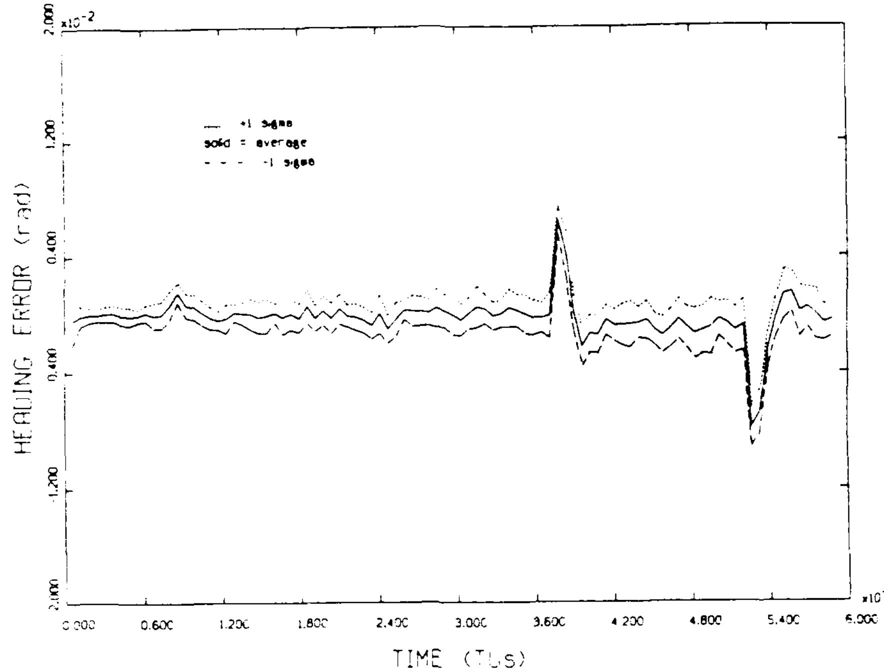

Figure 4.3. Monte Carlo Heading Error Statistics, 1 G, 1 Second Interval, Six State Filter

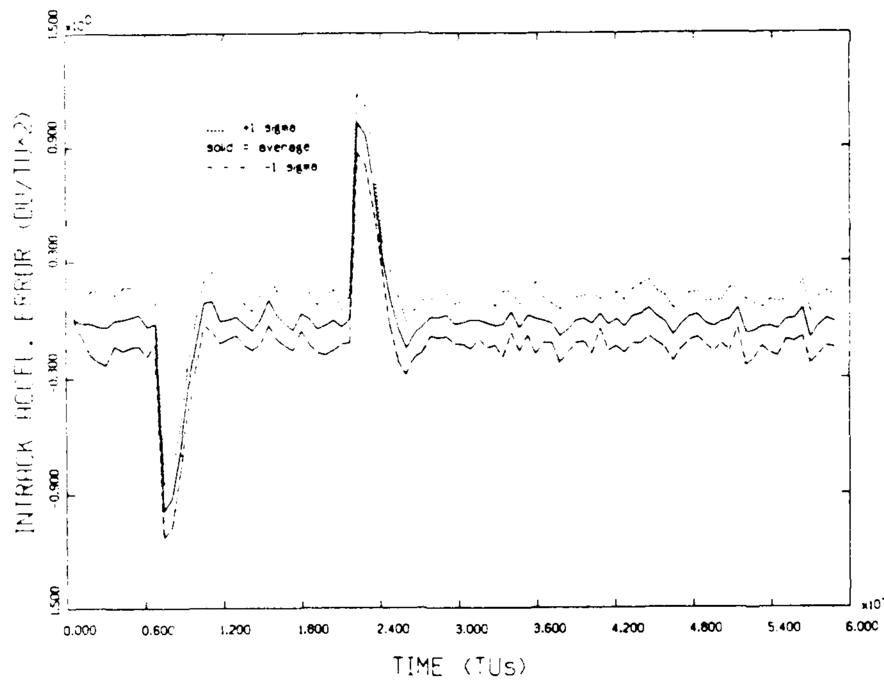

Figure 4.4. Monte Carlo a_I Error Statistics, 1 G, 1 Second Interval, Six State Filter

The other four states exhibited performance similar to the two states above. These plots are presented in Appendix A.

The ten second data interval also estimated the TAV's state over the trajectory defined in Table (IV.1) from the initial conditions listed in Table (IV.2). The dynamics noise matrix for this filter is listed in Table (IV.4). Heading and intrack acceleration covariance plots are given in Figures (4.5) and (4.6).

Table IV.4. Dynamics Noise Strengths, Six State Filter, 10 Second Data Interval

$Q_{\lambda\lambda}$	= 3.e-10	$(\text{rads})^2$
$Q_{\delta\delta}$	= 5.e-10	$(\text{rads})^2$
Q_{hh}	= 1.e-12	$(\text{rads})^2$
Q_{VV}	= 1.e-9	$(DU/TU)^2$
Q_{II}	= 6.e-2	$(DU/TU^2)^2$
Q_{TT}	= 6.e-2	$(DU/TU^2)^2$

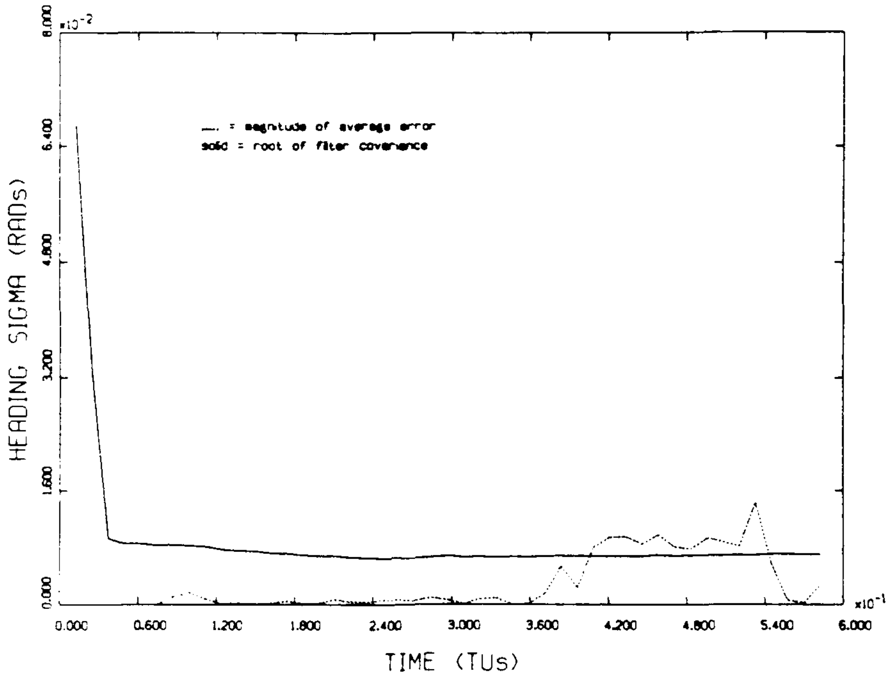

Figure 4.5. Heading Covariance and Error, 1 G, 10 Second Data Interval, Six State Filter

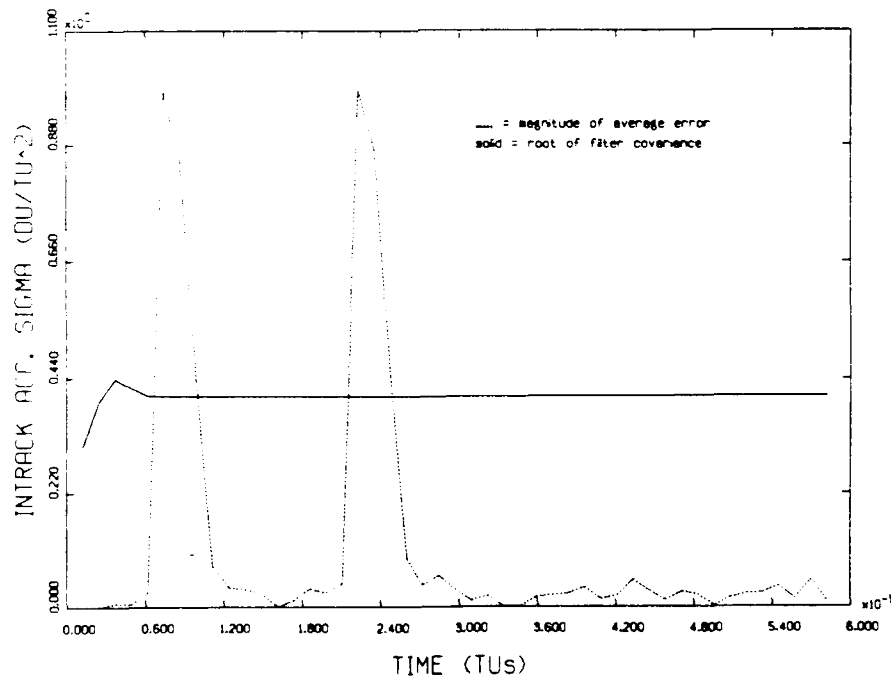

Figure 4.6. a_I Covariance and Error, 1 G, 10 Second Data Interval, Six State Filter

Monte Carlo error statistics for the ten second data interval filter were slightly degraded compared to the one second data interval filter. Heading and intrack acceleration error statistics are presented in Figures (4.7) and (4.8). The other states' covariance plots are presented in Appendix A. All remaining error $\pm\sigma$ plots are presented in Appendix C.

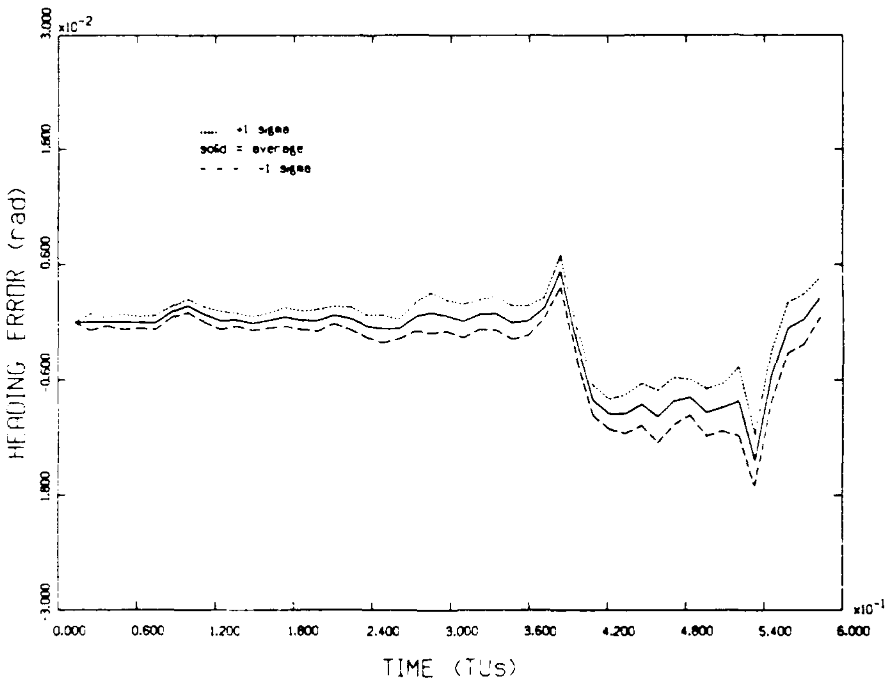

Figure 4.7. Monte Carlo Heading Error Statistics, 1 G, 10 Second Interval, Six State Filter

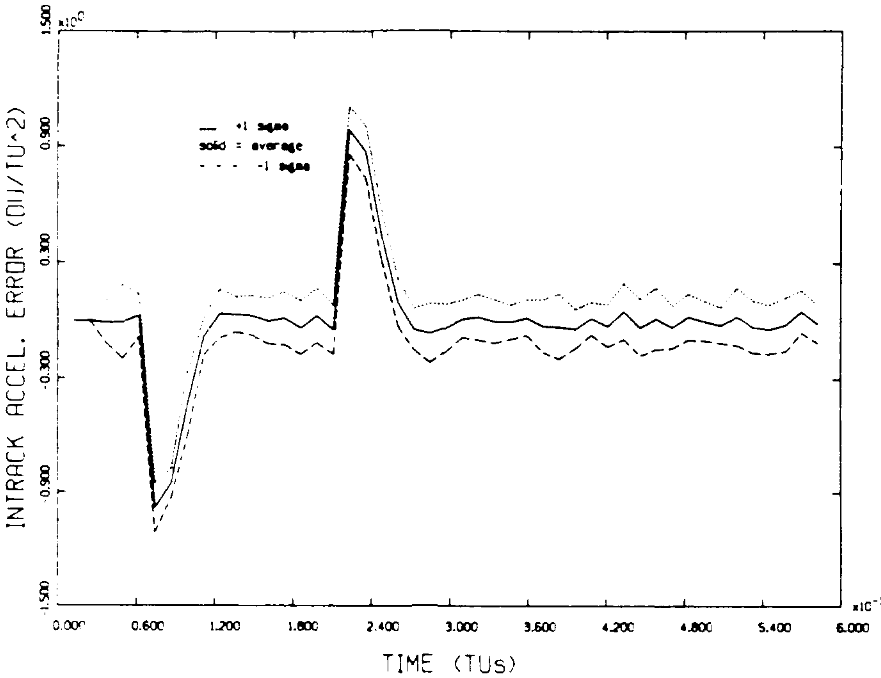

Figure 4.8. Monte Carlo a_I Error statistics, 1 G, 10 Second Interval, Six State Filter

Filter Performance

In order to evaluate the filter's ability to properly estimate states for a TAV located anywhere within view of the sensor, two additional sets of initial conditions were used with the flight profile given in Table (IV.1) and the dynamics noise matrix given in Table (IV.3). The first set was a northward trajectory starting from a point closer to the north pole.

Table IV.5. North Trajectory Initial Conditions

State	Covariance
λ = 0.0 rads	$P_{\lambda\lambda}$ = 1.25e-5 rads^2
δ = 1.0472 rads	$P_{\delta\delta}$ = 1.25e-5 rads^2
h = 0.0 rads	P_{hh} = 3.e-3 rads^2
V = 0.5 DU/TU	P_{VV} = 3.e-2 (DU/TU^2)^2
a_I = 0.0 DU/TU^2	P_{II} = 3.5e-2 (DU/TU^2)^2
a_T = 0.0 DU/TU^2	P_{TT} = 2.5 (DU/TU^2)^2

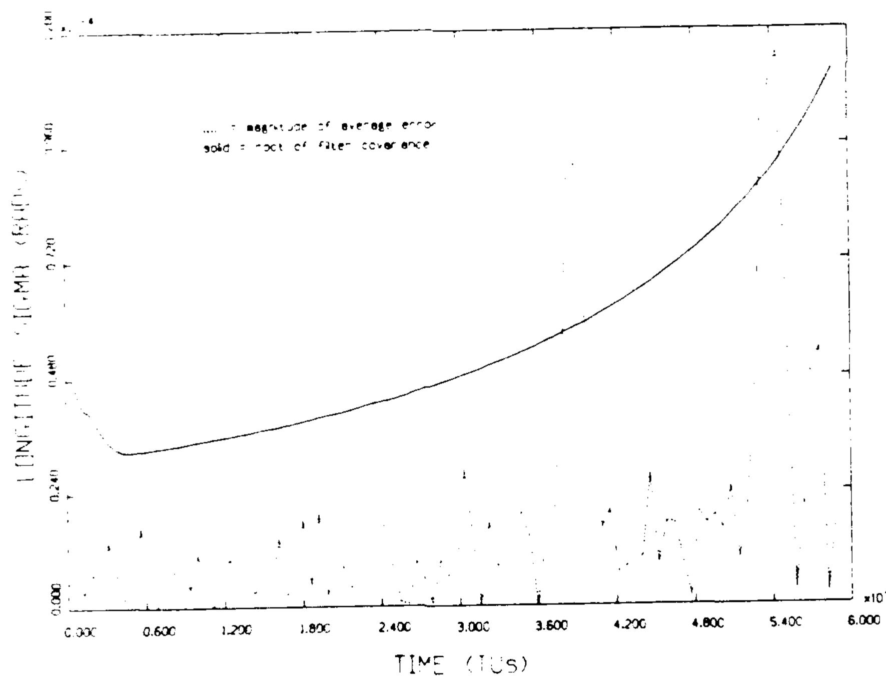

Figure 4.9. North Trajectory Longitude Covariance and Error, 1 G, 1 Second Interval, Six State Filter

Longitude becomes less certain near the north pole due to the longitude singularity at the pole, and Figure (4.9) is clearly consistent with this fact. As before, the other states' covariance plots are presented in Appendix A.

Another trajectory used the flight profile in Table (IV.1) with the initial conditions given in Table (IV.6). This east trajectory gave additional support that the six state filter remained viable near the eastward (and westward) limits of sensor view. All covariance plots for this trajectory are presented in Appendix A.

Table IV.6. East Trajectory Initial Conditions

State	Covariance
λ = 1.0472 rads	$P_{\lambda\lambda}$ = 1.25e-5 rads^2
δ = 0.1745 rads	$P_{\delta\delta}$ = 1.25e-5 rads^2
h = 1.5708 rads	P_{hh} = 3.e-3 rads^2
V = 0.5 DU/TU	P_{VV} = 3.e-2 (DU/TU^2)^2
a_I = 0.0 DU/TU^2	P_{II} = 3.5e-2 (DU/TU^2)^2
a_T = 0.0 DU/TU^2	P_{TT} = 2.5 (DU/TU^2)^2

A 9 G acceleration profile, Table (IV.7), was also investigated using the central trajectory initial conditions of Table (IV.1) and the appropriate dynamics noise matrices for the one and ten second interval filters. Although these

two filters had degraded performance, they still made adequate estimates of TAV states. Intrack acceleration curves, Figures (4.10) and (4.11), demonstrate adequate state estimation by both the one and ten second interval filters. The curves for the remaining five states are presented in Appendix B.

Table IV.7. Flight Profile, 9 G Accelerations

Time (sec)	Time (TU)	Maneuver
0 - 60	0 - .074	Constant Speed
61 - 180	.075 - .223	9 G Intrack Acceleration
181 - 300	.224 - .372	Constant Speed
301 - 420	.373 - .521	9 G Transverse Accel.
421 - 480	.522 - .595	Constant Speed

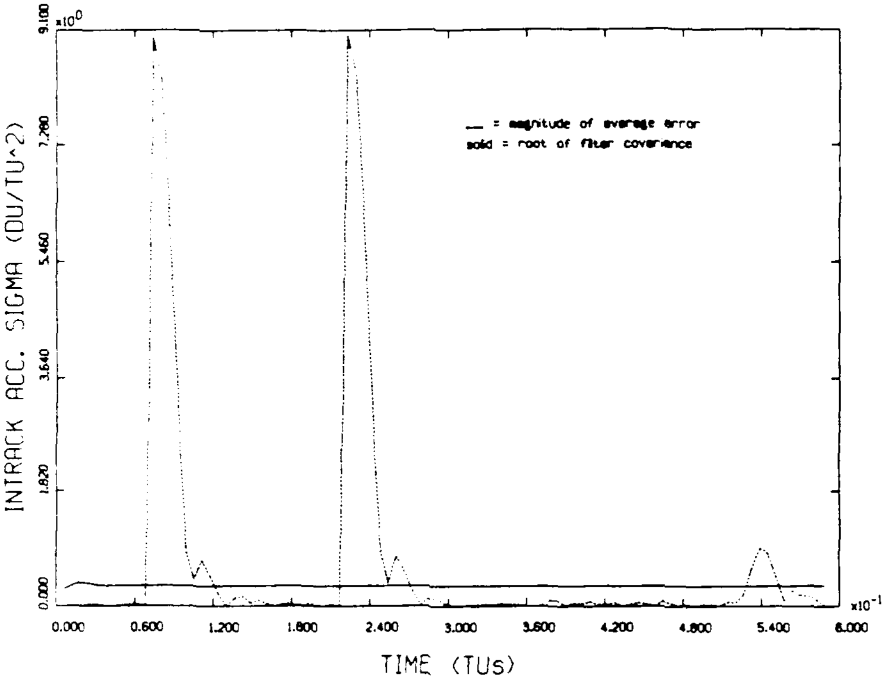

Figure 4.10. a_I Covariance and Error, 9 G, 1 Second Interval, Six State Filter

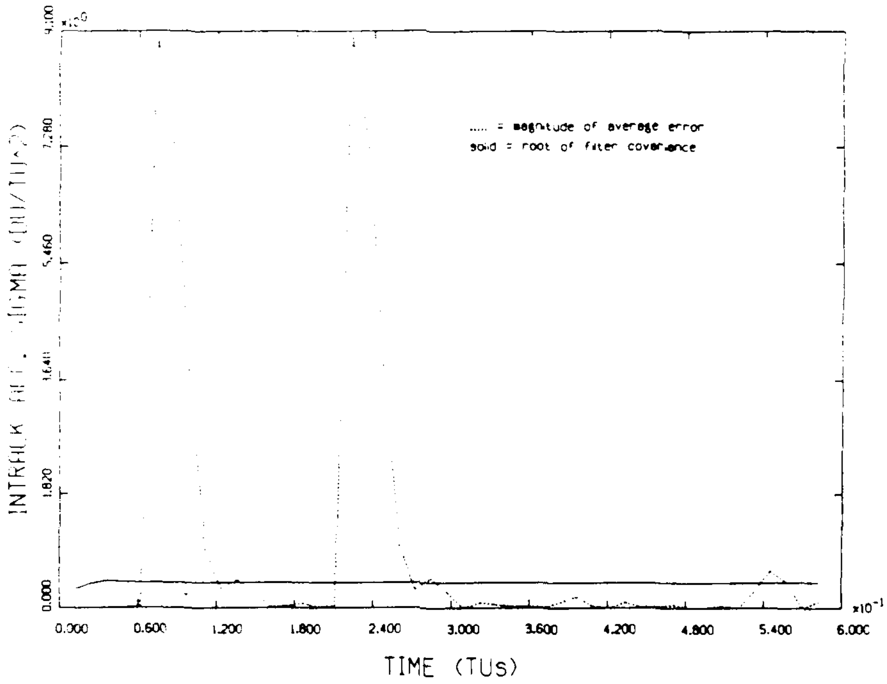

Figure 4.11. a_I Covariance and Error, 9 G, 10 Second Interval, Six State Filter

The six state filter, executed at both one and ten second data intervals, was found to adequately estimate all TAV states through 1 G and 9 G maneuvers. The remainder of this study sought a filtering algorithm which could exceed the six state filter's performance.

V. Four State Kalman Filter

The second filter developed for this tracking problem was a reduced order, four state Kalman filter. This chapter relates the motivation for a four state filter, the design and tuning process, and the filter's performance.

Motivation

The six state filter tracks the transatmospheric vehicle through periods with acceleration and periods without acceleration. Most current aircraft fly long periods of "cruise" at an essentially constant speed. The transatmospheric vehicle would also cruise in this manner when flying point-to-point missions, to align its ascent to orbit with a rendezvous target, and to return to its base after missions. During these quiescent (without intrack or transverse acceleration) periods, the two acceleration states are carried along in the six state filter for no useful purpose. The four state filter is designed to track the target during these less computationally taxing periods, taking advantage of the reduced number of states by assuming zero acceleration, thus eliminating calculations containing any acceleration terms.

State Equation

With the elimination of the acceleration states, the dynamics of the transatmospheric vehicle, Equation (2.20), reduce to the linear approximation

$$\begin{bmatrix} \lambda_{i+1} \\ \delta_{i+1} \\ h_{i+1} \\ V_{i+1} \end{bmatrix} = \begin{bmatrix} (V_i \cdot \sin h_i / R_e \cdot \cos \delta_i) - \omega_e \\ (V_i \cdot \cos h_i) / R_e \\ -a_{Ti} / V_i + [V_i \cdot \sin h_i \cdot \sin\delta_i / (R_e \cdot \cos\delta_i)] \\ a_{Ii} \end{bmatrix} \cdot \Delta t + \begin{bmatrix} \lambda_i \\ \delta_i \\ h_i \\ V_i \end{bmatrix} \quad (5.1)$$

Assuming that acceleration will be zero during the use of this filter further reduces the state equation to

$$\begin{bmatrix} \lambda_{i+1} \\ \delta_{i+1} \\ h_{i+1} \\ V_{i+1} \end{bmatrix} = \begin{bmatrix} (V_i \cdot \sin h_i / (R_e \cdot \cos \delta_i)) - \omega_e \\ (V_i \cdot \cos h_i) / R_e \\ (V_i \cdot \sin h_i \cdot \sin \delta_i) / (R_e \cdot \cos \delta_i) \\ 0 \end{bmatrix} \cdot \Delta t + \begin{bmatrix} \lambda_i \\ \delta_i \\ h_i \\ V_i \end{bmatrix} \quad (5.2)$$

This equation is a model of the transatmospheric vehicle in a quiescent period. No attempt is made to accommodate accelerations because, in the presence of accelerations, the total, adaptive filter will execute the six state filter to properly estimate the acceleration states.

State Transition Matrix

Discrete time propagation of the state vector, $\bar{x}$, in Equation (5.2) is of the form

$$\bar{x}_{i+1}(t) = f[\bar{x}_i(t), \Delta t] \quad (5.3)$$

The state transition matrix is found by taking the gradient

$$[\Phi(t_{i+1},t_i)] = \nabla_{x_i}\left(f[\bar{x}_i(t),\ t]\right) \qquad (5.4)$$

which, expanded, is

$$[\Phi] = \begin{bmatrix} \frac{\partial\lambda_{i+1}}{\partial\lambda_i} & \frac{\partial\lambda_{i+1}}{\partial\delta_i} & \frac{\partial\lambda_{i+1}}{\partial h_i} & \frac{\partial\lambda_{i+1}}{\partial V_i} \\ \frac{\partial\delta_{i+1}}{\partial\lambda_i} & \frac{\partial\delta_{i+1}}{\partial\delta_i} & \frac{\partial\delta_{i+1}}{\partial h_i} & \frac{\partial\delta_{i+1}}{\partial V_i} \\ \frac{\partial h_{i+1}}{\partial\lambda_i} & \frac{\partial h_{i+1}}{\partial\delta_i} & \frac{\partial h_{i+1}}{\partial h_i} & \frac{\partial h_{i+1}}{\partial V_i} \\ \frac{\partial V_{i+1}}{\partial\lambda_i} & \frac{\partial V_{i+1}}{\partial\delta_i} & \frac{\partial V_{i+1}}{\partial h_i} & \frac{\partial V_{i+1}}{\partial V_i} \end{bmatrix} \qquad (5.5)$$

where

$$\frac{\partial\lambda_{i+1}}{\partial\delta_i} = \frac{V_i\cdot\sin h_i\cdot\sin\delta_i}{R_e\cdot\cos^2\delta_i}\cdot\Delta t$$

$$\frac{\partial\lambda_{i+1}}{\partial h_i} = \frac{V_i\cdot\cos h_i}{R_e\cdot\cos\delta_i}\cdot\Delta t$$

$$\frac{\partial\lambda_{i+1}}{\partial V_i} = \frac{\sin h_i}{R_e\cdot\cos\delta_i}\cdot\Delta t$$

$$\frac{\partial\delta_{i+1}}{\partial h_i} = \frac{-V_i\cdot\sin h_i}{R_e}\cdot\Delta t$$

$$\frac{\partial\delta_{i+1}}{\partial V_i} = \frac{\cos h_i}{R_e}\cdot\Delta t$$

$$\frac{\partial h_{i+1}}{\partial\delta_i} = \left(V_i\cdot\sin h_i + \frac{V_i\cdot\sin h_i\cdot\sin^2\delta_i}{\cos^2\delta_i}\right)\cdot\frac{\Delta t}{R_e}$$

$$\frac{\partial h_{i+1}}{\partial h_i} = \frac{V_i\cdot\cos h_i\cdot\sin\delta_i}{R_e\cdot\cos\delta_i}\cdot\Delta t + 1$$

$$\frac{\partial h_{i+1}}{\partial V_i} = \frac{\sin h_i \cdot \sin \delta_i}{R_e \cdot \cos \delta_i} \cdot \Delta t$$

$$\frac{\partial \lambda_{i+1}}{\partial \lambda_i} = \frac{\partial \delta_{i+1}}{\partial \delta_i} = \frac{\partial V_{i+1}}{\partial V_i} = 1$$

$$\frac{\partial h_{i+1}}{\partial \lambda_i} = \frac{\partial V_{i+1}}{\partial \lambda_i} = \frac{\partial V_{i+1}}{\partial \delta_i} = \frac{\partial V_{i+1}}{\partial h_i} = \frac{\partial \delta_{i+1}}{\partial \lambda_i} = 0$$

Measurements (3:44)

Data is assumed to consist of a deterministic portion and a zero-mean, white Gaussian noise, $\overline{v}_i$.

$$\overline{z} = h[\overline{x}(t_i),t_i] + \overline{v}_i \tag{5.6}$$

where

$$\overline{h}[\overline{x}(t_i),t_i] = \begin{bmatrix} 1 & 0 & 0 & 0 \\ 0 & 1 & 0 & 0 \end{bmatrix} \cdot \overline{x}$$

and $\overline{v}_i$ has strength

$$[Q] = [J][Q_{az,el}][J]^T$$

with [J] and $[Q_{az,el}]$ defined in Equations (3.13) and (3.1).

[H] is defined as

$$[H] = \frac{\partial \overline{h}[\overline{x}(t_i),t_i]}{\partial \overline{x}} = \begin{bmatrix} 1 & 0 & 0 & 0 \\ 0 & 1 & 0 & 0 \end{bmatrix} \tag{5.7}$$

State Covariance (3:44)

For convenience in starting the filter, each state variable at t = 0 is assumed independent of the other states, or

$$[P_o] = \lceil \sigma_\lambda^2 \quad \sigma_\delta^2 \quad \sigma_h^2 \quad \sigma_V^2 \rfloor \tag{5.8}$$

This allows the entry of four values as opposed to a fully populated 4×4 matrix.

Covariance is propagated via

$$[P_{i+1}] = [\Phi_{i+1,i}][P_i][\Phi_{i+1,i}]^T + [Q_n] \qquad (5.9)$$

where $[\Phi_{i+1,i}]$ is defined by Equation (5.5) and $[Q_n]$ is the dynamics noise matrix, which is assumed to be diagonal.

$$[Q_n] = \lceil Q_{n_\lambda} \quad Q_{n_\delta} \quad Q_{n_h} \quad Q_{n_V} \rfloor \qquad (5.10)$$

The four diagonal elements of $[Q_n]$ will be adjusted through the tuning process.

<u>Filter Algorithm</u> (5:100)

The extended Kalman filter equations are

$$[K(t_i)] = [P(t_i^-)][H]^T\left\{[H][P(t_i^-)][H]^T + [Q]\right\}^{-1} \qquad (5.11)$$

$$[P(t_i^+)] = \left\{[I] - [K(t_i)][H]\right\}[P(t_i^-)] \qquad (5.12)$$

$$\delta\bar{x}(t_i^+) = \delta\bar{x}(t_i^-) + [K(t_i)]\left\{\bar{r}_z - [H]\delta\bar{x}(t_i^-)\right\} \qquad (5.13)$$

which is the same as presented in Chapter IV.

<u>Tuning</u>

Just as in the case of the six state filter, the dynamics noise matrix, $[Q_n]$, was adjusted until the square root of the diagonal components of the filter's covariance matrix (after the measurement update) were just slightly higher than the average error found via Monte Carlo analysis. The four state filter was tuned for a flight profile without any applied accelerations. The initial conditions are the same as the central trajectory initial conditions from Chapter IV and are repeated in Table (V.1). The dynamics noise matrix values used for this study are

listed in Table (V.2) for the one second interval and in Table (V.3) for the ten second interval.

Table V.1. Central Trajectory Initial Conditions, Four State Filter

State	Covariance
λ = 0.0 rads	$P_{\lambda\lambda}$ = 1.25e-5 rads^2
δ = 0.0 rads	$P_{\delta\delta}$ = 1.25e-5 rads^2
h = 0.7854 rads	P_{hh} = 3.e-3 rads^2
V = 0.5 DU/TU	P_{VV} = 3.e-3 (DU/TU)^2
a_I = 0.0 DU/TU^2	
a_T = 0.0 DU/TU^2	

Table V.2. Dynamics Noise Strengths, Four State Filter, One Second Data Interval

$Q_{\lambda\lambda}$ = 0.0 rads^2
$Q_{\delta\delta}$ = 0.0 rads^2
Q_{hh} = 1.e-26 rads^2
Q_{VV} = 1.e-26 (DU/TU)^2

Table V.3. Dynamics Noise Strengths, Four State Filter, Ten Second Data Interval

$$Q_{\lambda\lambda} = 0.0 \text{ rads}^2$$
$$Q_{\delta\delta} = 0.0 \text{ rads}^2$$
$$Q_{hh} = 1.\text{e-}16 \text{ rads}^2$$
$$Q_{vv} = 1.\text{e-}16 \ (\text{DU/TU})^2$$

The four state filter's performance was demonstrated by the longitude covariance plots, Figures (5.1) and (5.2), for the one and ten second interval four state filters. Although the one second interval plot shows the error exceeding the square root of covariance halfway through the plot, this version of the four state filter gave the best performance when integrated into the adaptive filters.

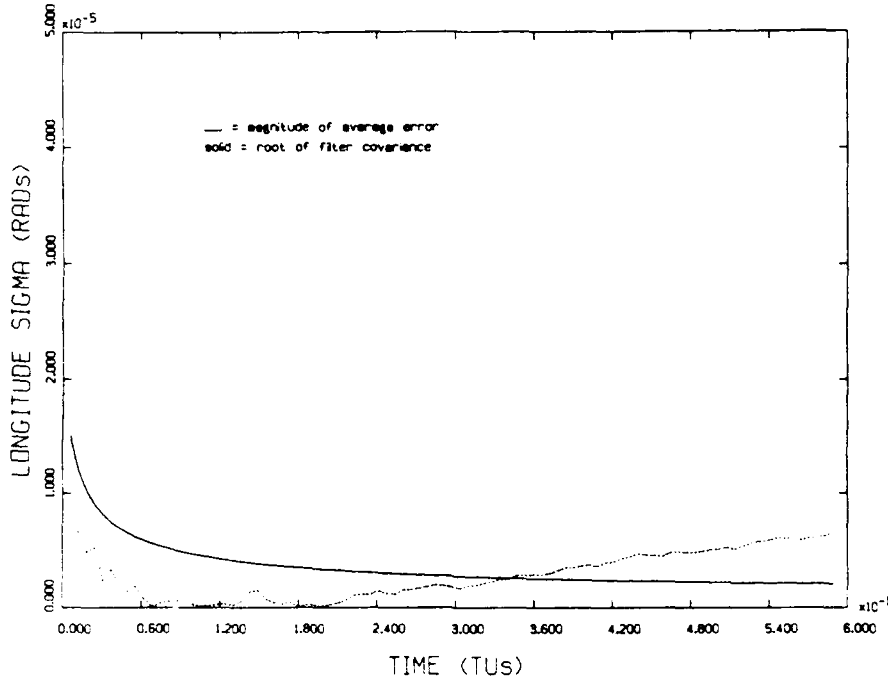

Figure 5.1. Longitude Covariance and Error, 1 G, 1 Second Data Interval, Four State Filter

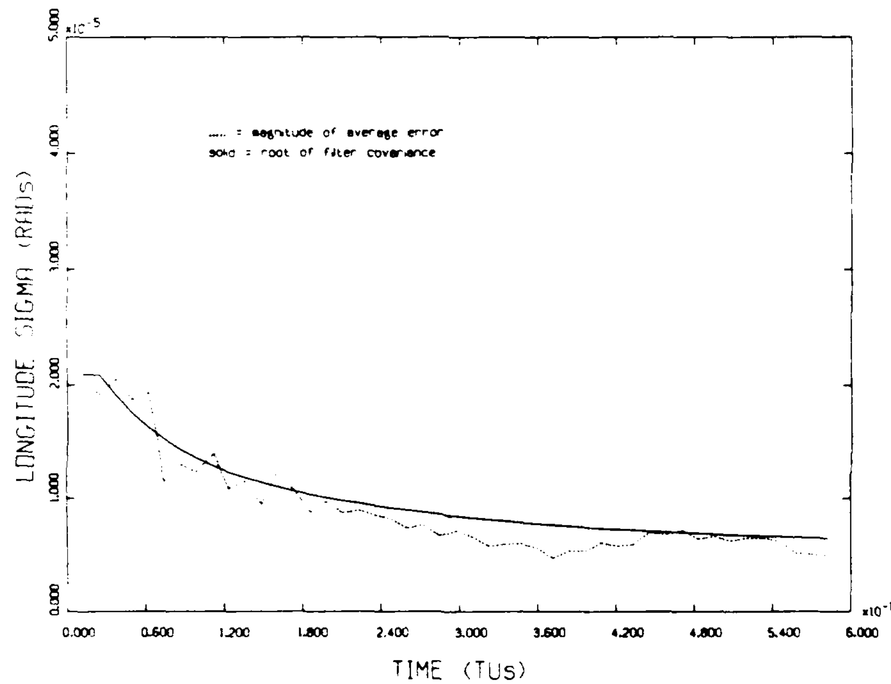

Figure 5.2. Longitude Covariance and Error, 1 G, 10 Second Data Interval, Four State Filter

VI. Multiple Model Adaptive Kalman Filters

When a system model itself may be subject to change, multiple model adaptive filtering can be used to compare the performance of several filters, each based upon a different system model. Sub-filter estimates could be used either individually or in weighted averages of those estimates. This section presents three different approaches for the application of adaptive filtering to this estimation problem. All of the adaptive filters presented estimated the states for the 1 G flight profile starting from the central trajectory initial conditions.

Acceleration Switched Adaptive Filter

The four state filter developed in chapter V was meant to model TAV dynamics in the absence of applied accelerations. The six state filter modeled the presence of accelerations. Rather than running both the six state and four state filters simultaneously, the first attempt at adaptation was to switch from the six state to the four state and back again based upon the six state estimate of acceleration and the four state filter's residuals. Residuals were measured before the measurement updates for each data interval. This was intended to decrease estimate errors and minimize computer time required for the adaptive filter.

The algorithm for the acceleration switched adaptive filter begins with the six state Kalman filter Equations (4.10), (4.11) and (4.12), repeated here with the subscript '6' to indicate the six state filter.

$$[K_6(t_i)] = [P_6(t_i^-)]\ [H_6]^T\left\{[H_6][P_6(t_i^-)][H_6]^T + [Q_6]\right\}^{-1} \quad (6.1)$$

$$[P_6(t_i^+)] = \left\{[I_6] - [K_6(t_i)][H_6]\right\}[P_6(t_i^-)] \quad (6.2)$$

$$\delta\bar{x}_6(t_i^+) = \delta\bar{x}_6(t_i^-) + [K_6(t_i)]\left\{\bar{r}_{z,6} - [H_6]\delta\bar{x}_6(t_i^-)\right\} \quad (6.3)$$

Normal six state filter operations continued until both $\bar{a}_T$ and $\bar{a}_T$ estimates dropped below 0.02 G's. At that point the accelerations were assumed to be zero and the four state filter was initiated using the first four components of the six-state state vector along with the corresponding 4×4 section of the covariance matrix. The remaining covariance values were stored to allow the six state filter to restart in the future. The four state filter equations (5.11), (5.12), and (5.13) are repeated below.

$$[K_4(t_i)] = [P_4(t_i^-)]\ [H_4]^T\left\{[H_4][P_4(t_i^-)][H_4]^T + [Q_4]\right\}^{-1} \quad (6.4)$$

$$[P_4(t_i^+)] = \left\{[I_4] - [K_4(t_i)][H_4]\right\}[P_4(t_i^-)] \quad (6.5)$$

$$\delta\bar{x}_4(t_i^+) = \delta\bar{x}_4(t_i^-) + [K_4(t_i)]\left\{\bar{r}_{z,4} - [H_4]\delta\bar{x}_4(t_i^-)\right\} \quad (6.6)$$

The four state filter continued to operate until either the average of the last two longitude residuals or the average of the last two latitude residuals exceeded 7×10^{-6} radians. At this point, the four state filter was assumed to be diverging, and the four-state state vector augmented

with two zeroes was fed into the six-state state vector. The four state covariance matrix, augmented with the unused values discussed above, was inserted into the six state covariance, and the adaptive filter switched back to six state filter operations until accelerations once again dropped below the lower bound. The two switching bounds, 0.02 G's for acceleration and 7×10^{-6} radians for position, were found to give the best state estimates for this algorithm.

Unfortunately, this ad hoc approach to adaptive filtering did not markedly decrease filter errors, nor was it an improvement during quiescent periods. Figure (6.1) depicts slight increases in heading covariance during the four state filter's activity. The rest of the curve is essentially the same as the curve for the six state filter.

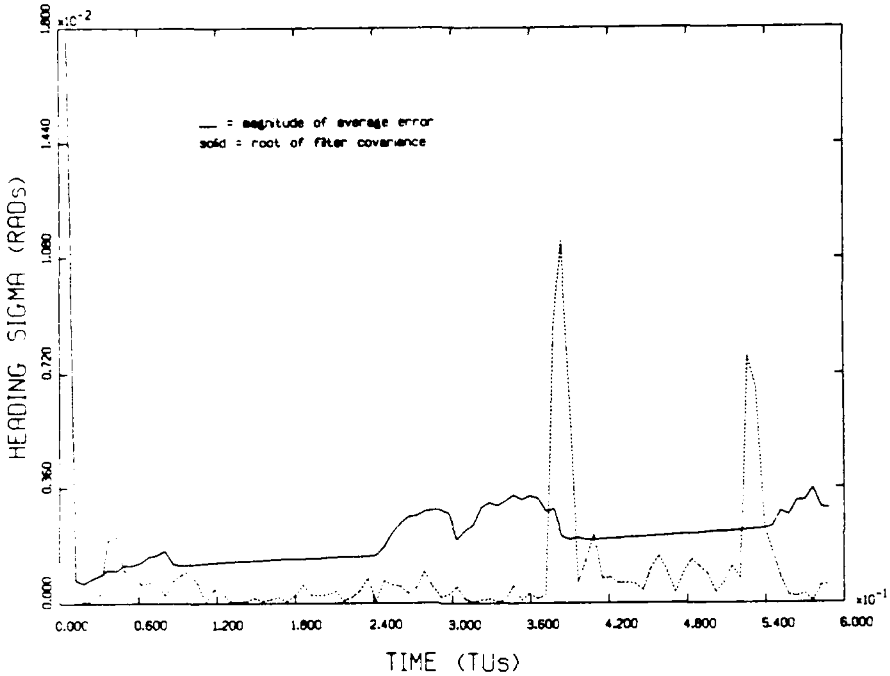

Figure 6.1 Heading Covariance and Error, 1 G, 1 Second Interval, Acceleration Switched Adaptation

<u>Residual Switched Adaptive Filter</u>

This second attempt at adaptation abandoned the idea of running only one filter at a time. For this adaptation the longitude and latitude residuals were monitored in order to choose which filter (model) best represented the TAV's dynamics during the current data interval.

The root-mean-squares of the longitude and latitude residuals for both the six state and four state filters were calculated. Residuals were measured before the measurement updates.

$$RMS_4 = \sqrt{0.5\cdot(r_{\lambda 4}^2 + r_{\delta 4}^2)} \qquad (6.7)$$

$$RMS_6 = \sqrt{0.5 \cdot (r_{\lambda 6}^2 + r_{\delta 6}^2)} \qquad (6.8)$$

The smaller of the two RMS's would indicate the sub-filter whose estimate was chosen for that time interval. If the four state filter was chosen, the current acceleration estimates would be set to zero.

This attempt at adaptation suffered from the same problem as the previous attempt: the four state model did not adequately improve the estimate even during quiescent periods. Figure 6.2 demonstrates behavior much worse than the six state filter's performance. This adaptive filter exhibited large errors and was abandoned.

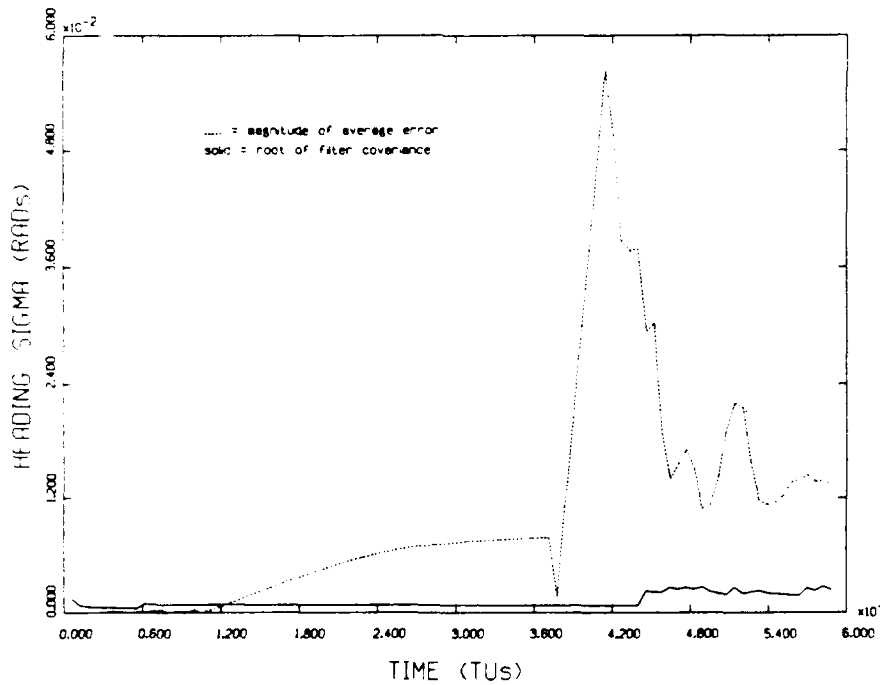

Figure 6.2 Heading Covariance and Error, 1 G, 1 Second Interval, Residual Switched Adaptation

Probability Weighting Adaptive Filter

Both the six state and four state sub-filters generate state estimates for each data point. Probability weighting used the sub-filters' residuals to generate the probability that either sub-filter model was the correct model for the system at any given time. The probability density, f_k, associated with the sub-filters is given by

$$f_k(t_i) = \frac{1}{2\pi|[\underline{A}_k]|^{1/2}} \cdot \exp\left\{-\frac{1}{2}\,\bar{r}_k^T\,[\underline{A}_k]^{-1}\,\bar{r}_k\right\} \qquad (6.9)\ (3:132)$$

where

$$\begin{aligned}[A_k] &= [H_k][P_k(t_i^-)][H_k]^T + [Q_k] \\ &= [H][P_k(t_i^-)][H]^T + [Q] \\ &= \begin{bmatrix} P_{k,11} & 0 \\ 0 & P_{k,22} \end{bmatrix} + [Q]\end{aligned}$$

$$[A_k] = \begin{bmatrix} P_{k,11} + Q_{11} & Q_{12} \\ Q_{21} & P_{k,22} + Q_{22} \end{bmatrix} \qquad (6.10)$$

Equation (6.9) is of the form

$$f_k(t_i) = \beta \cdot \exp\left\{-\frac{1}{2}\,\bar{r}_k^T\,[\underline{A}_k]^{-1}\,\bar{r}_k\right\} \qquad (6.11)$$

The β term is commonly set to one in order to enhance the sensitivity of the adaptive filter to the inadequacies of the sub-filters. (1:a) With β set to one the adaptive filter switches more quickly to the more correct sub-filter, and the probability density becomes

$$f_k(t_i) = \exp\left\{-\frac{1}{2}\,\bar{r}_k^T\,[\underline{A}_k]^{-1}\,\bar{r}_k\right\} \qquad (6.12)$$

The probability that the k-state sub-filter is the best model is given by

$$p_k(t_i) = f_k(t_i)\cdot p_k(t_{i-1}) / \{f_4(t_i)\cdot p_4(t_{i-1}) + f_6(t_i)\cdot p_6(t_{i-1})\} \qquad (6.13)$$

Adaptive filter state estimates are given by

$$\hat{x}(t_i^+) = p_4(t_i) \cdot \hat{x}_4(t_i^+) + p_6(t_i) \cdot \hat{x}_6(t_i^+) \qquad (6.13)$$

(3:131)

and covariance by

$$[P(t_i^+)] = p_4(t_i) \cdot \left\{[P_4(t_i^+)] + [\hat{x}_4(t_i^+) - \hat{x}(t_i^+)] \cdot [\hat{x}_4(t_i^+) - \hat{x}(t_i^+)]^T\right\} + p_6(t_i) \cdot \left\{[P_6(t_i^+)] + [\hat{x}_6(t_i^+) - \hat{x}(t_i^+)] \cdot [\hat{x}_6(t_i^+) - \hat{x}(t_i^+)]\right\} \qquad (6.14)$$

(3:131)

For this application, the sub-filters should be tuned optimistically as opposed to the pessimistic tunings performed in chapter IV. By allowing sub-filter covariance to be close to, or slightly less than, the actual error, the residuals should more clearly indicate the relative "goodness" of the sub-filter models. Best adaptive filter estimates, however, occurred when the six state filter utilized the dynamics noise matrices presented in Tables (IV.3) and (IV.4), and when the four state filter retained the dynamics noise matrices presented in Tables (V.2) and (V.3). These four matrices are summarized in Tables (VI.1) and (VI.2).

Table VI.1. Adaptive Filter Dynamics Noise Matrices, 1 Second Data Interval

	Four State Filter	Six State Filter
$Q_{\lambda\lambda}$	0.0 $rads^2$	1.e-14 $rads^2$
$Q_{\delta\delta}$	0.0 $rads^2$	2.e-14 $rads^2$
Q_{hh}	1.e-26 $rads^2$	1.e-13 $rads^2$
Q_{VV}	1.e-26 $(DU/TU)^2$	6.e-11 $(DU/TU)^2$
Q_{II}	N/A	8.e-3 $(DU/TU^2)^2$
Q_{TT}	N/A	4.5e-3 $(DU/TU^2)^2$

Table VI.2. Adaptive Filter Dynamics Noise Matrices, 10 Second Data Interval

	Four State Filter	Six State Filter
$Q_{\lambda\lambda}$	0.0 $rads^2$	3.e-10 $rads^2$
$Q_{\delta\delta}$	0.0 $rads^2$	5.e-10 $rads^2$
Q_{hh}	1.e-26 $rads^2$	1.e-12 $rads^2$
Q_{VV}	1.e-26 $(DU/TU)^2$	1.e-9 $(DU/TU)^2$
Q_{II}	N/A	6.e-2 $(DU/TU^2)^2$
Q_{TT}	N/A	6.e-2 $(DU/TU^2)^2$

The heading and intrack acceleration covariance plots for the one and ten second interval adaptive filters, Figures (6.3) through (6.6), demonstrated a slight improvement in intrack acceleration for a short period with some degradation in heading. The other states were also slightly improved or degraded, but there was little overall improvement as compared to the six state Kalman filter of Chapter IV. For the sake of completeness, this adaptive filter was carried forward into Chapter VII's comparisons. The other two adaptive filters were not.

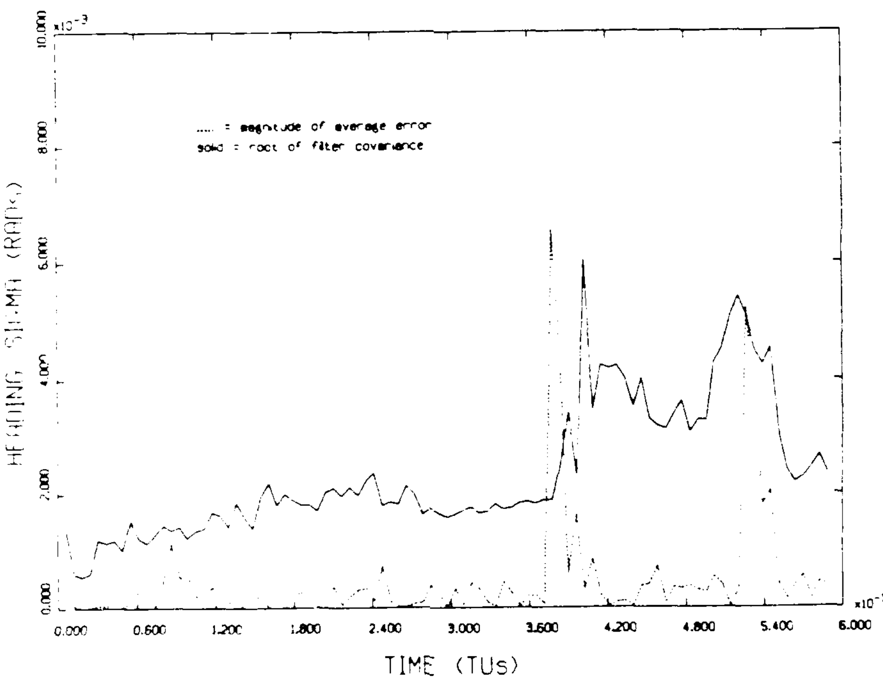

Figure 6.3. Heading Covariance and Error, 1 Second Interval, Probability Weighting Adaptation

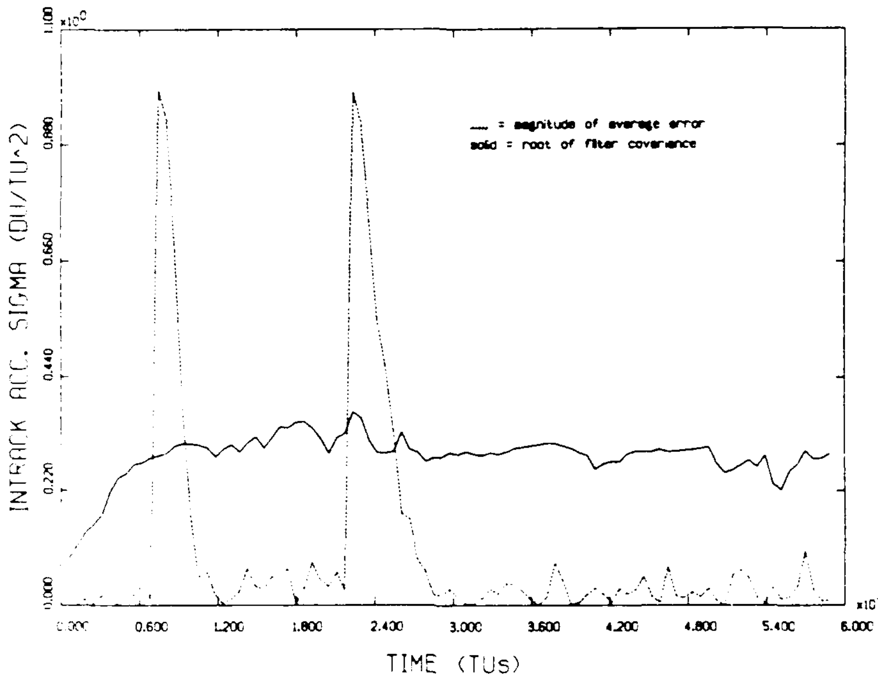

Figure 6.4. a_I Covariance and Error, 1 Second Interval, Probability Weighting Adaptation

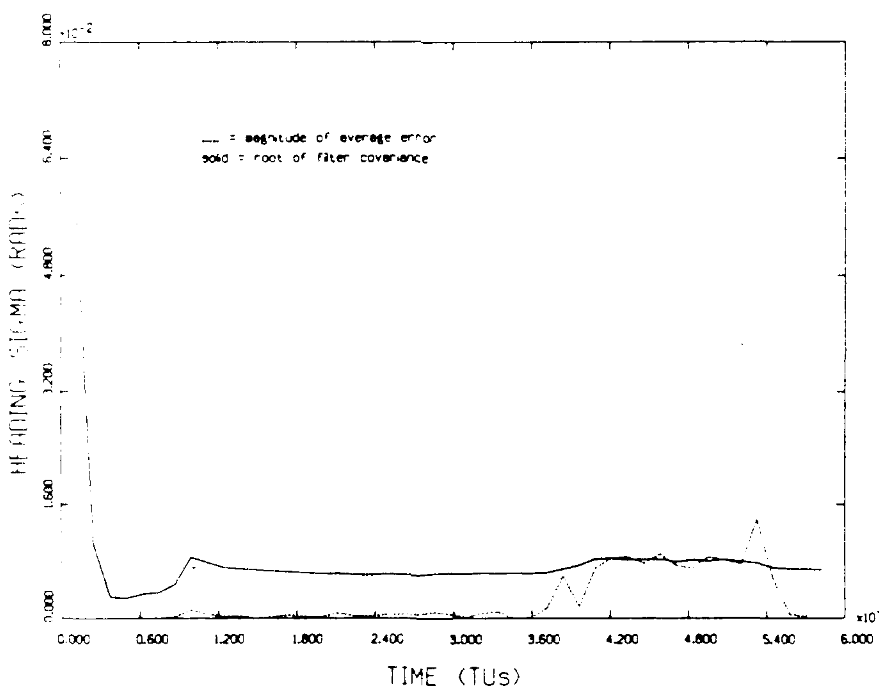

Figure 6.5. Heading Covariance and Error, 10 Second Interval, Probability Weighting Adaptation

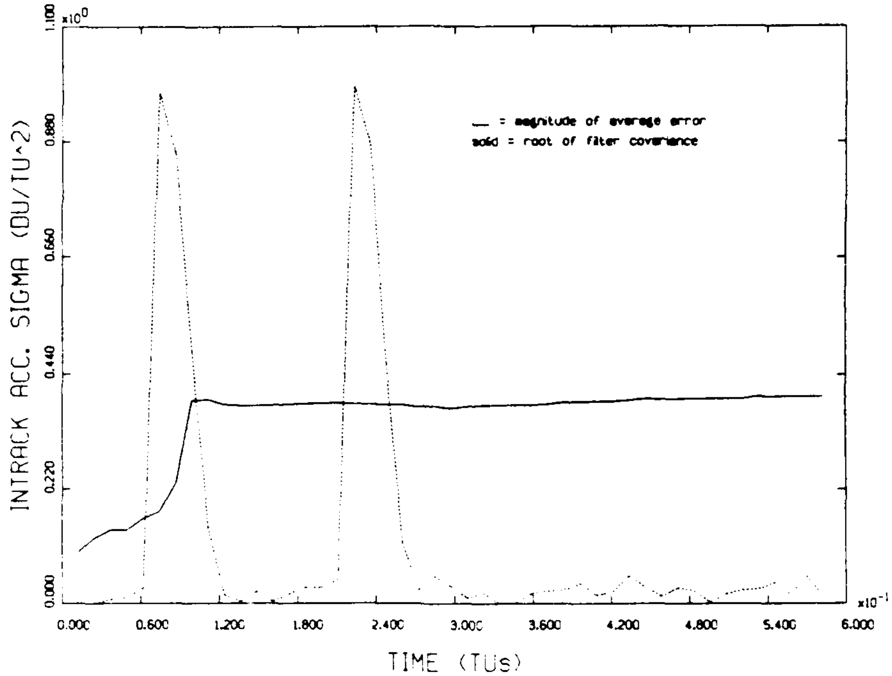

Figure 6.6. a_I Covariance and Error, 10 Second Interval, Probability Weighting Adaptation

VII. Smoother

A Kalman filter estimates the current state based upon the data collected prior to the current time. After collecting all of the data, another filter could be run backwards in time from the end of the data to estimate the state based upon all of the data collected from the current time until the end of the data. The two estimates could be optimally combined to produce an estimate of the state based upon all of the data collected. This process is called smoothing, and the algorithm is known as a smoother. (2:2) This chapter explains the motivation for the smoother and its derivation.

Motivation

All of the previous methods were potentially real-time algorithms that would take TAV position data and immediately estimate the six state variables. Adaptation failed to decrease errors, necessitating another approach to better estimate acceleration states. A smoother, although a form of Kalman filter, is a "post-flight" analysis tool also known to improve state estimates, including the acceleration states.

Forward Filter

The forward filter is the same as the six state filter developed in Chapter V where

$$\bar{x}_{F,i+1}(t) = f[\bar{x}_{F,i}(t),\Delta t] \quad (7.1)$$

$$[\Phi_F(t_{i+1},t_i)] = \nabla_{x_{F,i}}\Big(f[\bar{x}_{F,i}(t),\Delta t] \Big) \quad (7.2)$$

$$[K_F(t_i)] = [P_F(t_i^-)][H]^T\Big\{[H][P_F(t_i^-)][H]^T + [Q]\Big\}^{-1} \quad (7.3)$$

$$[P_F(t_i^+)] = \Big\{[I] - [K_F(t_i)][H]\Big\}[P_F(t_i^-)] \quad (7.4)$$

$$\delta\bar{x}_F(t_i^+) = \delta\bar{x}_F(t_i^-) + [K_F(t_i)]\Big\{ \bar{r}_{F,Z} - [H]\cdot\delta\bar{x}_F(t_i^-)\Big\} \quad (7.5)$$

Backward Filter

While Equation (7.1) propagates the system dynamics forward in time, replacing the Δt with $-\Delta t$ will propagate the system backward in time.

$$\bar{x}_{B,i-1}(t) = f[\bar{x}_{B,i}(t),-\Delta t] \quad (7.6)$$

Thus

$$[\Phi_B(t_{i-1},t_i)] = \nabla_{x_{B,i}}\Big(f[\bar{x}_{B,i}(t),-\Delta t] \Big) \quad (7.7)$$

$$[K_B(t_i)] = [P_B(t_i^-)][H]^T\Big\{[H][P_B(t_i^-)][H]^T + [Q]\Big\}^{-1} \quad (7.9)$$

$$[P_B(t_i^+)] = \Big\{[I] - [K_B(t_i)][H]\Big\}[P_B(t_i^-)] \quad (7.10)$$

$$\delta\bar{x}_B(t_i^+) = \delta\bar{x}_B(t_i^-) + [K_B(t_i)]\Big\{ \bar{r}_{B,Z} - [H]\cdot\delta\bar{x}_B(t_i^-)\Big\} \quad (7.11)$$

Combining the Estimates

Smoothed covariance was found via least squares where

$$[P_S] = \Big\{[P_F]^{-1} + [P_B]^{-1}\Big\}^{-1} \quad (7.12)$$

The smoothed state vector was also found via least squares where

$$\bar{x}_S = [P_S]\cdot\Big\{[P_F]^{-1}\cdot\bar{x}_F + [P_B]^{-1}\cdot\bar{x}_B\Big\} \quad (7.13)$$

This algorithm uses the "current" data point in both the forward and the backwards filters. This causes a double weighting of that data point in the smoother estimates.

One and ten second data interval smoothers estimated the states for the 1 G flight profile from the central trajectory initial conditions. Longitude and latitude estimates suffered large errors for both data intervals as demonstrated in Figures (7.1) and (7.2). Acceleration states were fairly well estimated for the one second data interval as shown in the intrack acceleration covariance plot, Figure (7.3). The ten second interval smoother showed some bias in acceleration estimates during accelerations, as shown in Figure (7.4). The other states' covariance plots are presented in Appendix A.

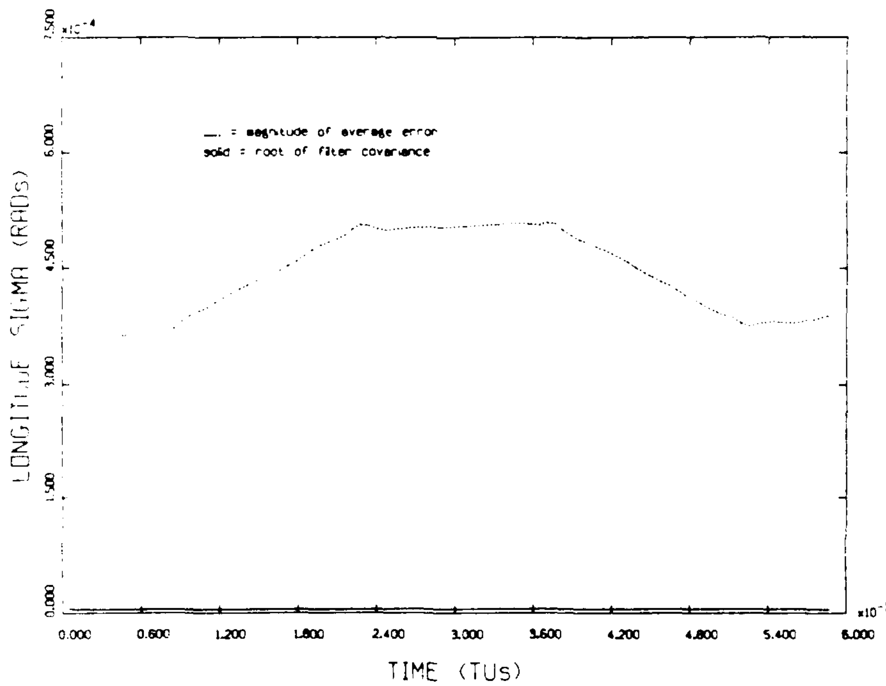

Figure 7.1. Longitude Covariance and Error, 1 G, 1 Second Data Interval, Smoother

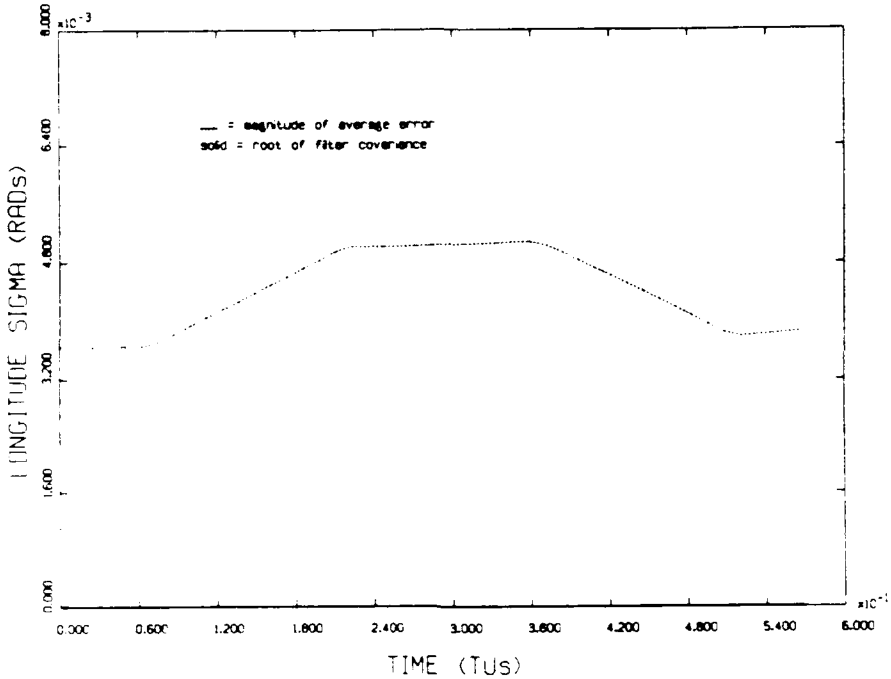

Figure 7.2. Longitude Covariance and Error, 1 G, 10 Second Data Interval, Smoother

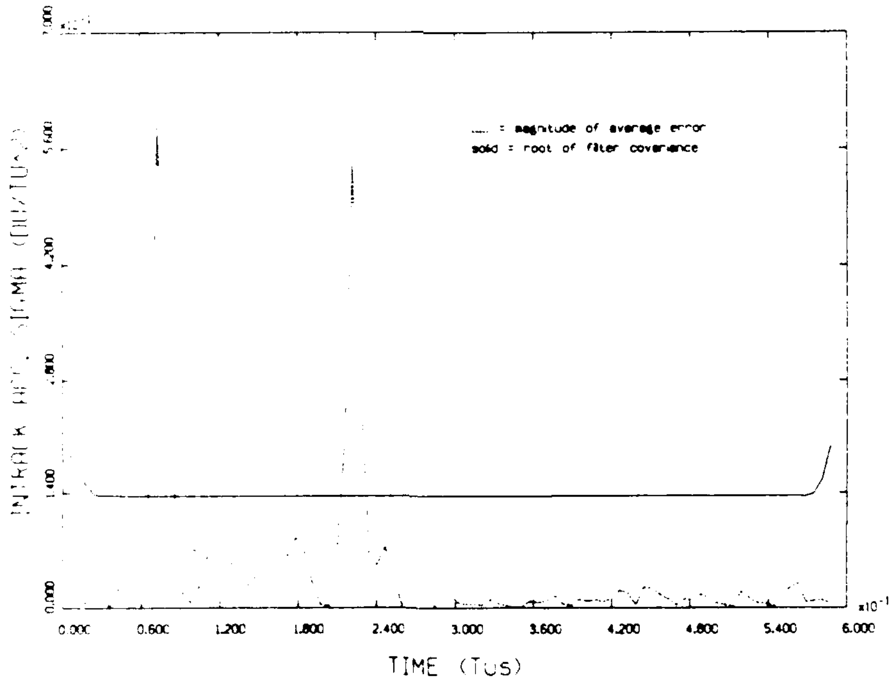

Figure 7.3. a_I Covariance and Error, 1 G, 1 Second Data Interval, Smoother

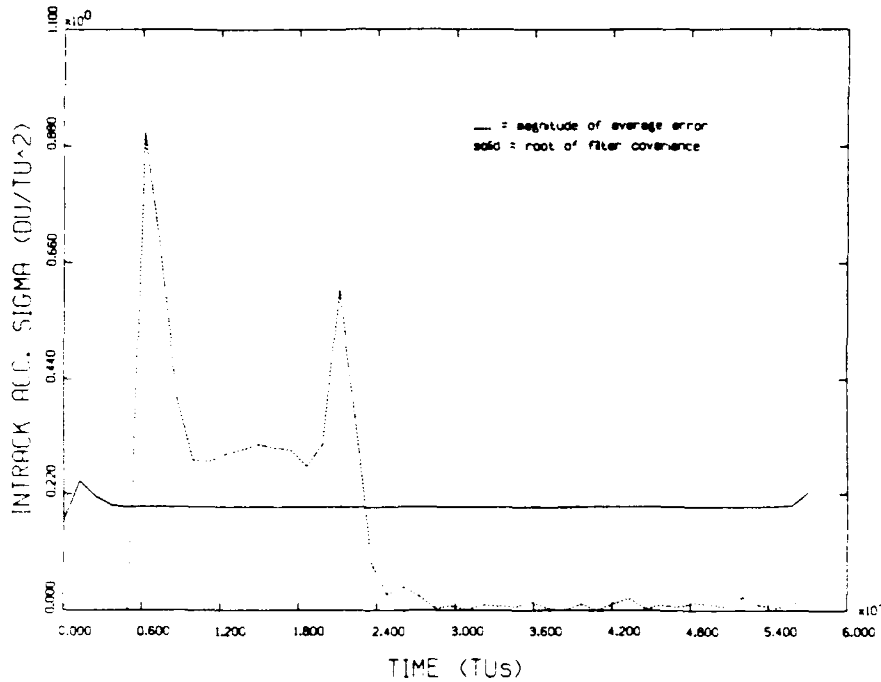

Figure 7.4. a_I Covariance and Error, 10 Second Data Interval, Smoother

Theoretically, smoother estimates should be no worse than the forward filter. Investigation indicated that the biases in the acceleration states may have been due to forward and backward filter oscillations in response to step changes in acceleration. All of the states suffered from the numerical imprecision inherent in the standard Kalman filter. This imprecision may have been worsened by the multiple matrix inversions in Equation (7.12). Longitude and latitude covariance magnitudes were approximately 10^{-10} radians^2, but acceleration covariances were as large as 10^{-1} $(DU/TU^2)^2$. Such a matrix is poorly suited for numerical inversion routines and may have induced estimate errors.

VIII. Filter Comparisons

In order to compare the smoother, probability weighting adaptive filter, and the six state Kalman filter, Monte Carlo average error magnitudes for all three estimators were plotted on the same graphs. Smoother errors during accelerations were consistently the largest. This is well demonstrated by the longitude error plot, Figure (8.1), which shows smoother error of approximately 4×10^{-4} radians. This equates to roughly 2.5 kilometers, as compared to 76 meters for the six state filter's position errors.

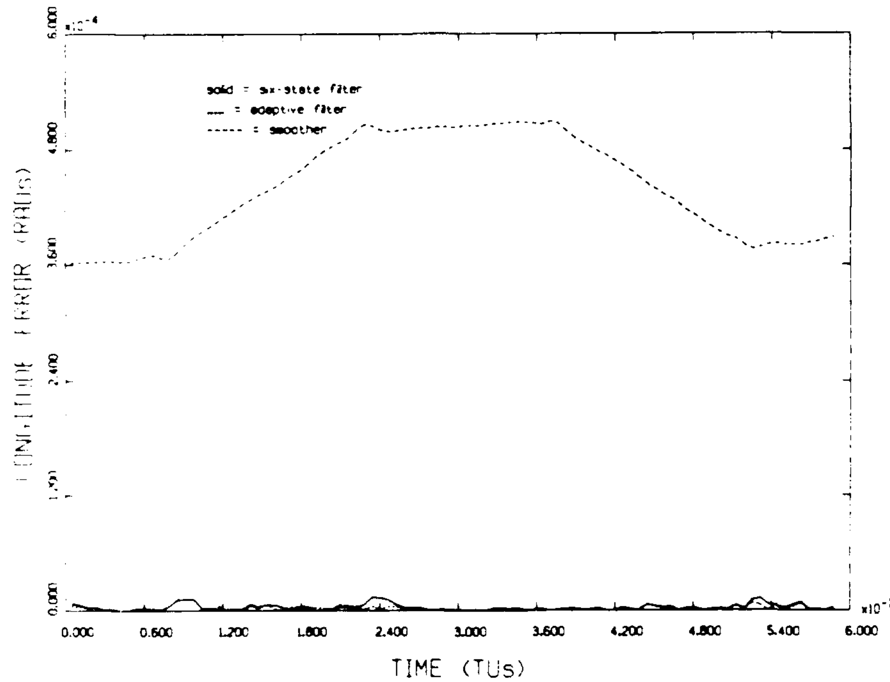

Figure 8.1. Longitude Error Comparison, 1 Second Interval

The adaptive filter showed slightly lower heading errors, Figures (8.2) and (8.3), but had performance similar to the six state filter for the remaining states.

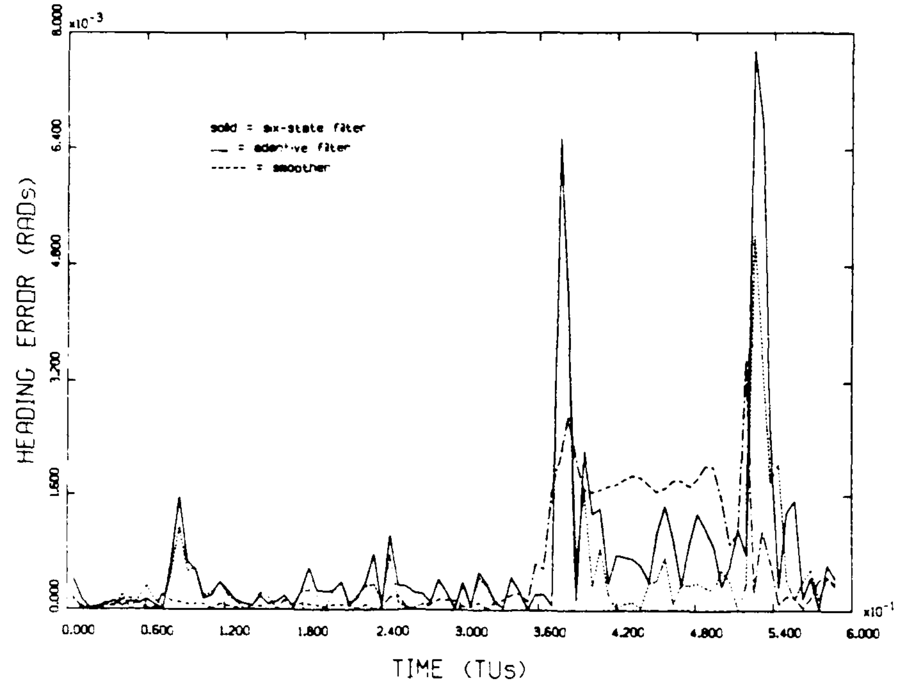

Figure 8.2. Heading Error Comparison, 1 Second Interval

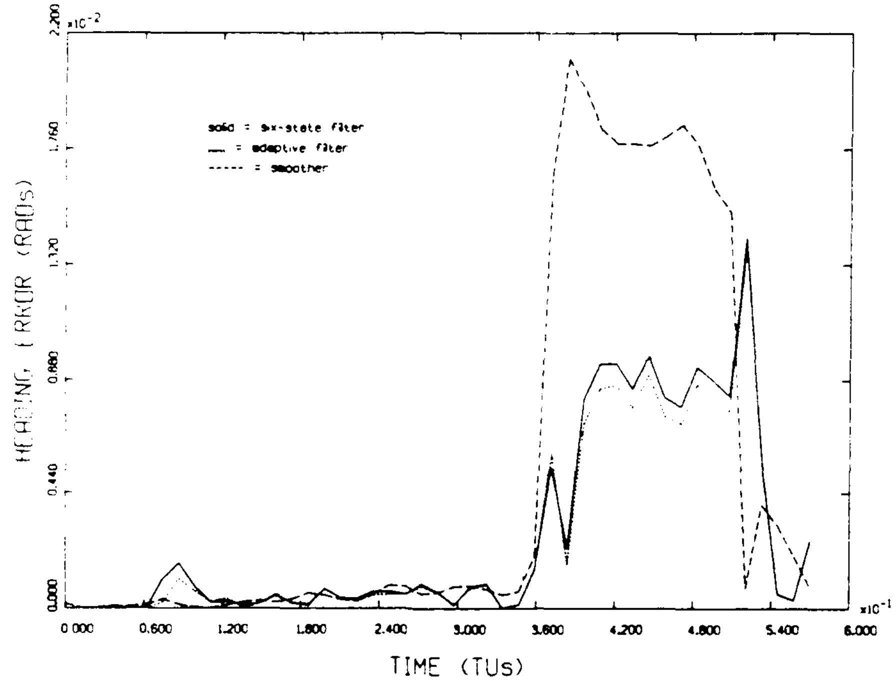

Figure 8.3. Heading Error Comparison, 10 Second Interval

The distinct spikes in Figure (8.4) demonstrate the smoother's superior ability to follow abrupt changes in acceleration, but the six state Kalman filter had the lowest errors overall. The attempts at adaptation and smoothing, then, were no improvement over the six state Kalman filter. Appendix D presents the remaining error comparison plots.

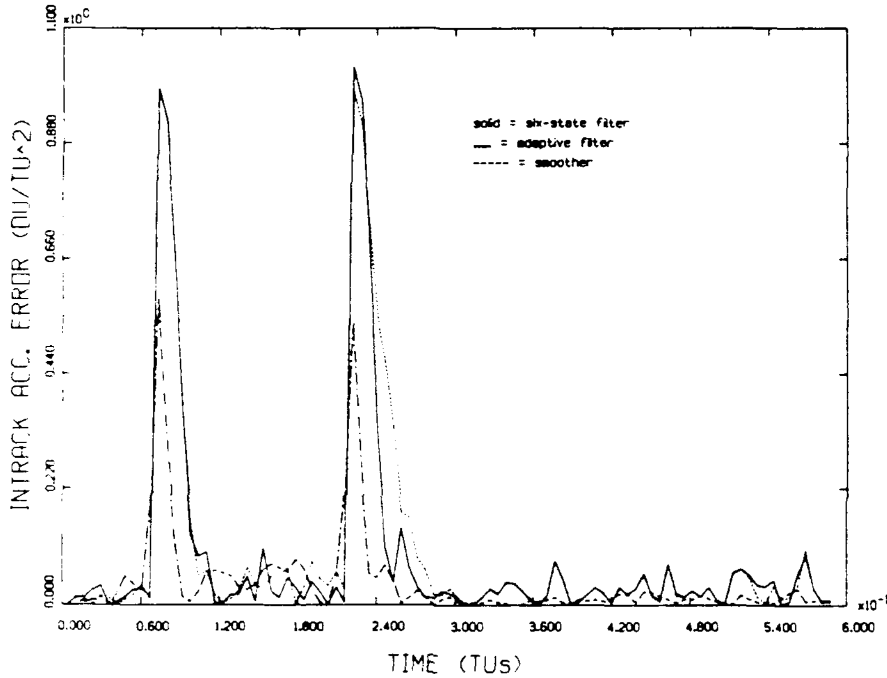

Figure 8.4. Intrack Acceleration Error Comparison,

1 Second Data Interval

IX. Recommendations

Attempts at adaptation and smoothing were no improvement over the six state Kalman filter. Numerical imprecision problems could be lessened by rescaling the problem such that the covariance values for all states had similar magnitudes. This would allow more accurate covariance matrix inversion and possibly improved smoother performance. Numerical precision for all of the estimators could be improved by using a factored form of the Kalman filter. In a factored form, the Cholesky square root of the covariance matrix is propagated, preventing the loss of significant digits when the covariance magnitude is much less than one.

The probability weighting adaptive filter could be improved by using the exponential of the unweighted square of the residuals in the probability density in Equation (6.12). This further enhances quick recognition of changes in the appropriateness of the sub-filter system models. (1:b)

Further effort to validate the six state Kalman filter could focus on applying the filter to data generated from actual, high-speed aircraft flights. This would expose any inadequacies in the truth model. This actual data could be corrupted by mathematical representations of atmospheric effects.

Singularities exist in the dynamics equations near the poles where many military flights are likely to orbit. A second Kalman filter could be derived using a coordinate system 90° away from the longitude/latitude system. This filter could be used when the TAV flies near the poles, or it could be combined in a multiple model adaptive filter much the same as the four and six state filters were combined in Chapter VI.

Finally, although the adaptive filters presented in this thesis gave no appreciable improvement, a bank of six state filters (tuned to best estimate various accelerations) could still be tried as a multiple model adaptive filter. (6:8-2) By already having a sub-filter tuned for various accelerations, multiple model adaptive filters generally have faster response to changes in acceleration.

Appendix A: 1 G Covariance and Error Plots

This appendix provides covariance plots for the six state Kalman filter, the probability weighting adaptive filter, and the smoother. Tables representing initial conditions are presented before each grouping of plots.

Table A.1. Flight Profile, 1 G Accelerations

Time (sec)	Time (TU)	Maneuver
0 - 60	0 - .074	Constant Speed
61 - 180	.075 - .223	1 G Intrack Acceleration
181 - 300	.224 - .372	Constant Speed
301 - 420	.373 - .521	1 G Transverse Accel.
421 - 480	.522 - .595	Constant Speed

Table A.2. Central Trajectory Initial Conditions

State	Covariance
λ = 0.0 rads	$P_{\lambda\lambda}$ = 1.25e-5 rads^2
δ = 0.0 rads	$P_{\delta\delta}$ = 1.25e-5 rads^2
h = 0.7854 rads	P_{hh} = 3.e-3 rads^2
V = 0.5 DU/TU	P_{VV} = 3.e-2 (DU/TU)^2
a_I = 0.0 DU/TU^2	P_{II} = 3.5e-2 (DU/TU^2)^2
a_T = 0.0 DU/TU^2	P_{TT} = 2.5 (DU/TU^2)^2

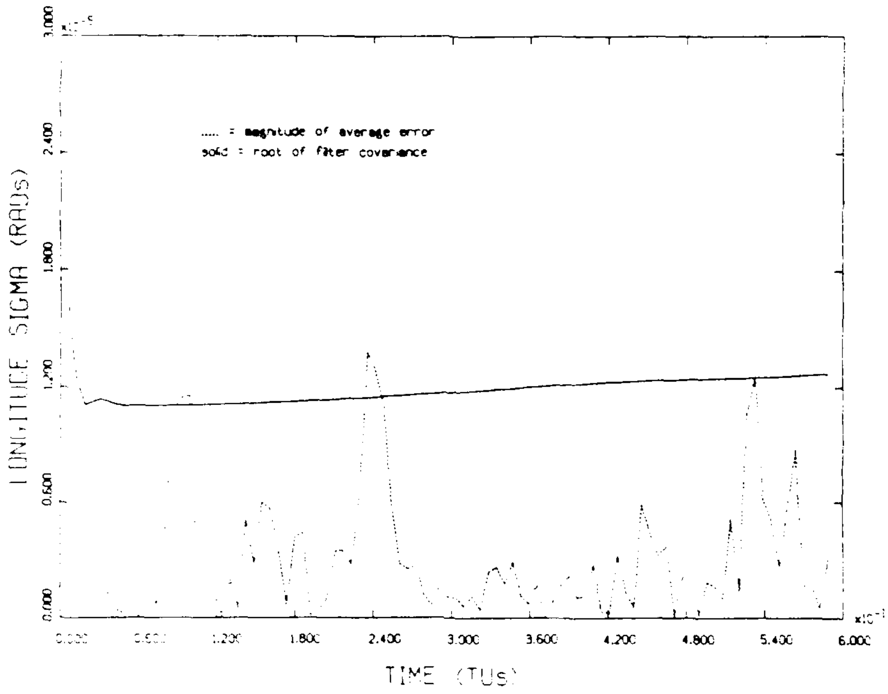

Figure A.1. Longitude Covariance and Error, 1 G, 1 Second Data Interval, Six State Filter

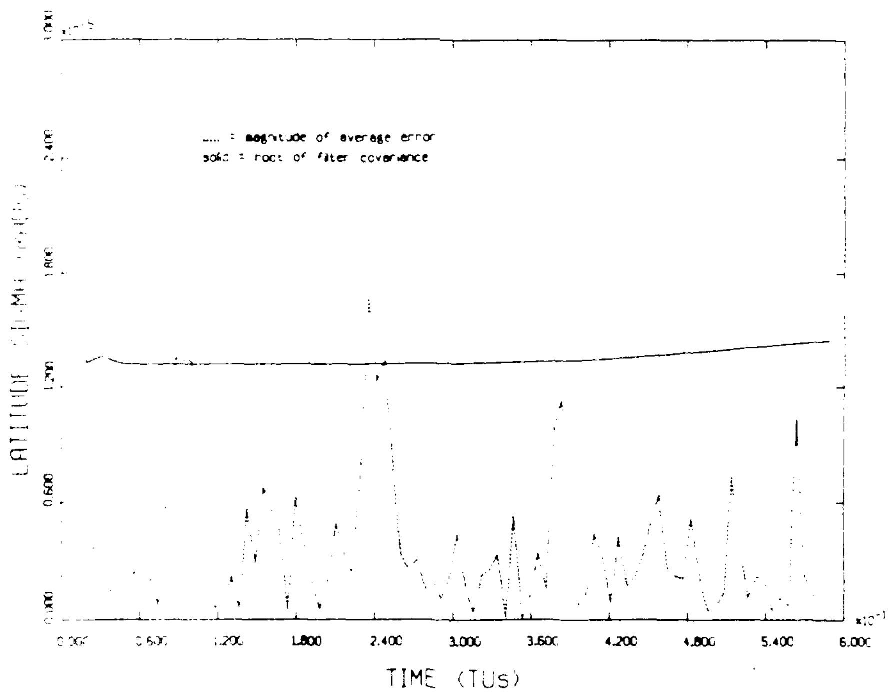

Figure A.2. Latitude Covariance and Error, 1 G, 1 Second Data Interval, Six State Filter

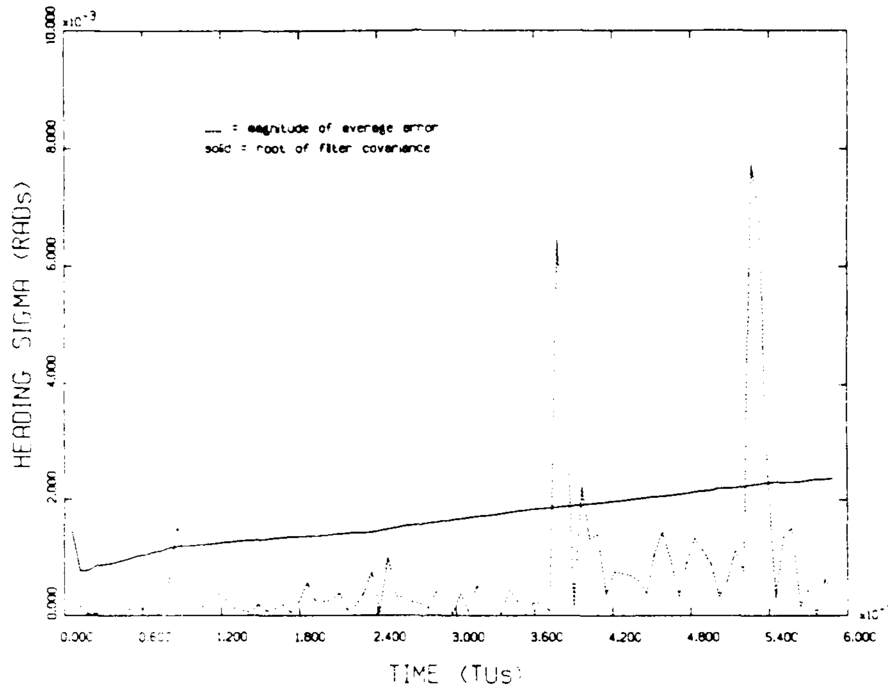

Figure A.3. Heading Covariance and Error, 1 G, 1 Second Data Interval, Six State Filter

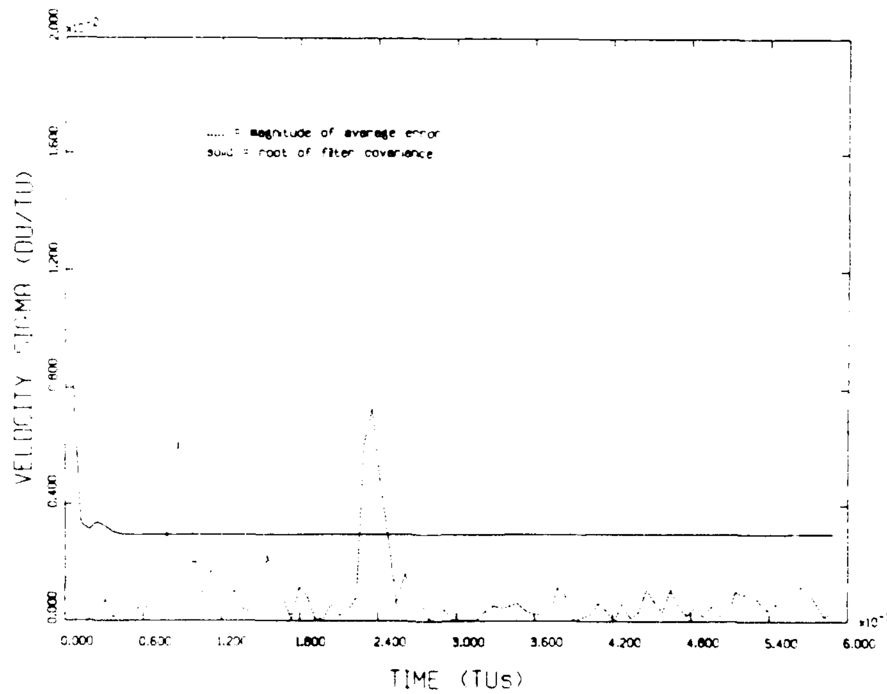

Figure A.4. Velocity Covariance and Error, 1 G, 1 Second Data Interval, Six State Filter

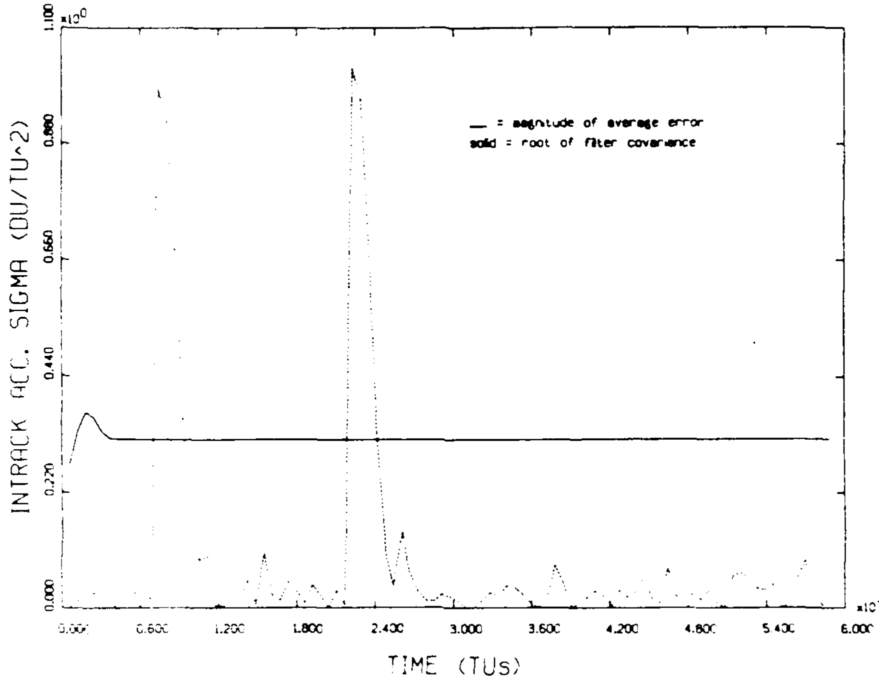

Figure A.5. a_I Covariance and Error, 1 G, 1 Second Data Interval, Six State Filter

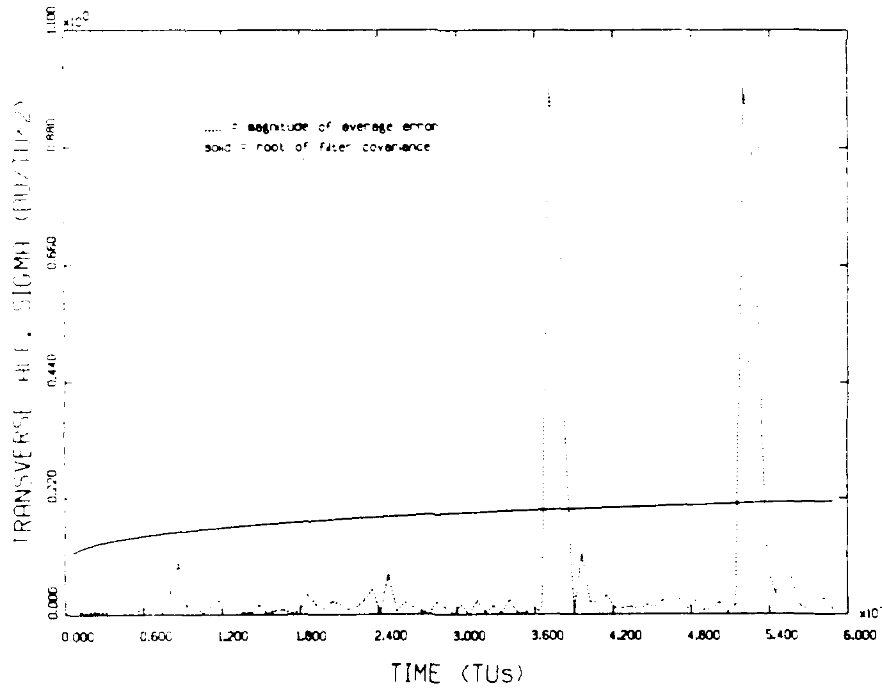

Figure A.6. a_T Covariance and Error, 1 G, 1 Second Data Interval, Six State Filter

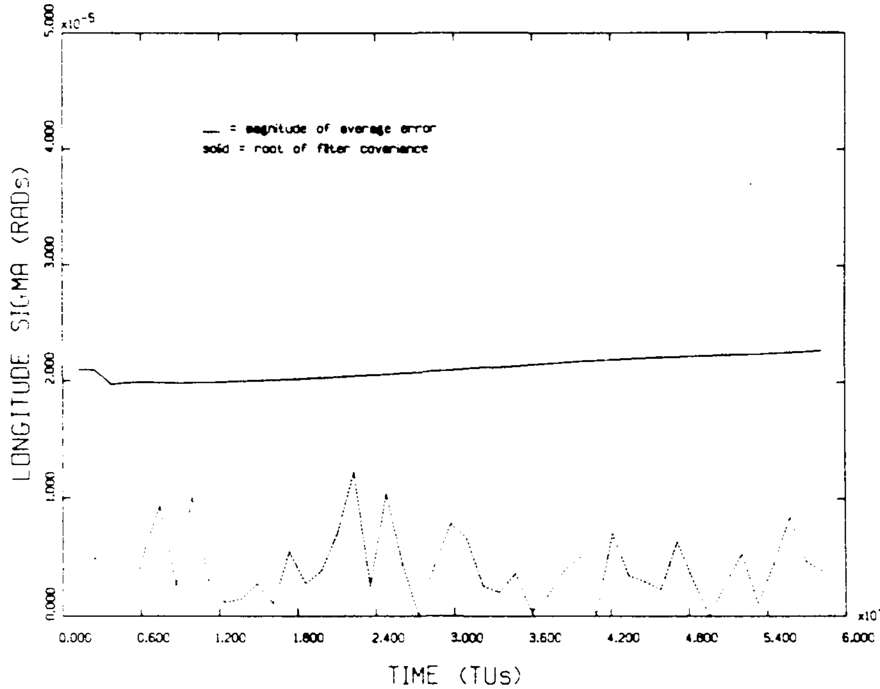

Figure A.7. Longitude Covariance and Error, 1 G, 10 Second Data Interval, Six State Filter

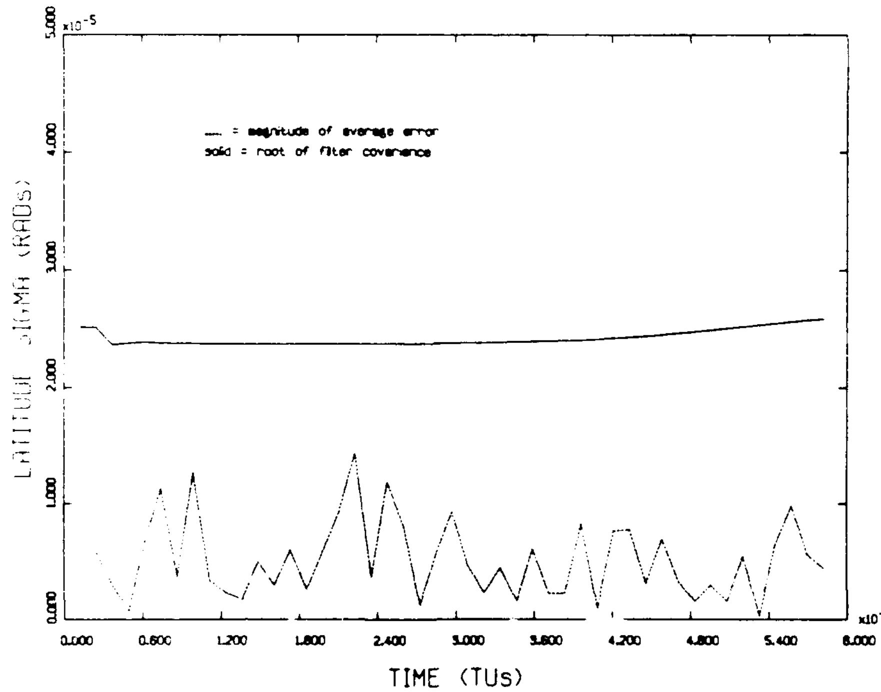

Figure A.8. Latitude Covariance and Error, 1 G, 10 Second Data Interval, Six State Filter

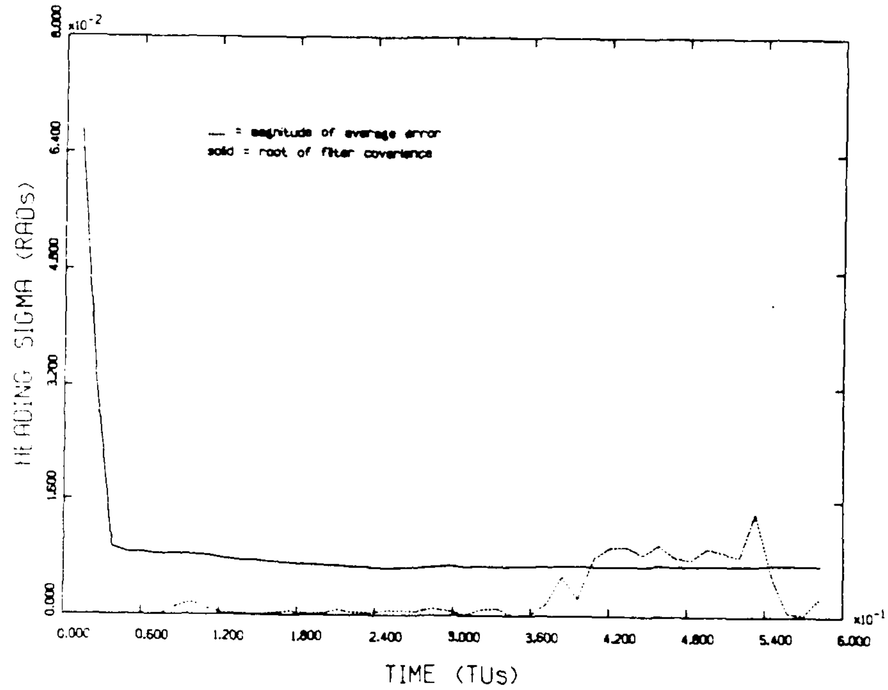

Figure A.9. Heading Covariance and Error, 1 G, 10 Second Data Interval, Six State Filter

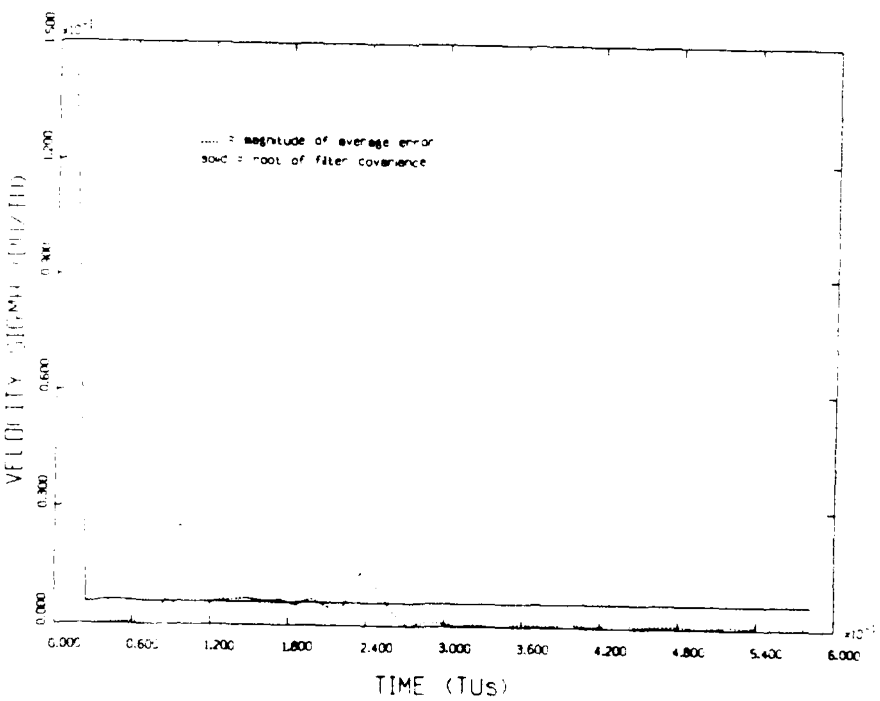

Figure A.10. Velocity Covariance and Error, 1 G, 10 Second Data Interval, Six State Filter

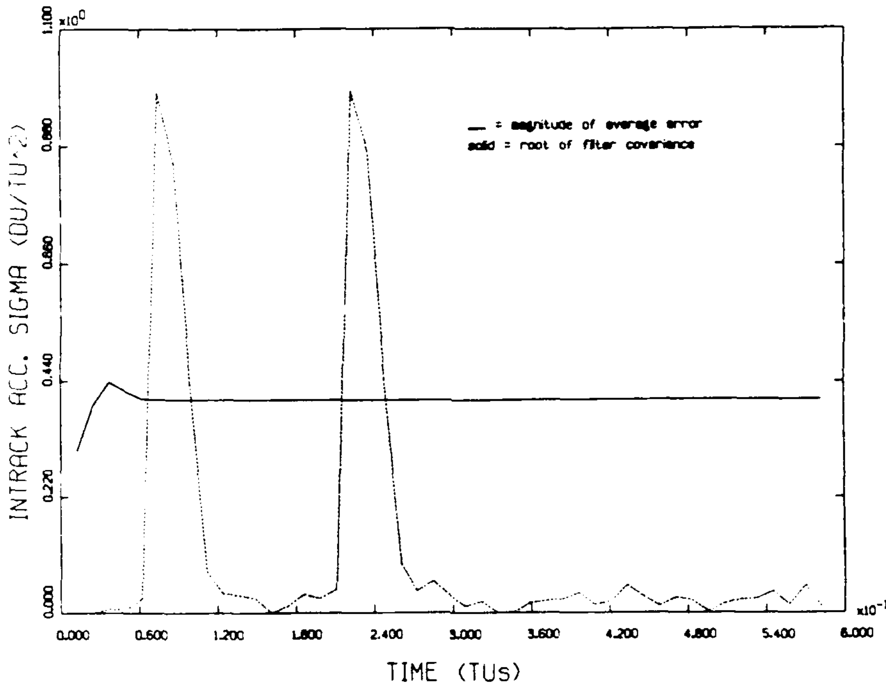

Figure A.11. a_I **Covariance and Error, 1 G,**

10 Second Data Interval, Six State Filter

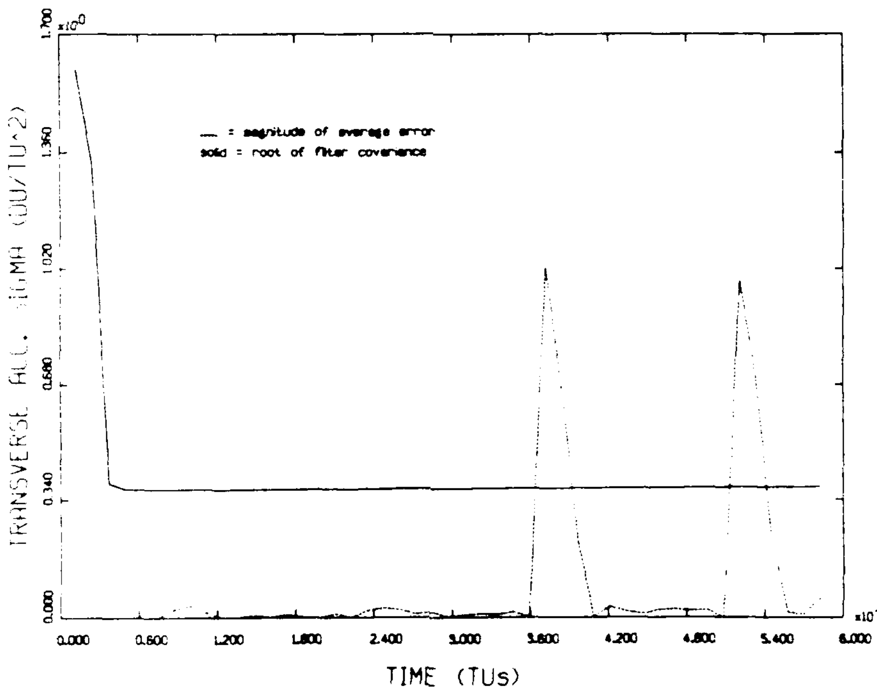

Figure A.12. a_T **Covariance and Error, 1 G,**

10 Second Data Interval, Six State Filter

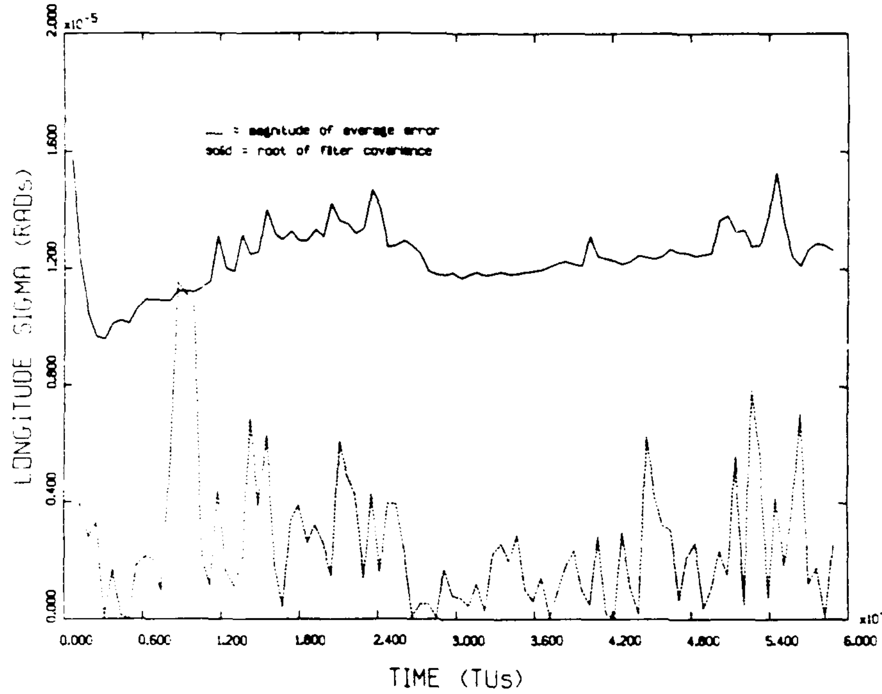

Figure A.13. Longitude Covariance and Error, 1 G, 1 Second Data Interval, Probability Weighting Adaptation

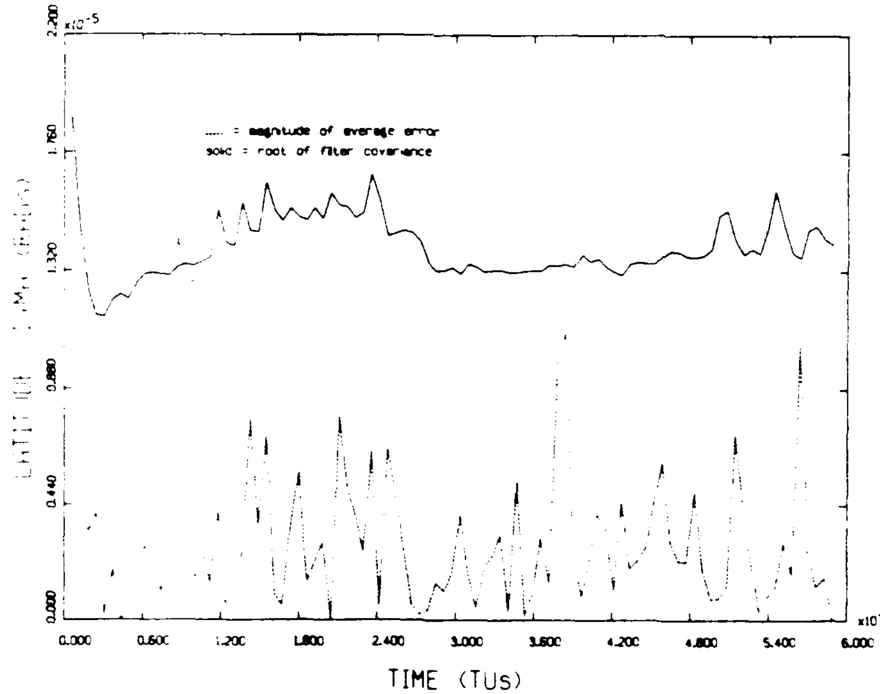

Figure A.14. Latitude Covariance and Error, 1 G, 1 Second Data Interval, Probability Weighting Adaptation

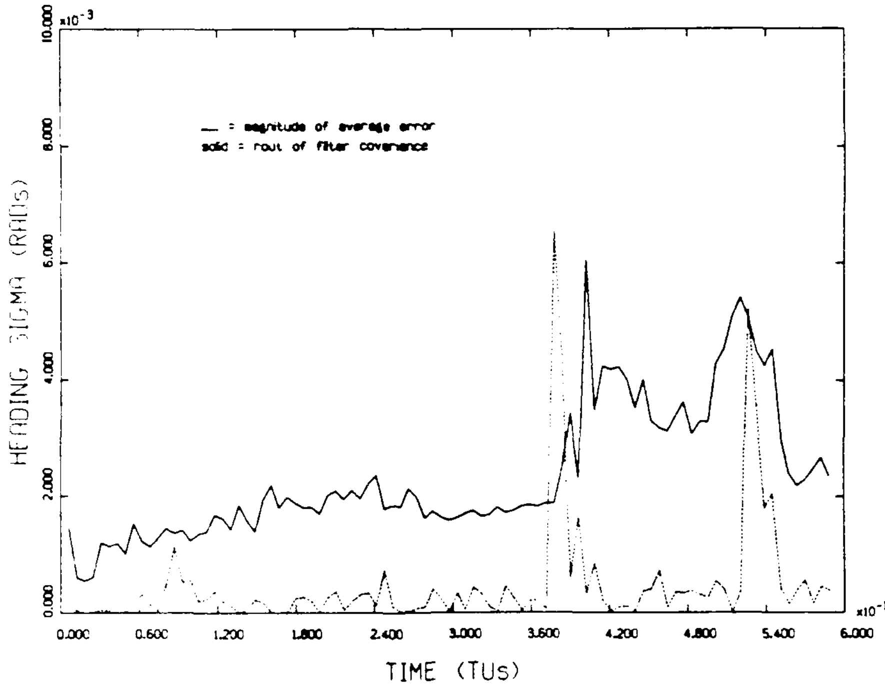

Figure A.15. Heading Covariance and Error, 1 G, 1 Second Data Interval, Probability Weighting Adaptation

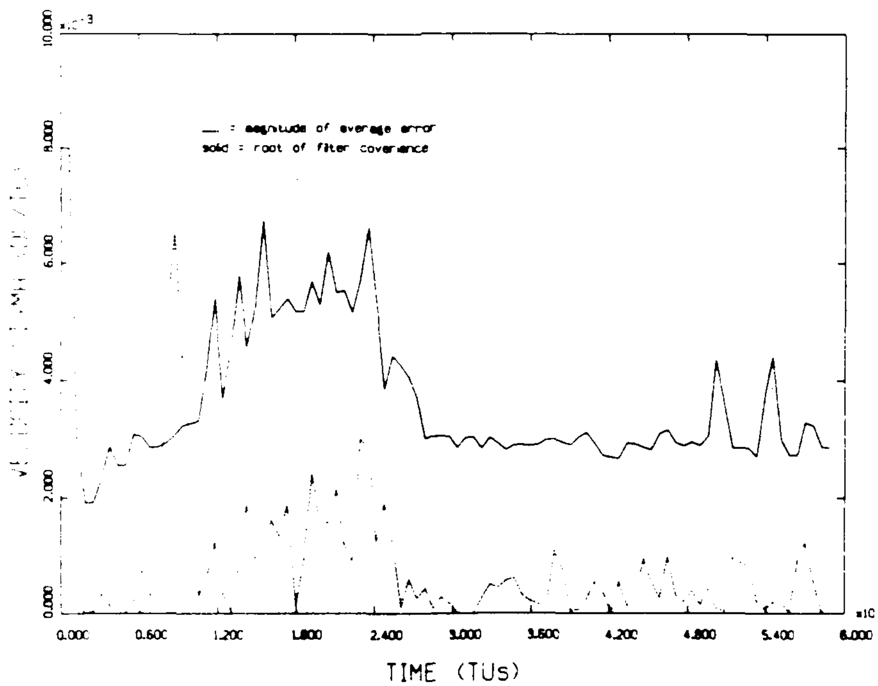

Figure A.16. Velocity Covariance and Error, 1 G, 1 Second Data Interval, Probability Weighting Adaptation

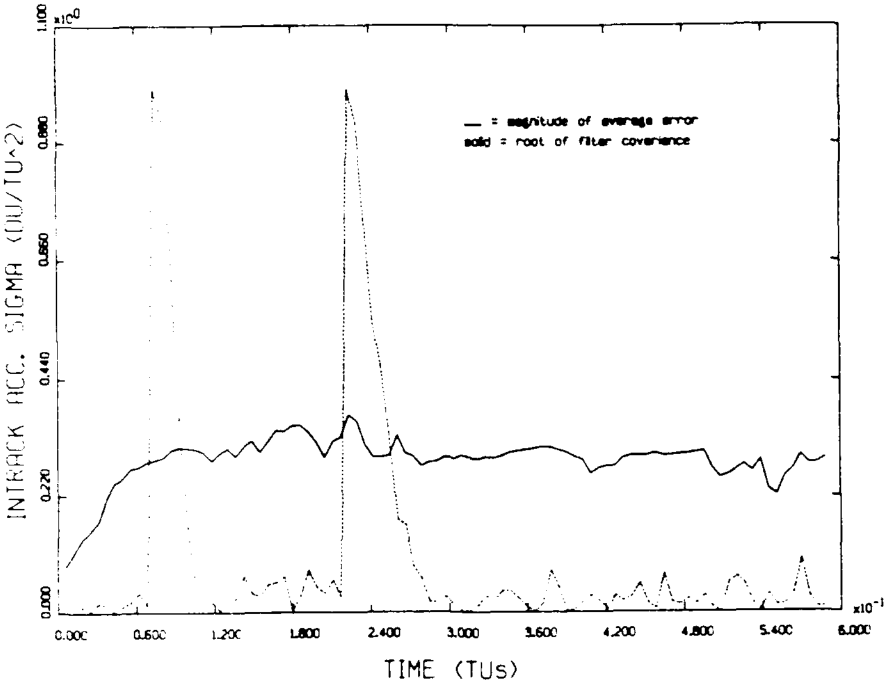

Figure A.17. a_I Covariance and Error, 1 G, 1 Second Data Interval, Probability Weighting Adaptation

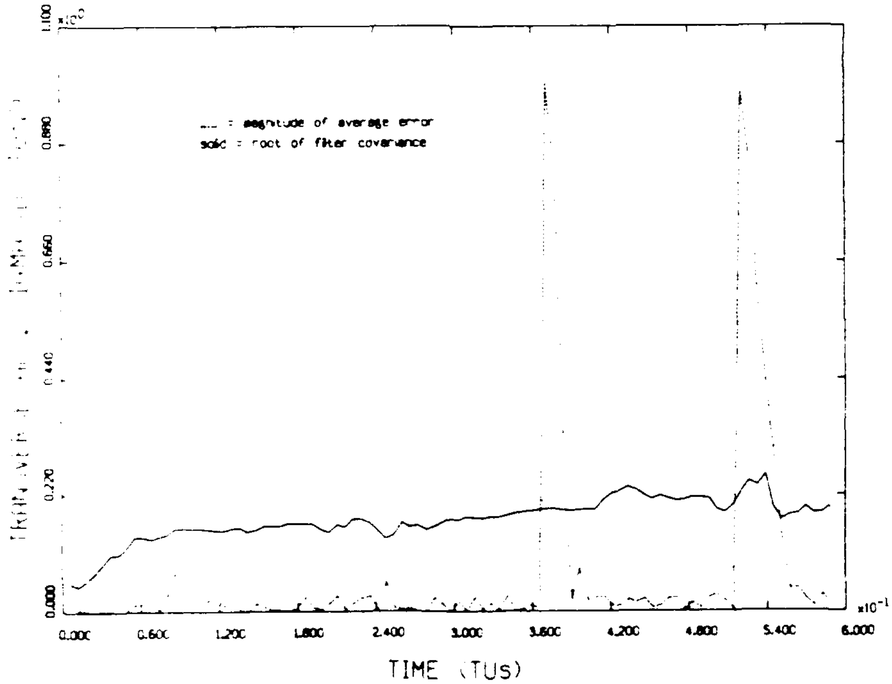

Figure A.18. a_T Covariance and Error, 1 G, 1 Second Data Interval, Probability Weighting Adaptation

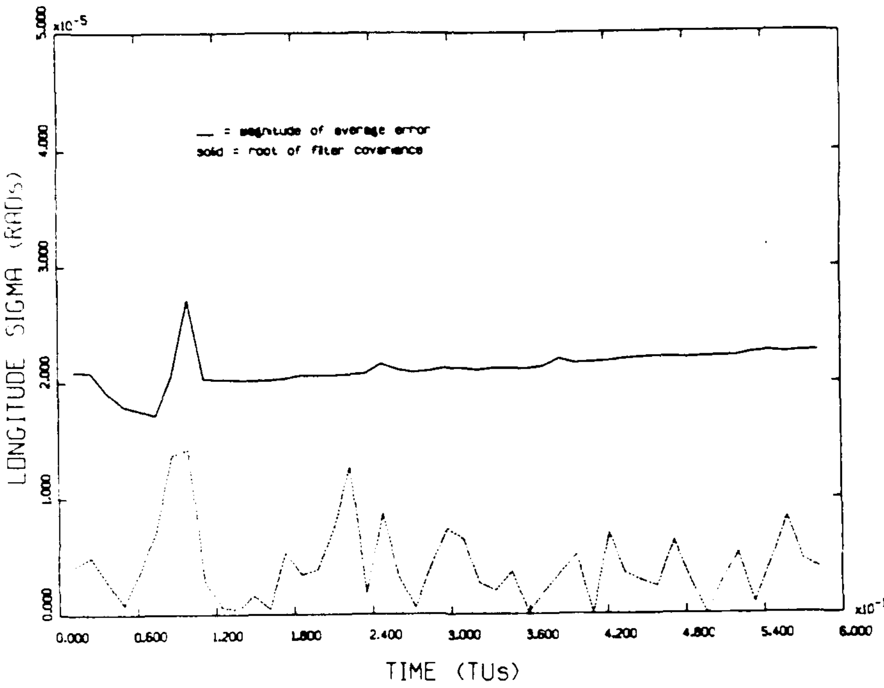

Figure A.19. Longitude Covariance and Error, 1 G, 10 Second Data Interval, Probability Weighting Adaptation

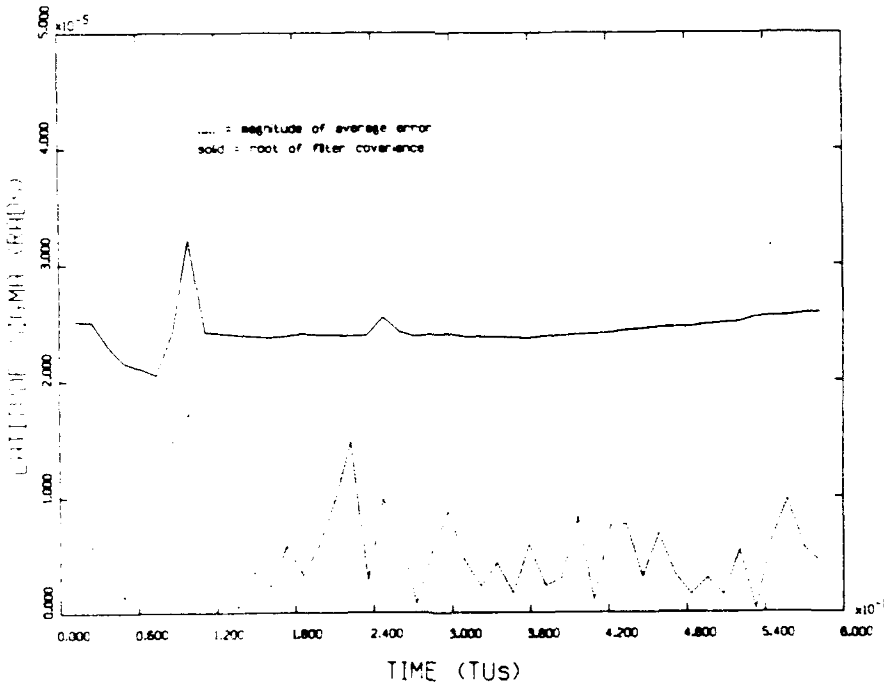

Figure A.20. Latitude Covariance and Error, 1 G, 10 Second Data Interval, Probability Weighting Adaptation

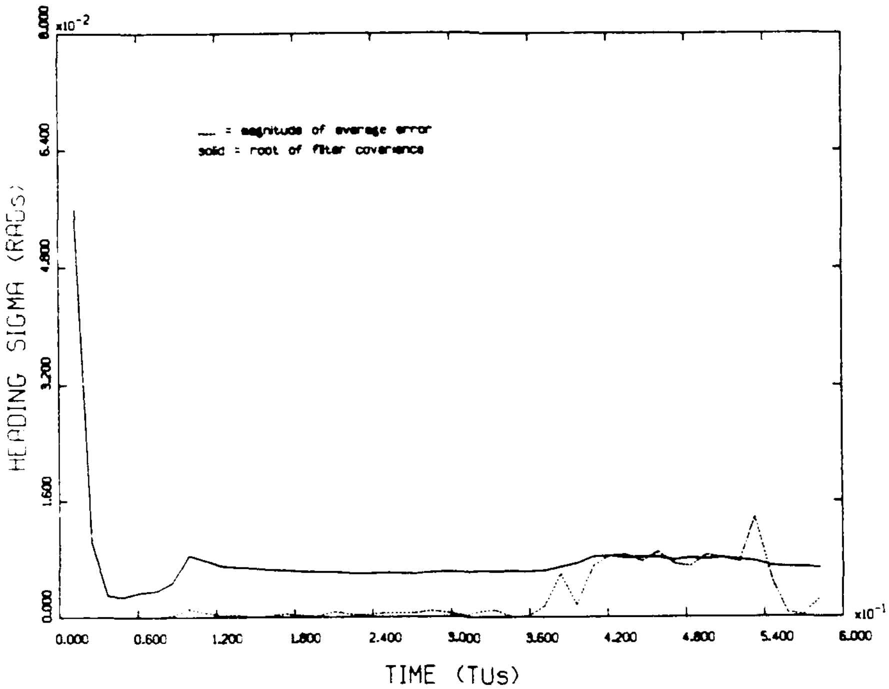

Figure A.21. Heading Covariance and Error, 1 G, 10 Second Data Interval, Probability Weighting Adaptation

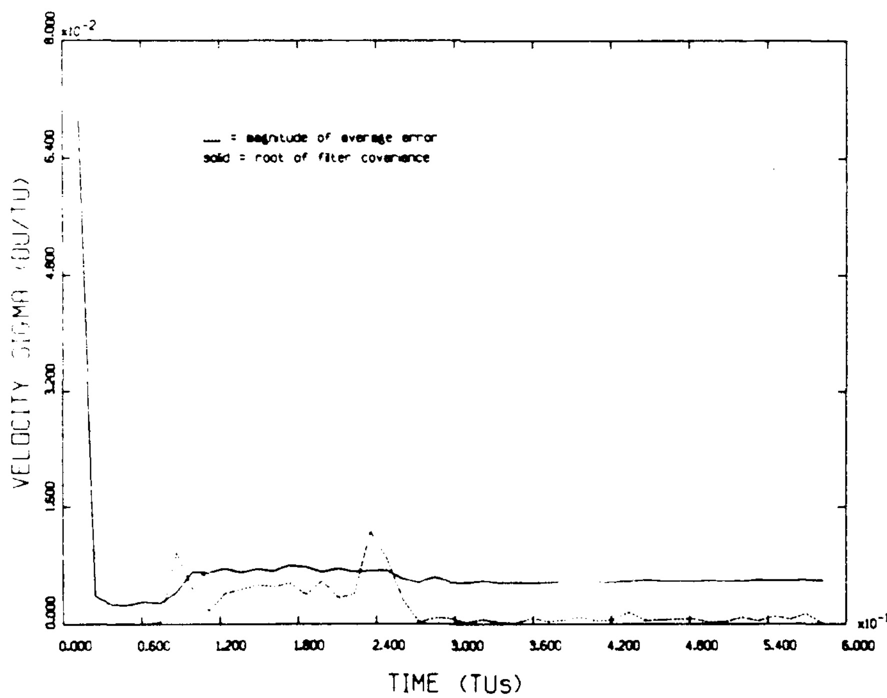

Figure A.22. Velocity Covariance and Error, 1 G, 10 Second Data Interval, Probability Weighting Adaptation

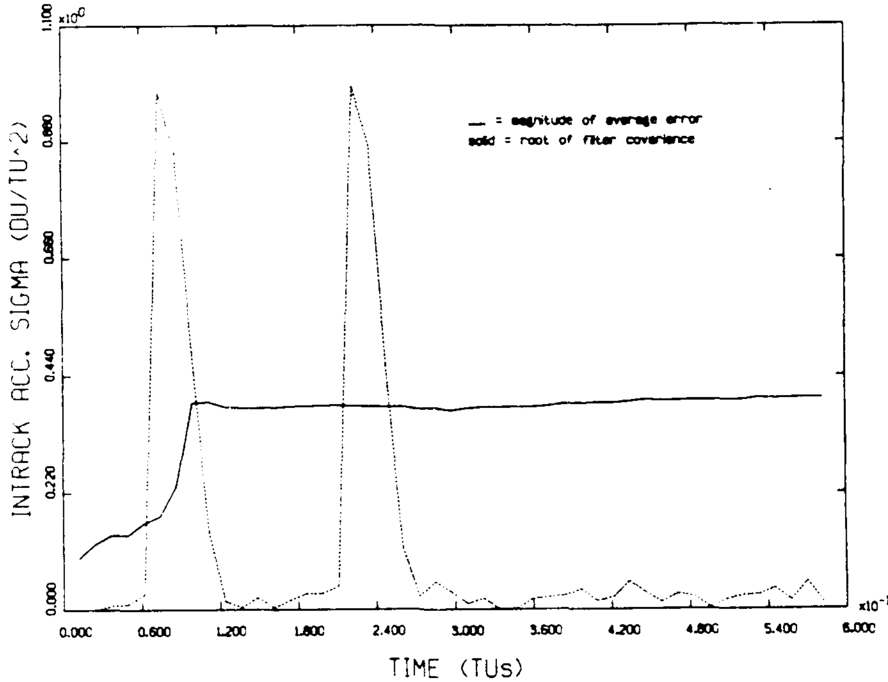

Figure A.23. a_I **Covariance and Error, 1 G, 10 Second Data Interval, Probability Weighting Adaptation**

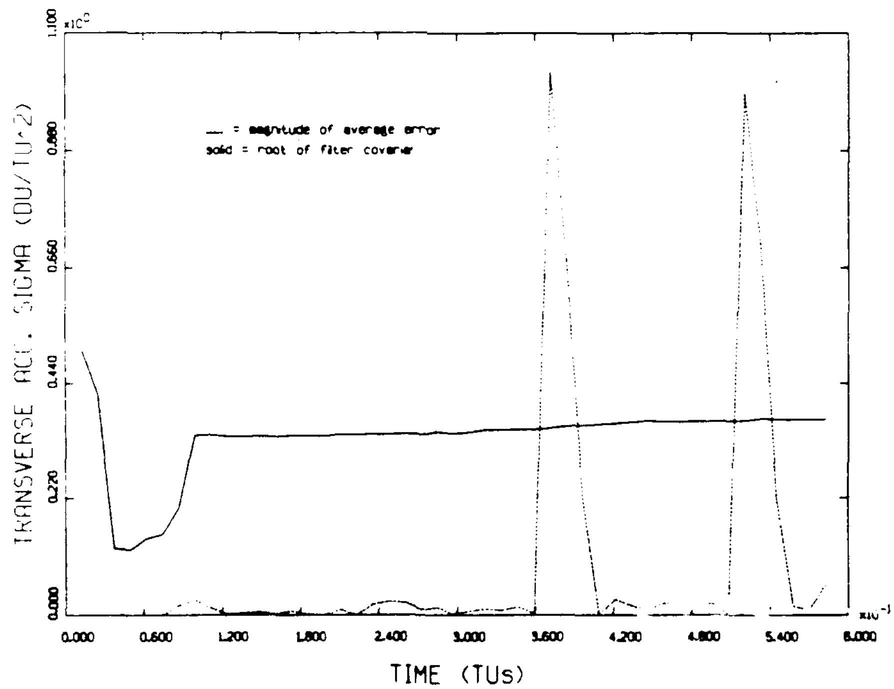

Figure A.24. a_T **Covariance and Error, 1 G, 10 Second Data Interval, Probability Weighting Adaptation**

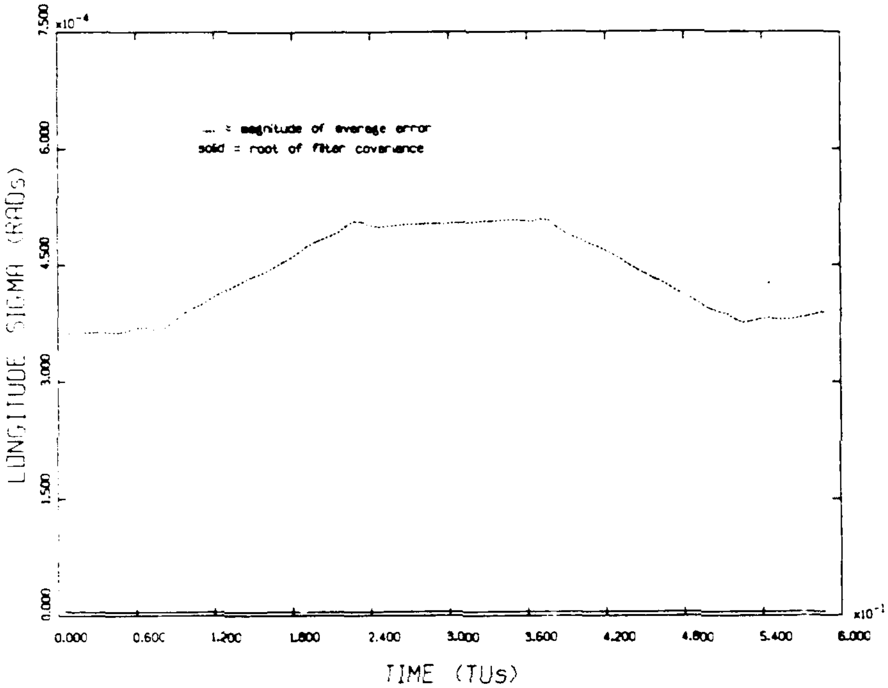

Figure A.25. Longitude Covariance and Error, 1 G, 1 Second Data Interval, Smoother

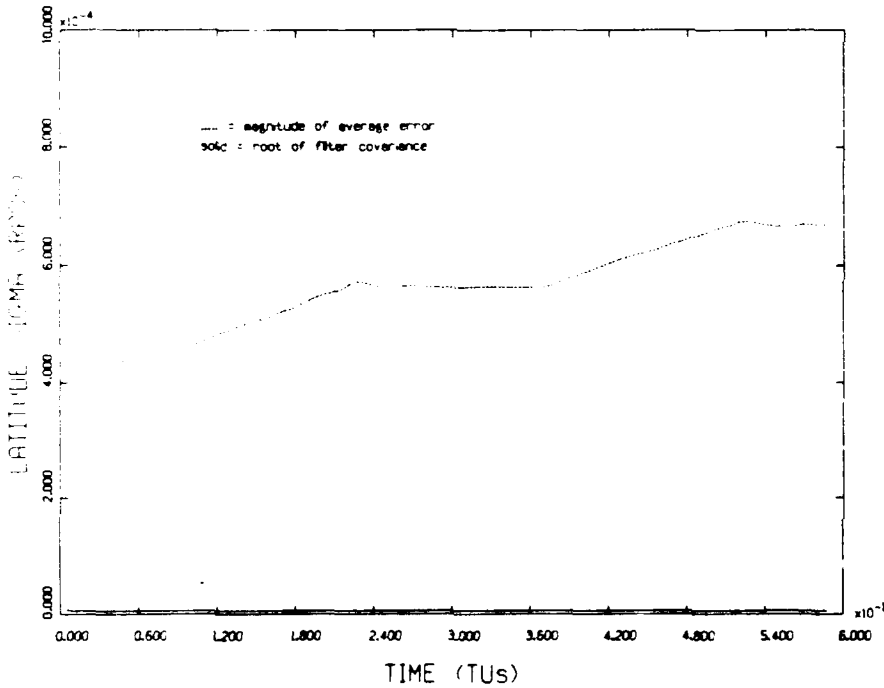

Figure A.26. Latitude Covariance and Error, 1 G, 1 Second Data Interval, Smoother

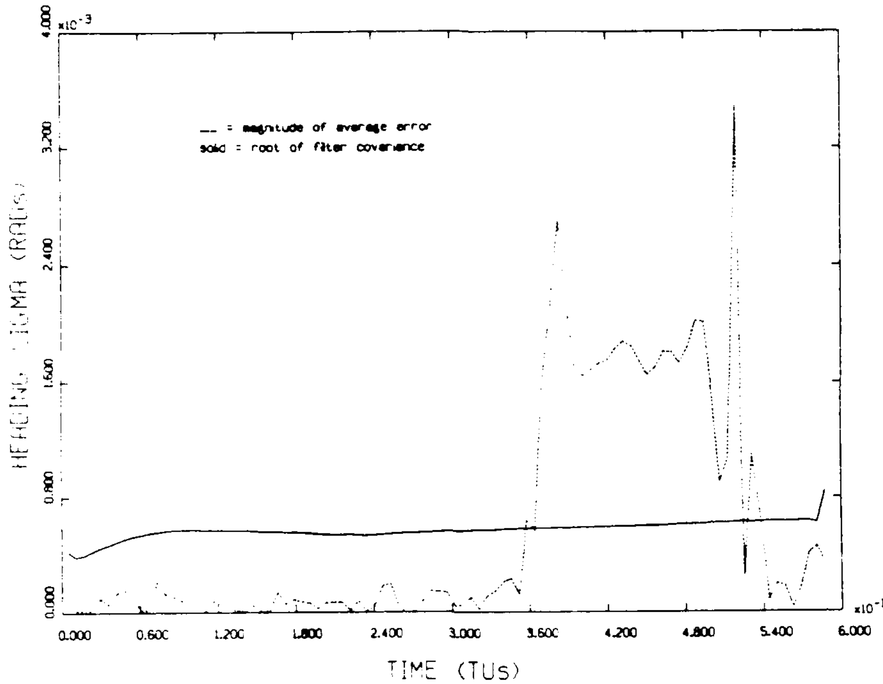

Figure A.27. Heading Covariance and Error, 1 G, 1 Second Data Interval, Smoother

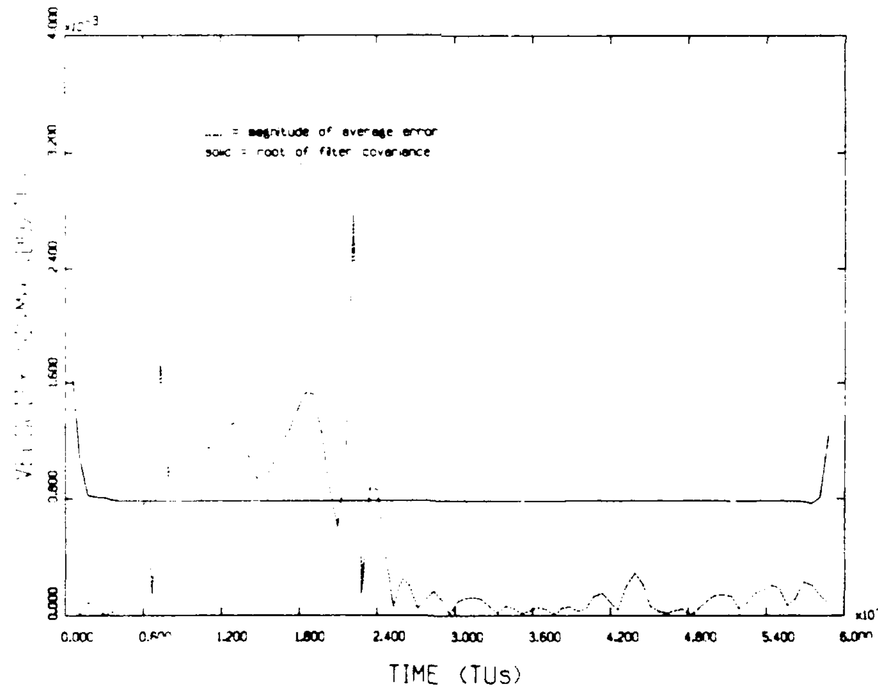

Figure A.28. Velocity Covariance and Error, 1 G, 1 Second Data Interval, Smoother

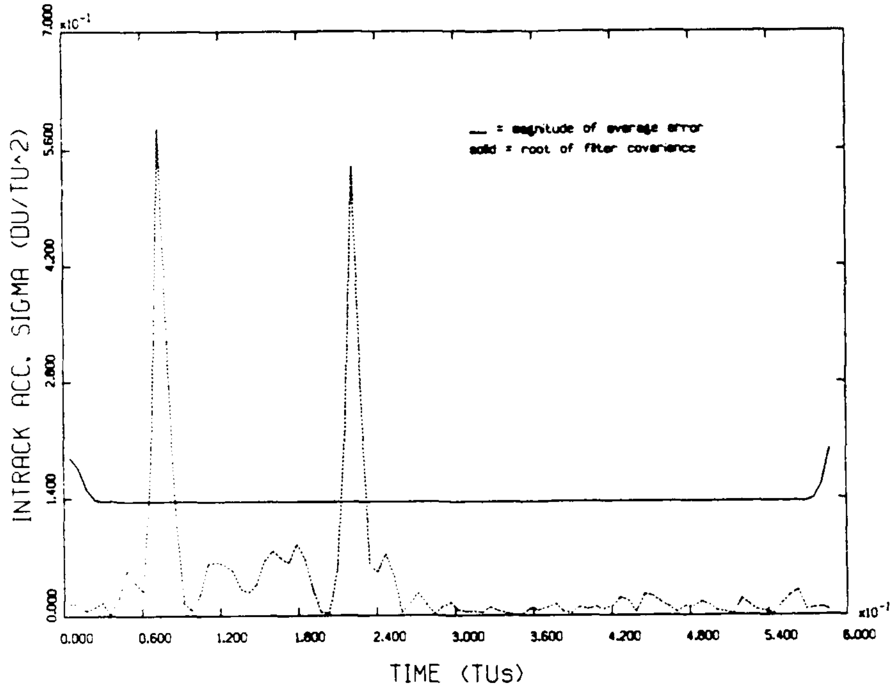

Figure A.29. a_I Covar:ance and Error, 1 G, 1 Second Data Interval, Smoother

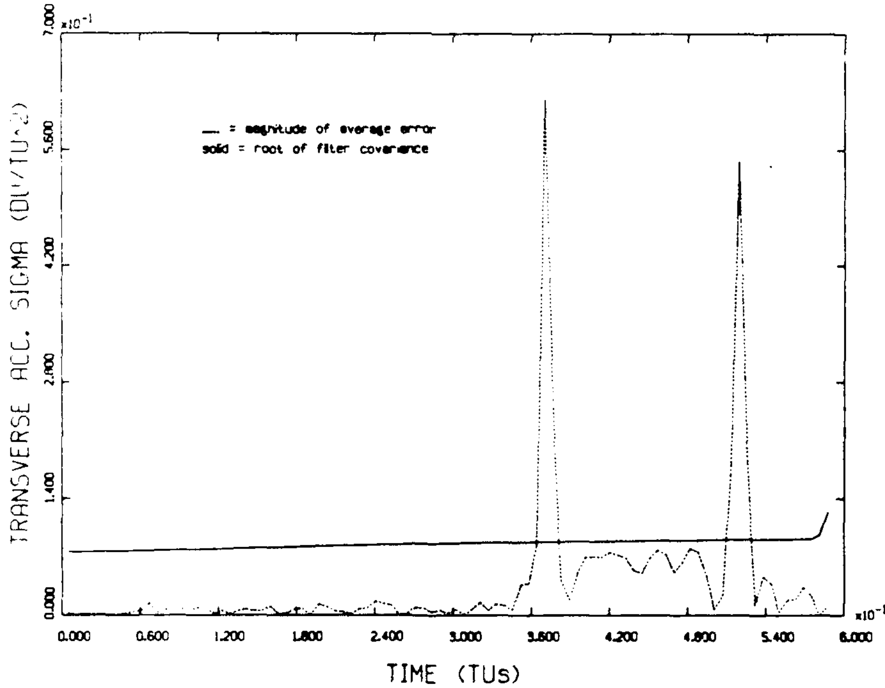

Figure A.30. a_T Covariance and Error, 1 G, 1 Second Data Interval, Smoother

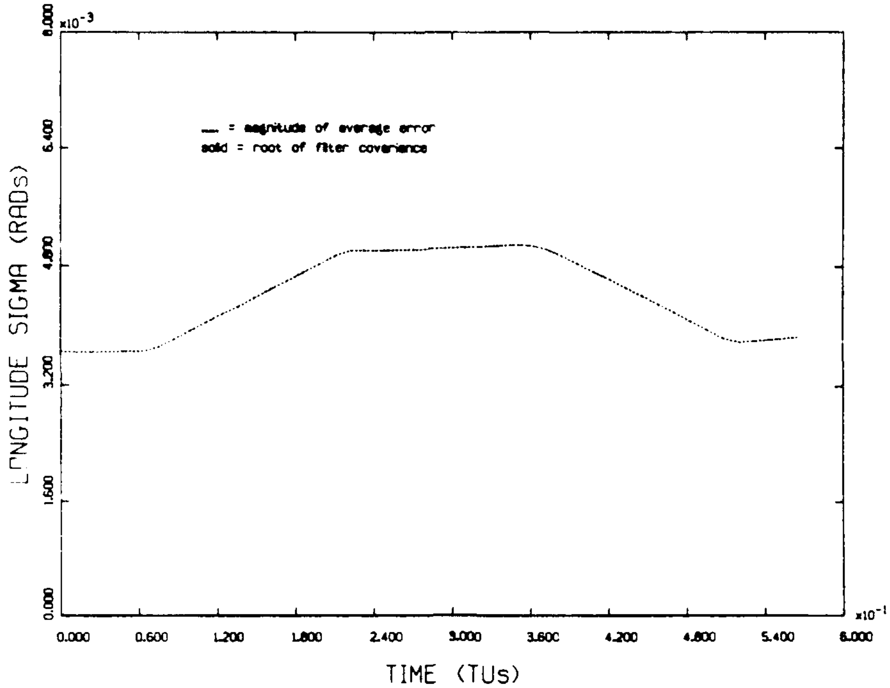

Figure A.31. Longitude Covariance and Error, 1 G, 10 Second Data Interval, Smoother

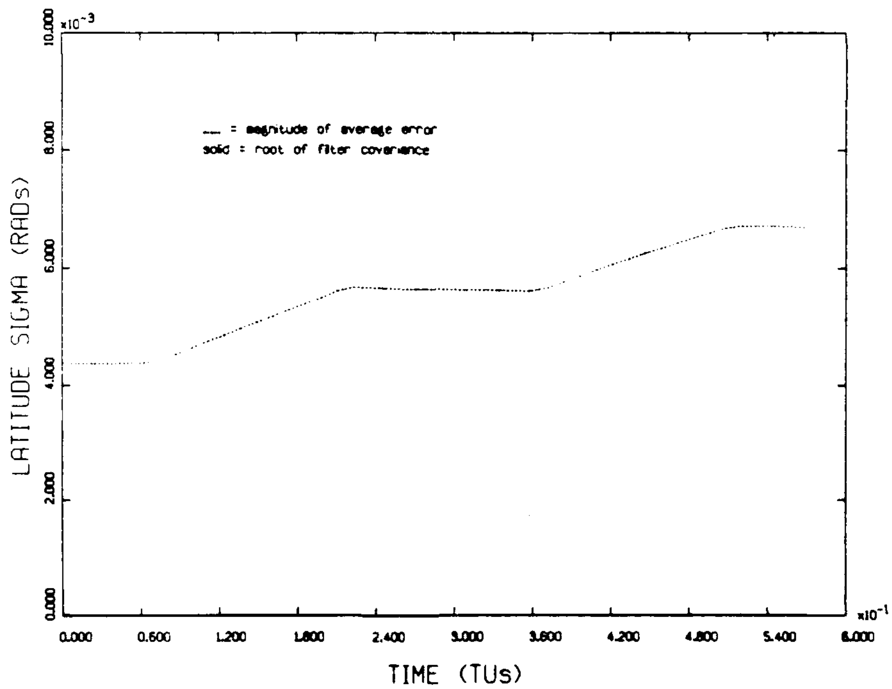

Figure A.32. Latitude Covariance and Error, 1 G, 10 Second Data Interval, Smoother

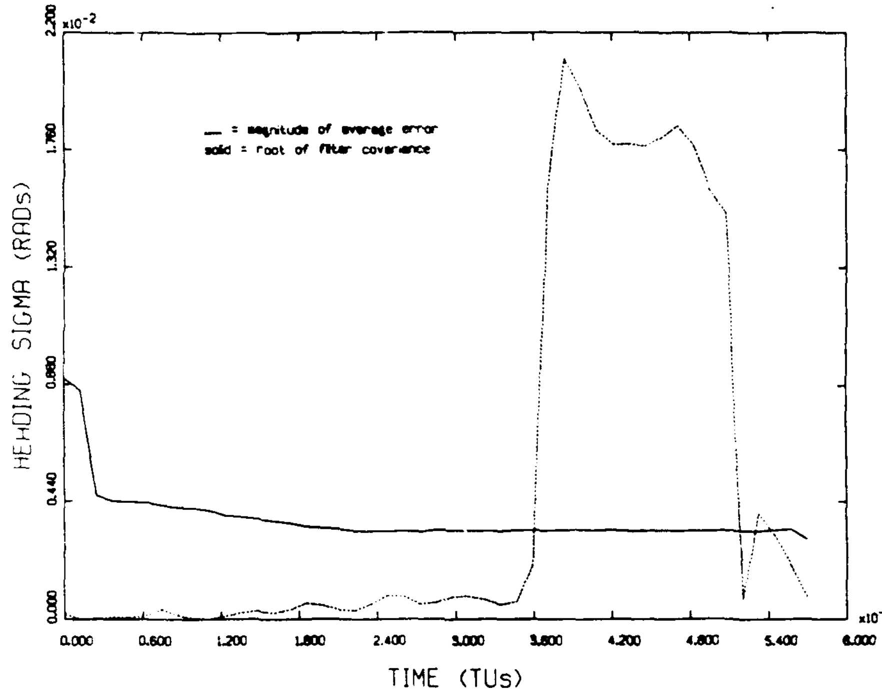

Figure A.33. Heading Covariance and Error, 1 G, 10 Second Data Interval, Smoother

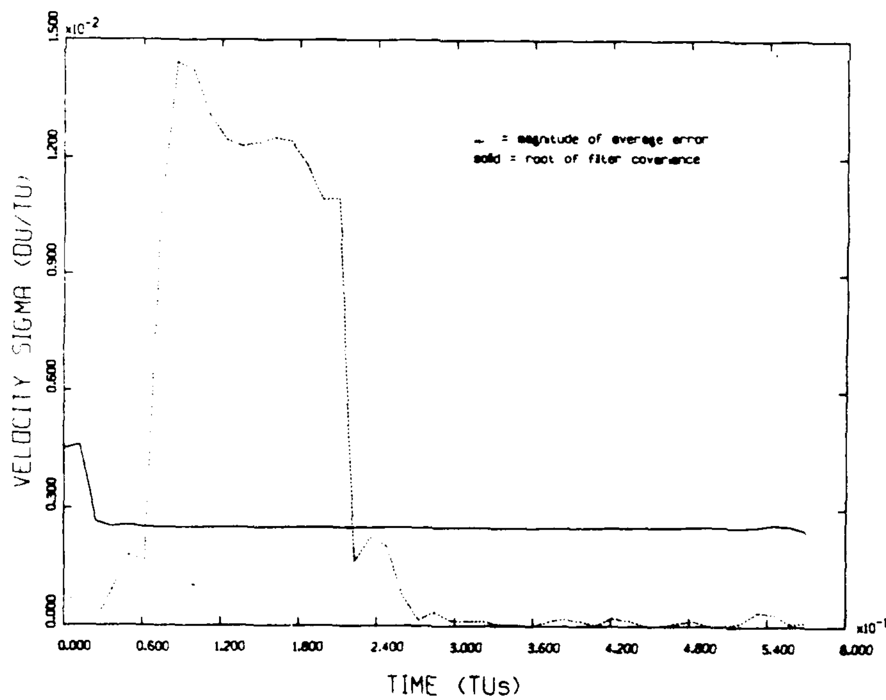

Figure A.34. Velocity Covariance and Error, 1 G, 10 Second Data Interval, Smoother

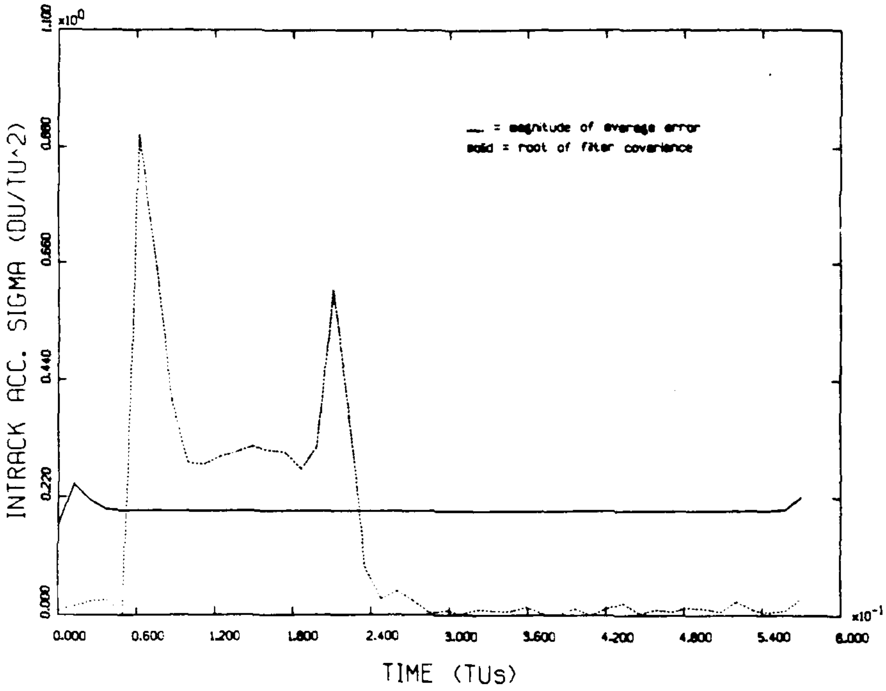

Figure A.35. a_I **Covariance and Error, 1 G, 10 Second Data Interval, Smoother**

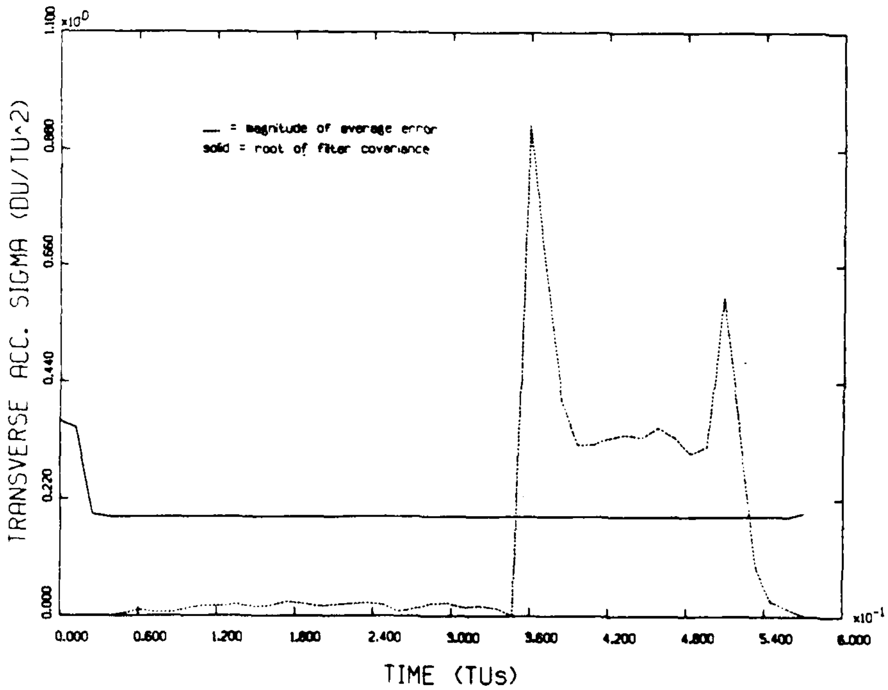

Figure A.36. a_T **Covariance and Error, 1 G, 10 Second Data Interval, Smoother**

Table A.3. North Trajectory Initial Conditions

State	Covariance
λ = 0.0 rads	$P_{\lambda\lambda}$ = 1.25e-5 rads^2
δ = 1.0472 rads	$P_{\delta\delta}$ = 1.25e-5 rads^2
h = 0.0 rads	P_{hh} = 3.e-3 rads^2
V = 0.5 DU/TU	P_{VV} = 3.e-2 (DU/TU)^2
a_I = 0.0 DU/TU^2	P_{II} = 3.5e-2 (DU/TU^2)^2
a_T = 0.0 DU/TU^2	P_{TT} = 2.5 (DU/TU^2)^2

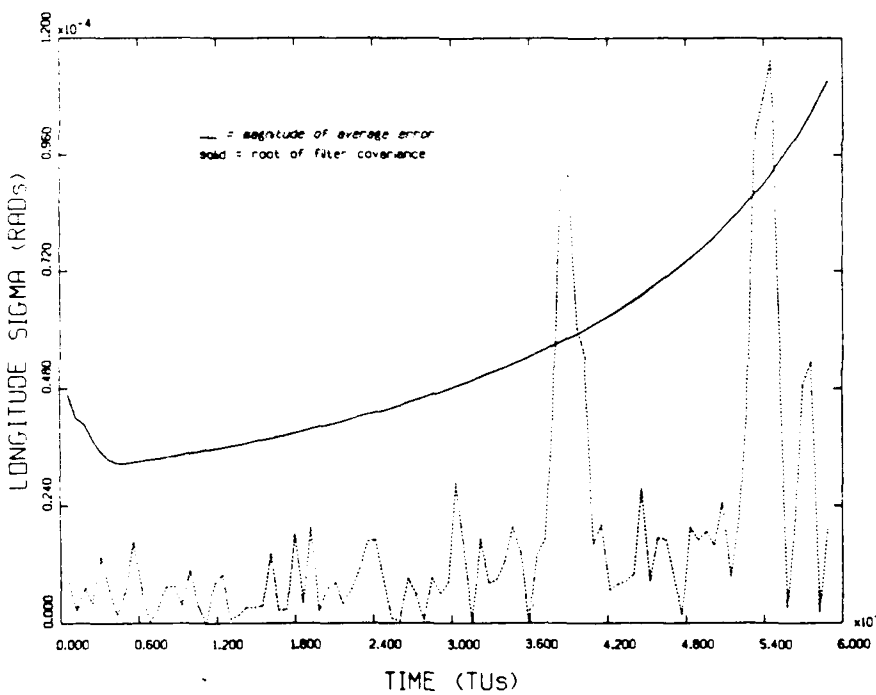

Figure A.37. Longitude Covariance and Error, 1 G, 1 Second Interval, North Trajectory, Six State Filter

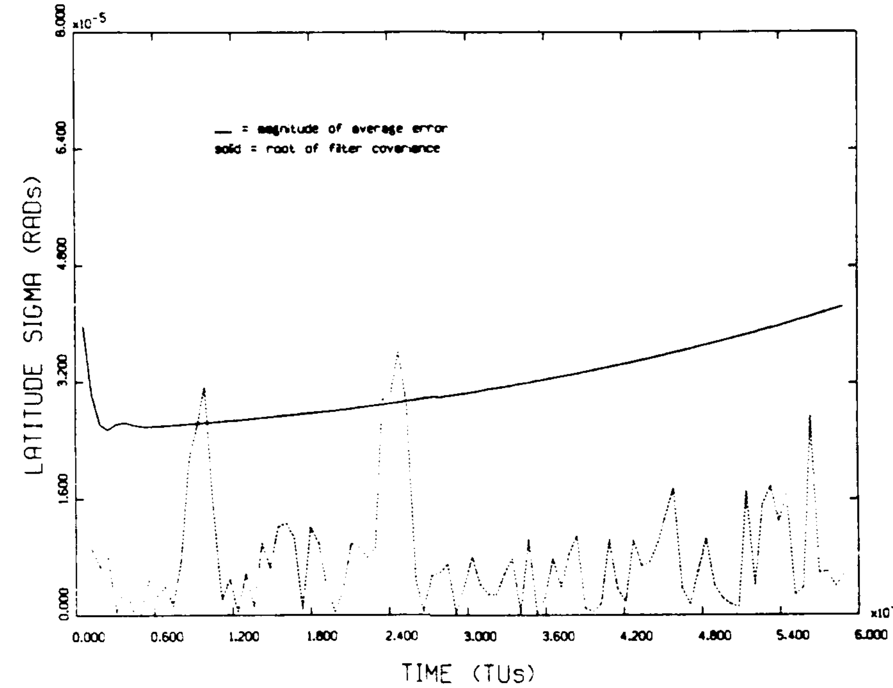

Figure A.38. Latitude Covariance and Error, 1 G, 1 Second Interval, North Trajectory, Six State Filter

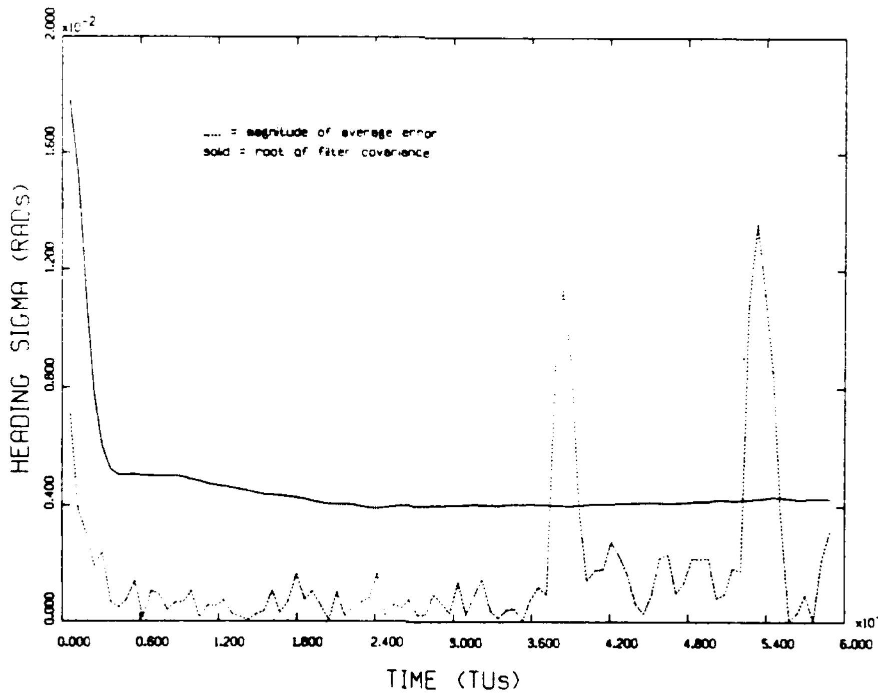

Figure A.39. Heading Covariance and Error, 1 G, 1 Second Interval, North Trajectory, Six State Filter

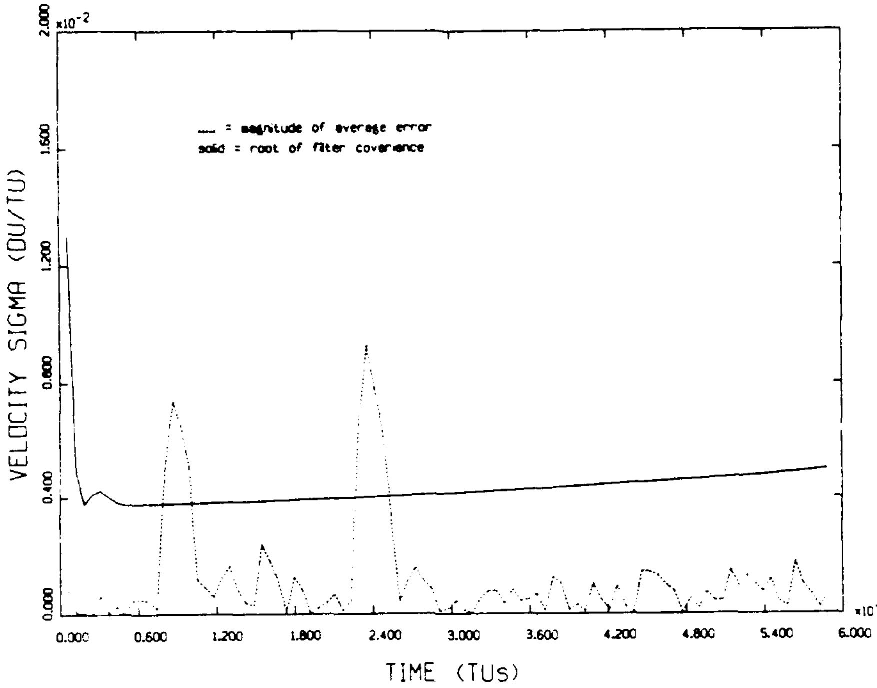

Figure A.40. Velocity Covariance and Error, 1 G, 1 Second Interval, North Trajectory, Six State Filter

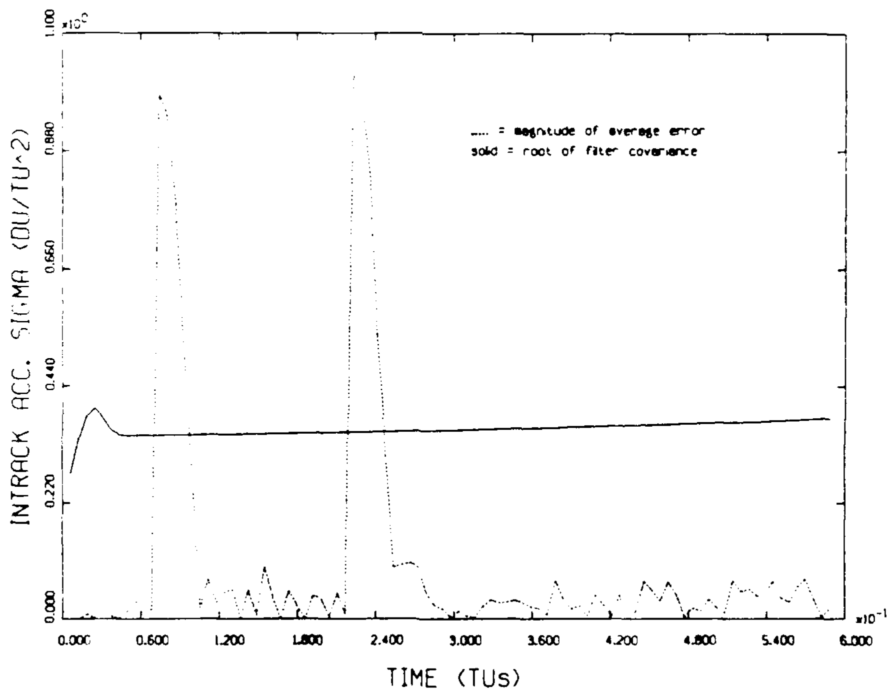

Figure A.41. a_I Covariance and Error, 1 G, 1 Second Interval, North Trajectory, Six State Filter

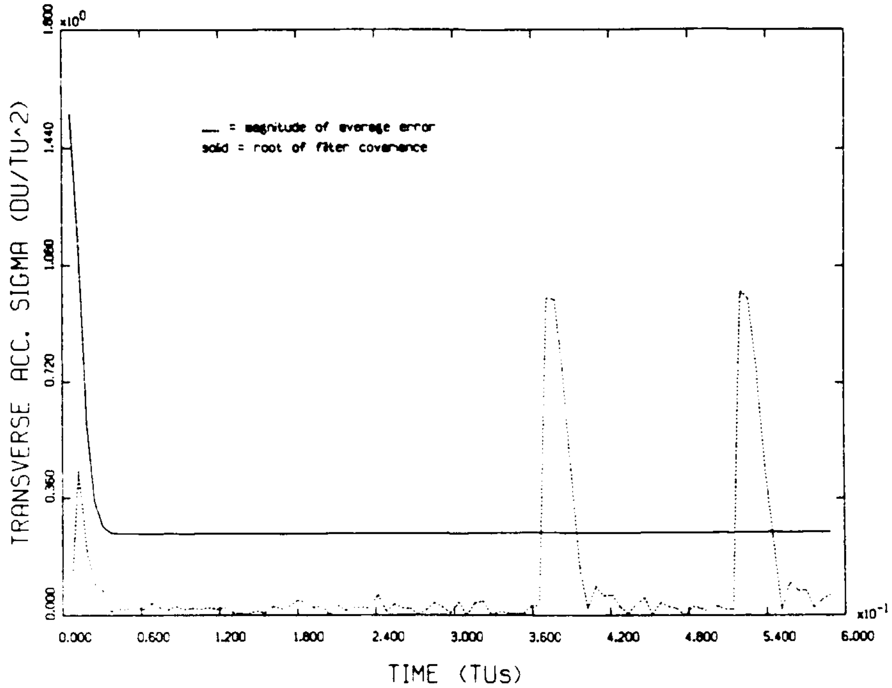

Figure A.42. a_T Covariance and Error, 1 G, 1 Second Interval, North Trajectory, Six State Filter

Table A.4. East Trajectory Initial Conditions

State	Covariance
λ = 1.0472 rads	$P_{\lambda\lambda}$ = 1.25e-5 rads^2
δ = 0.1745 rads	$P_{\delta\delta}$ = 1.25e-5 rads^2
h = 1.5708 rads	P_{hh} = 3.e-3 rads^2
V = 0.5 DU/TU	P_{VV} = 3.e-2 (DU/TU)^2
a_I = 0.0 DU/TU^2	P_{II} = 3.5e-2 (DU/TU^2)^2
a_T = 0.0 DU/TU^2	P_{TT} = 2.5 (DU/TU^2)^2

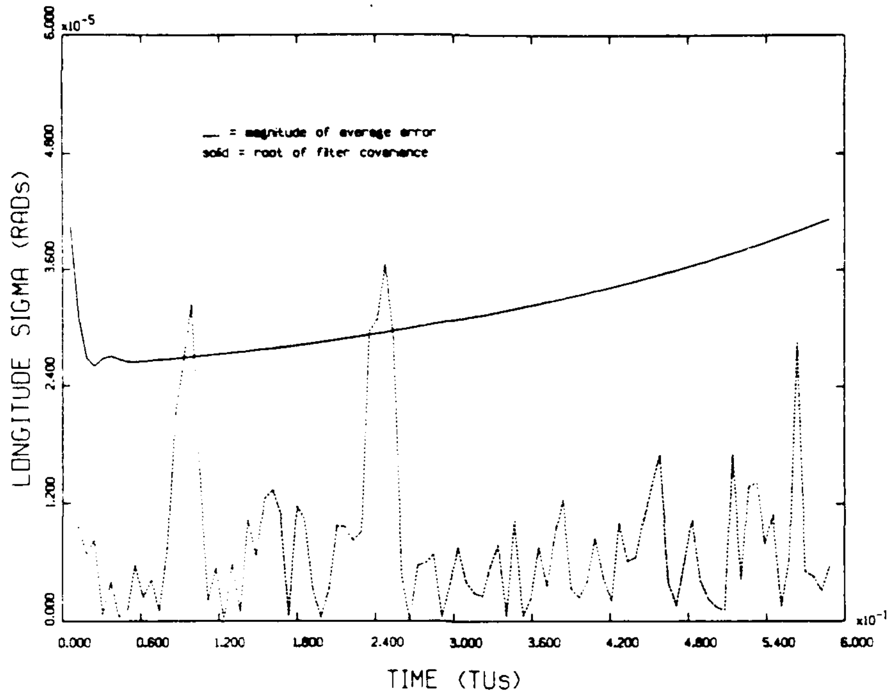

Figure A.43. Longitude Covariance and Error, 1 G, 1 Second Interval, East Trajectory, Six State Filter

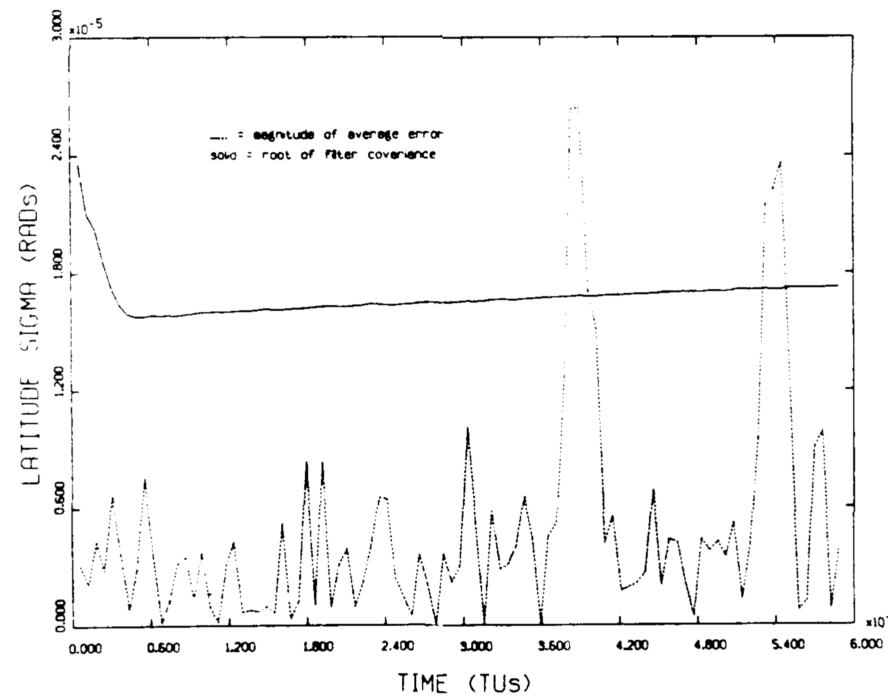

Figure A.44. Latitude Covariance and Error, 1 G, 1 Second Interval, East Trajectory, Six State Filter

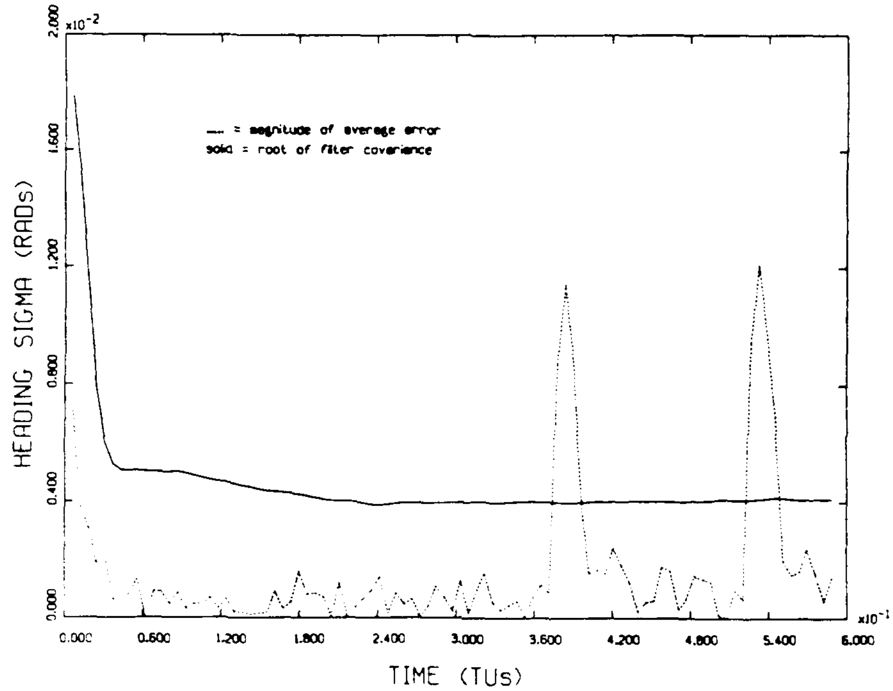

Figure A.45. Heading Covariance and Error, 1 G, 1 Second Interval, East Trajectory, Six State Filter

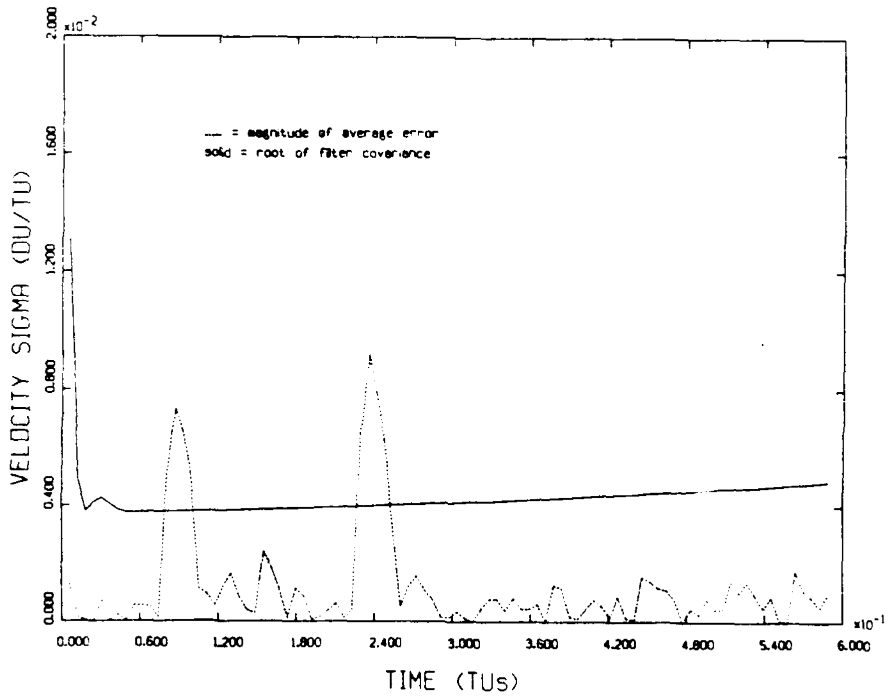

Figure A.46. Velocity Covariance and Error, 1 G, 1 Second Interval, East Trajectory, Six State Filter

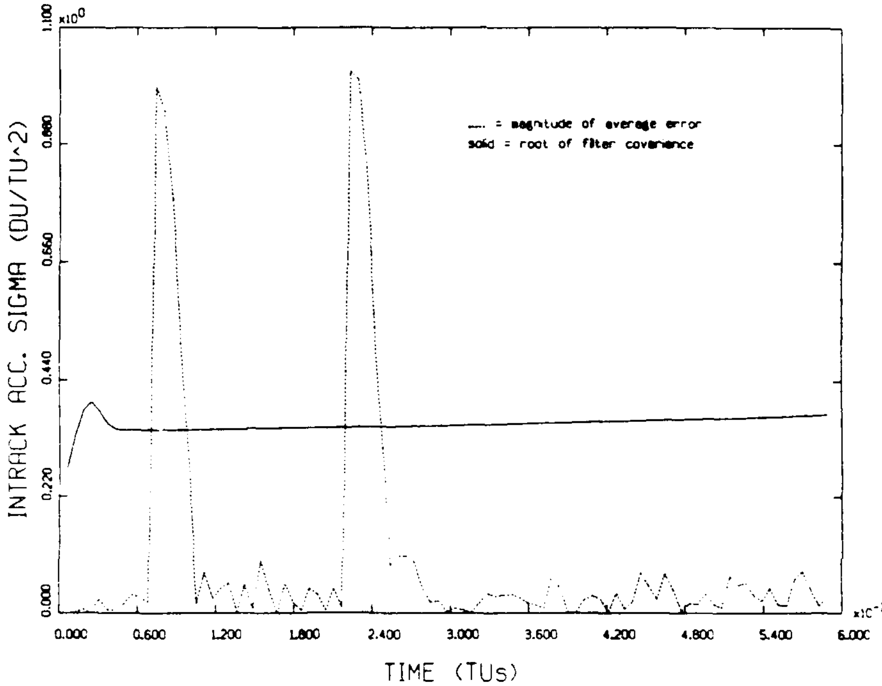

Figure A.47. a_I **Covariance and Error, 1 G, 1 Second Interval, East Trajectory, Six State Filter**

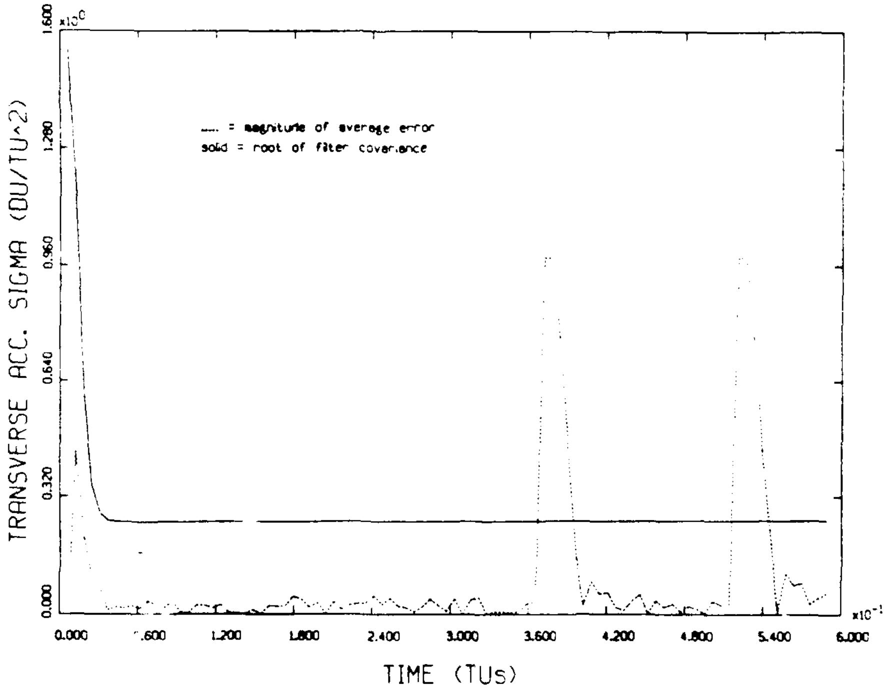

Figure A.48. a_T **Covariance and Error, 1 G, 1 Second Interval, East Trajectory, Six State Filter**

Appendix B: 9 G Covariance and Error Plots

Chapter 4 applied the six state Kalman filter to a 9 G flight profile. The covariance plots for the one and ten second data interval filters are presented below.

Table B.1. Flight Profile, 9 G Accelerations

Time (sec)	Time (TU)	Maneuver
0 - 60	0 - .074	Constant Speed
61 - 180	.075 - .223	9 G Intrack Acceleration
181 - 300	.224 - .372	Constant Speed
301 - 420	.373 - .521	9 G Transverse Accel.
421 - 480	.522 - .595	Constant Speed

Table B.2. Central Trajectory Initial Conditions

State	Covariance
λ = 0.0 rads	$P_{\lambda\lambda}$ = 1.25e-5 rads^2
δ = 0.0 rads	$P_{\delta\delta}$ = 1.25e-5 rads^2
h = 0.7854 rads	P_{hh} = 3.e-3 rads^2
V = 0.5 DU/TU	P_{VV} = 3.e-2 (DU/TU)^2
a_I = 0.0 DU/TU^2	P_{II} = 3.5e-2 (DU/TU^2)^2
a_T = 0.0 DU/TU^2	P_{TT} = 2.5 (DU/TU^2)^2

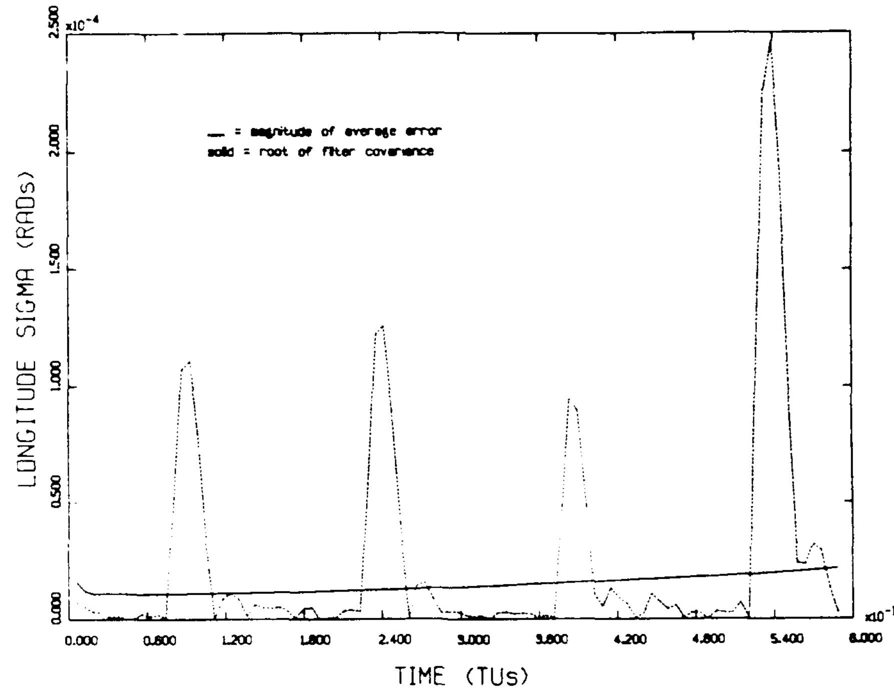

Figure B.1. Longitude Covariance and Error, 9 G, 1 Second Data Interval, Six State Filter

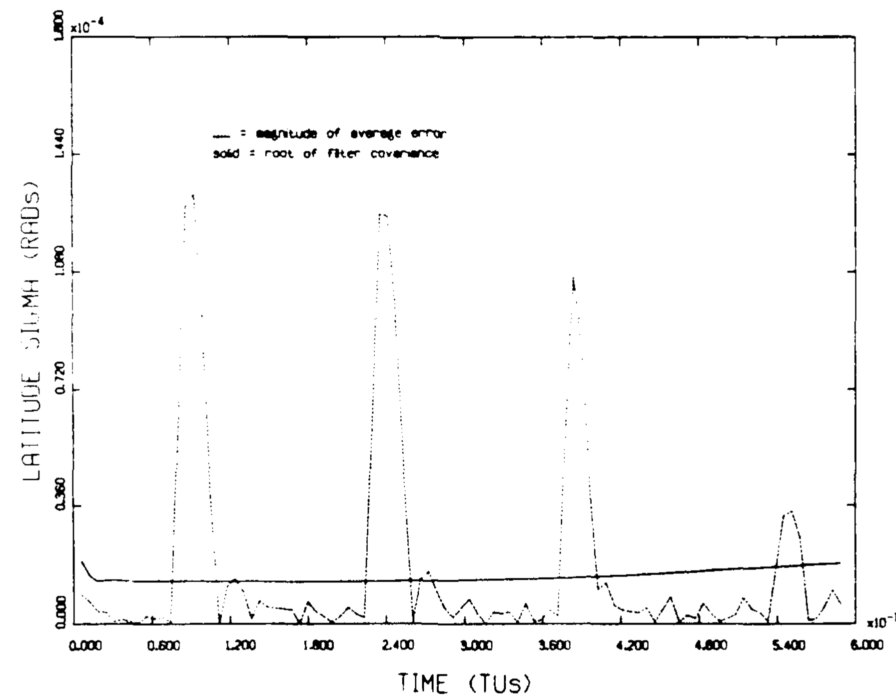

Figure B.2. Latitude Covariance and Error, 9 G, 1 Second Data Interval, Six State Filter

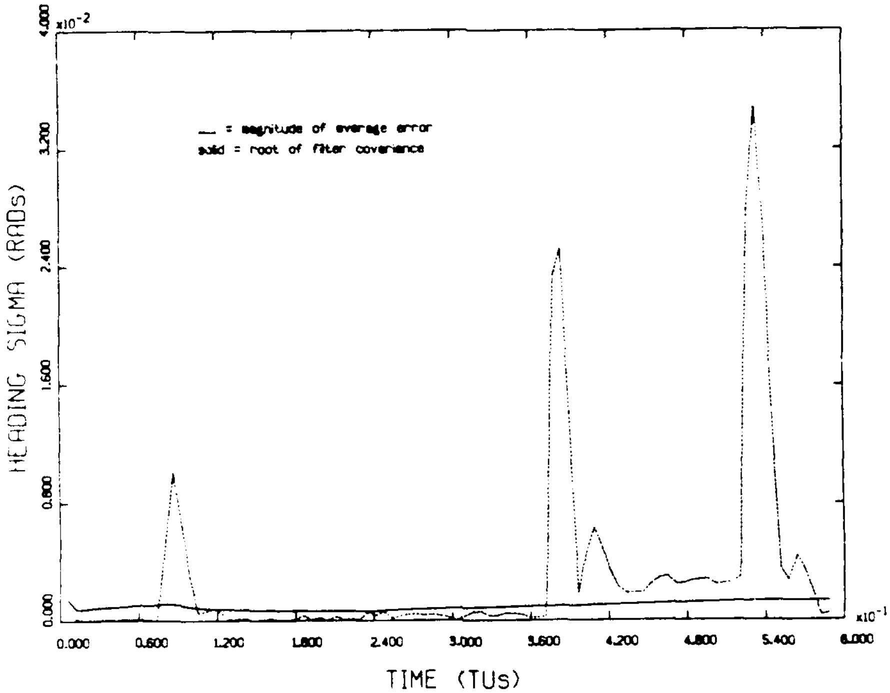

Figure B.3. Heading Covariance and Error, 9 G, 1 Second Data Interval, Six State Filter

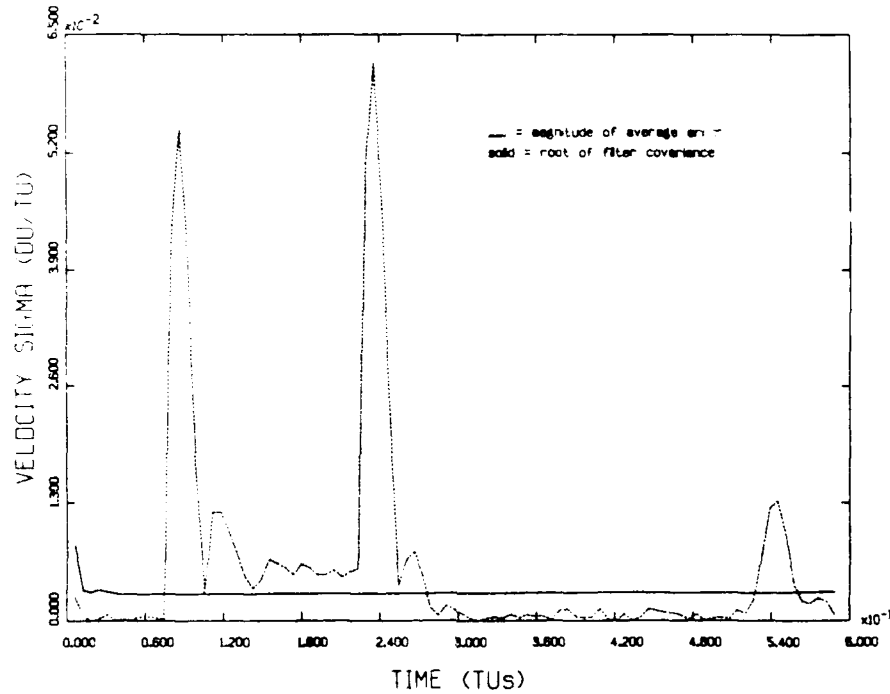

Figure B.4. Velocity Covariance and Error, 9 G, 1 Second Data Interval, Six State Filter

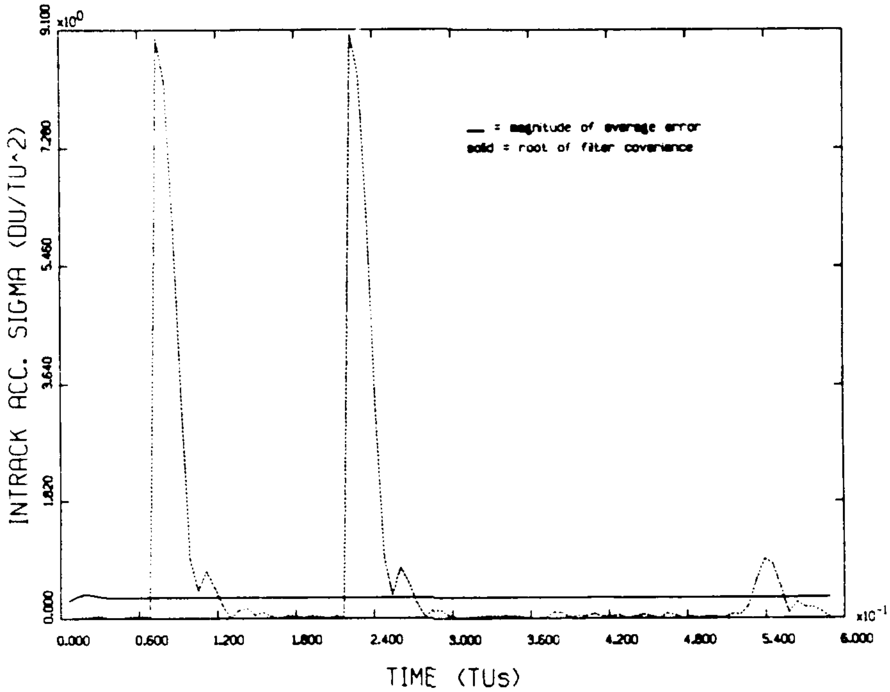

Figure B.5. a_I Covariance and Error, 9 G, 1 Second Data Interval, Six State Filter

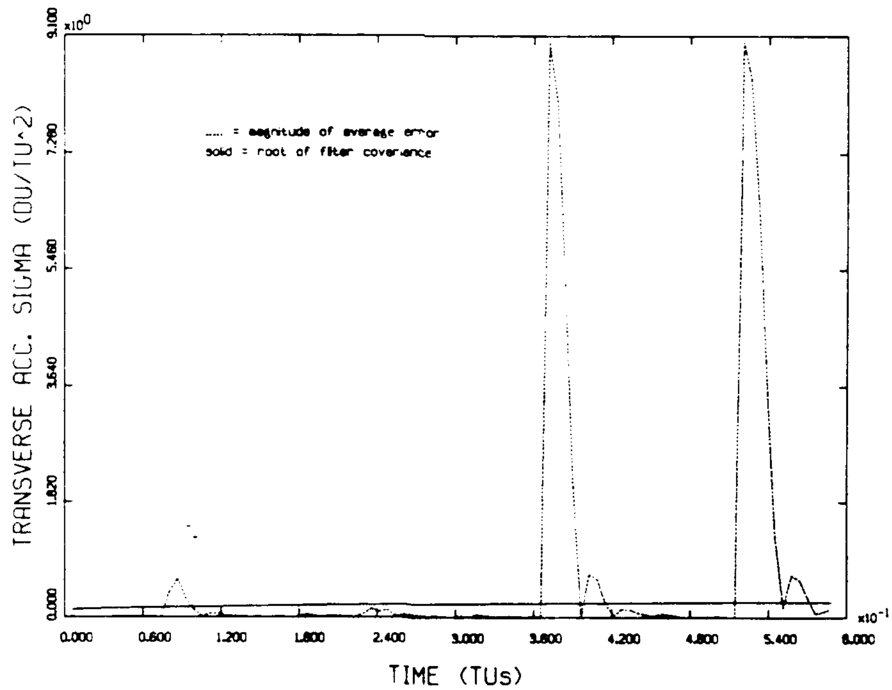

Figure B.6. a_T Covariance and Error, 9 G, 1 Second Data Interval, Six State Filter

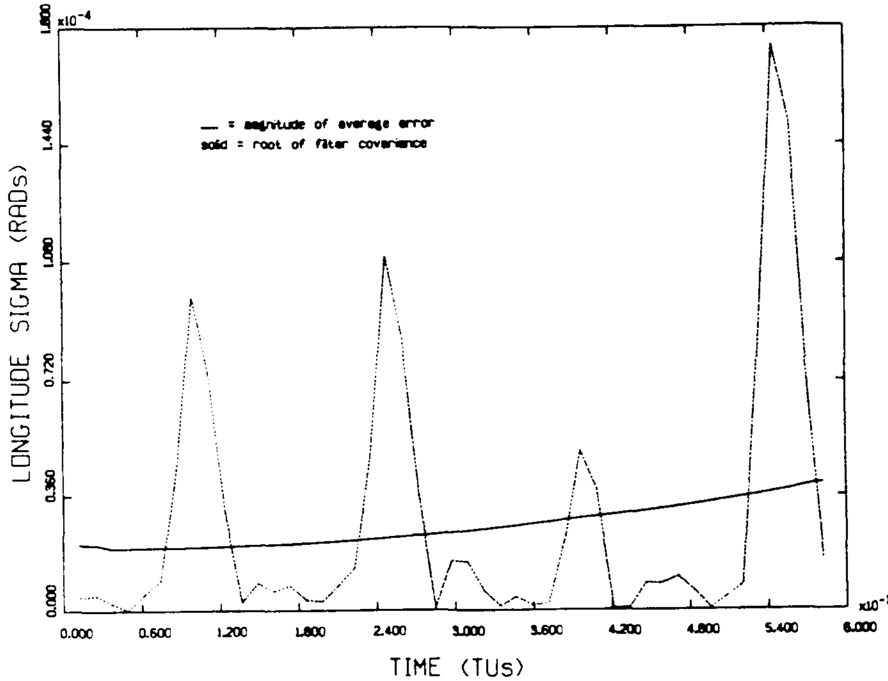

Figure B.7. Longitude Covariance and Error, 9 G,

10 Second Data Interval, Six State Filter

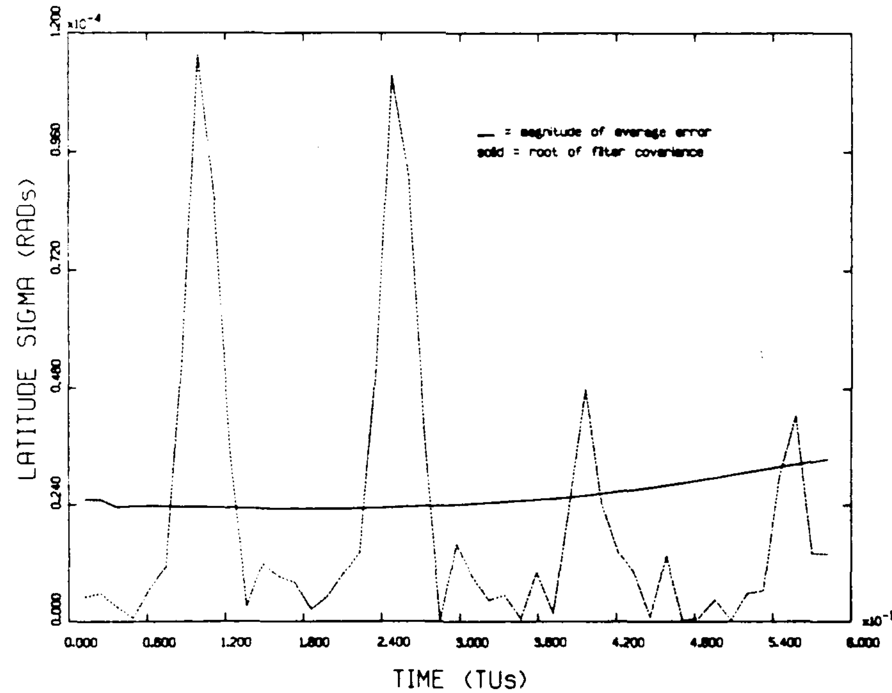

Figure B.8. Latitude Covariance and Error, 9 G,

10 Second Data Interval, Six State Filter

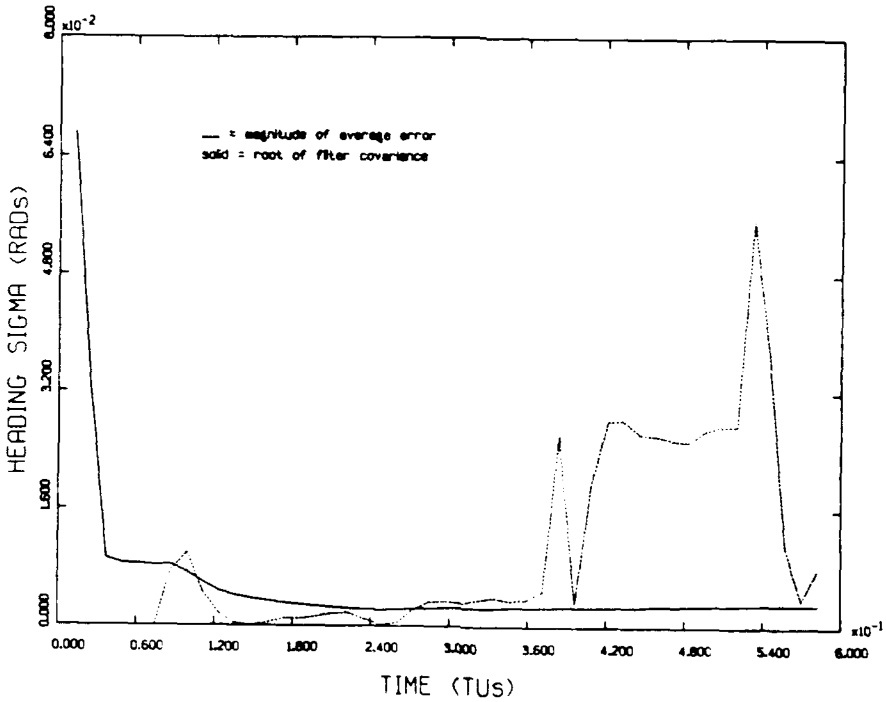

Figure B.9. Heading Covariance and Error, 9 G, 10 Second Data Interval, Six State Filter

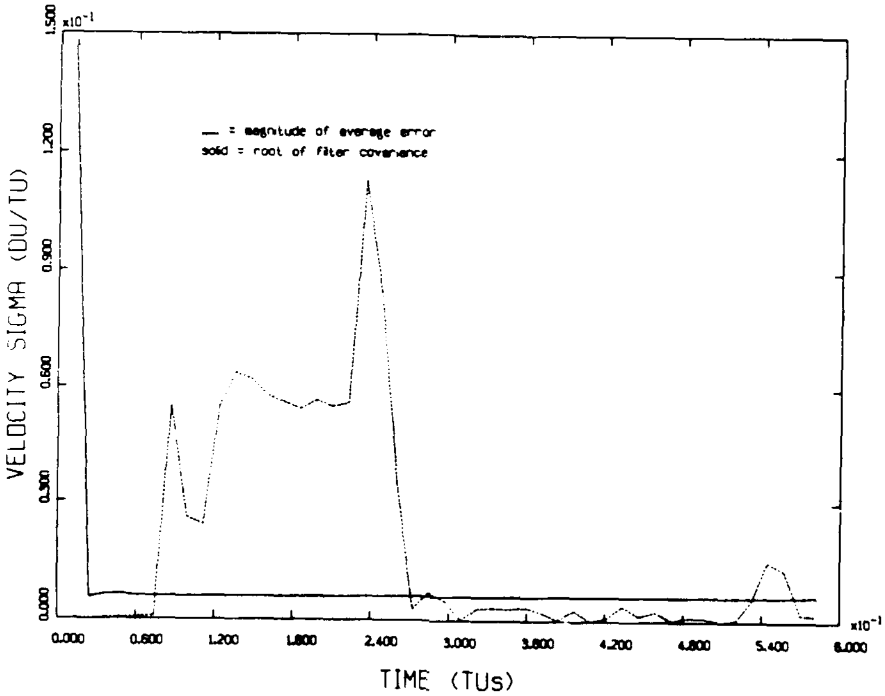

Figure B.10. Velocity Covariance and Error, 9 G, 10 Second Data Interval, Six State Filter

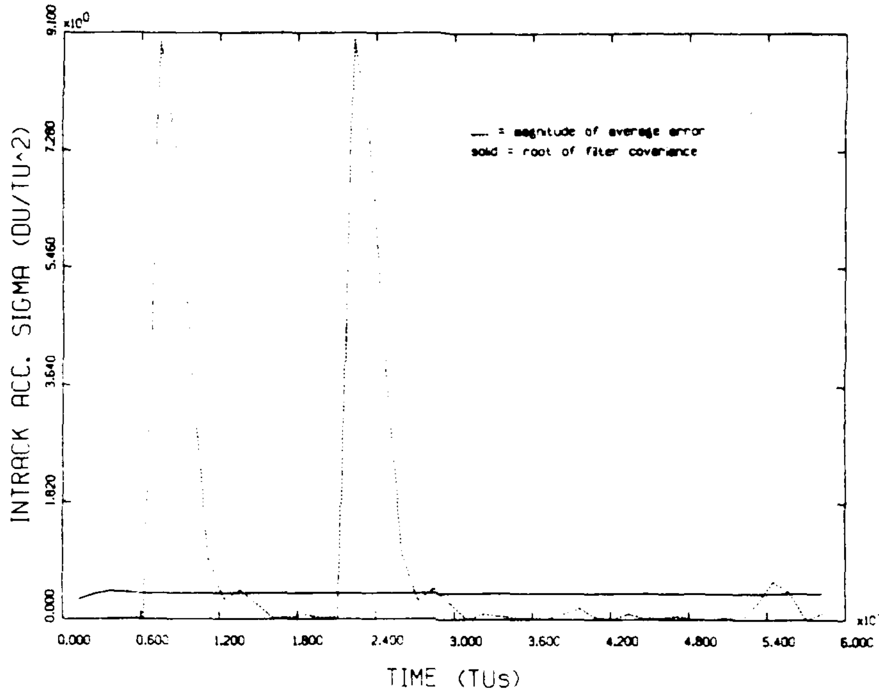

Figure B.11. a_I **Covariance and Error, 9 G, 10 Second Data Interval, Six State Filter**

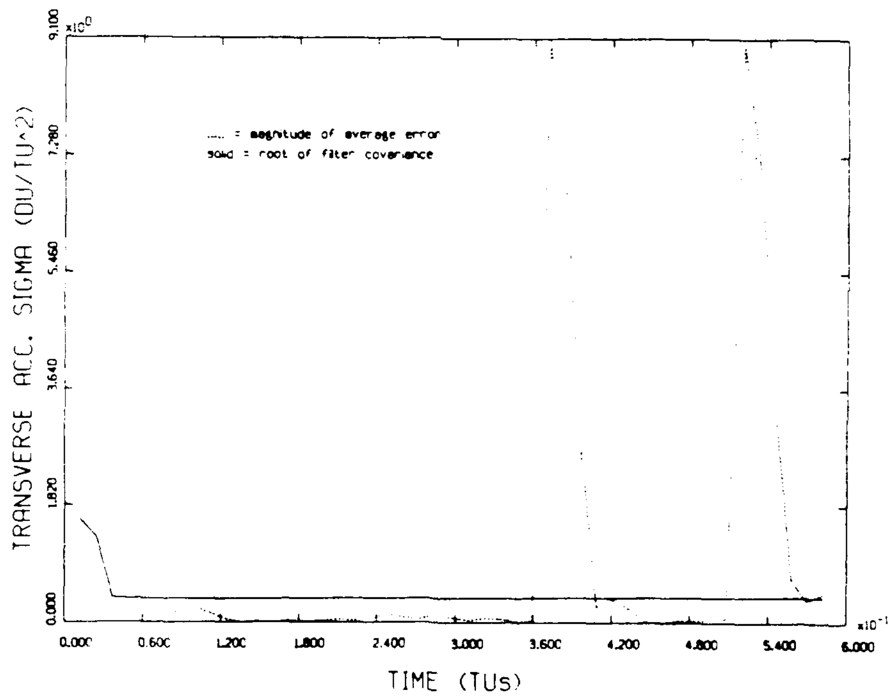

Figure B.12. a_T **Covariance and Error, 9 G, 10 Second Data Interval, Six State Filter**

Appendix C: Error $\pm$ 1 σ Plots, Central Trajectory

To show the consistency in state estimation for the six state Kalman filter, Chapter 4 presented four error statistics plots. All six states' plots for both the one and ten second interval filters are presented below.

Table C.1. Central Trajectory Initial Conditions

State	Covariance
λ = 0.0 rads	$P_{\lambda\lambda}$ = 1.25e-5 rads^2
δ = 0.0 rads	$P_{\delta\delta}$ = 1.25e-5 rads^2
h = 0.7854 rads	P_{hh} = 3.e-3 rads^2
V = 0.5 DU/TU	P_{VV} = 3.e-2 (DU/TU)^2
a_I = 0.0 DU/TU^2	P_{II} = 3.5e-2 (DU/TU^2)^2
a_T = 0.0 DU/TU^2	P_{TT} = 2.5 (DU/TU^2)^2

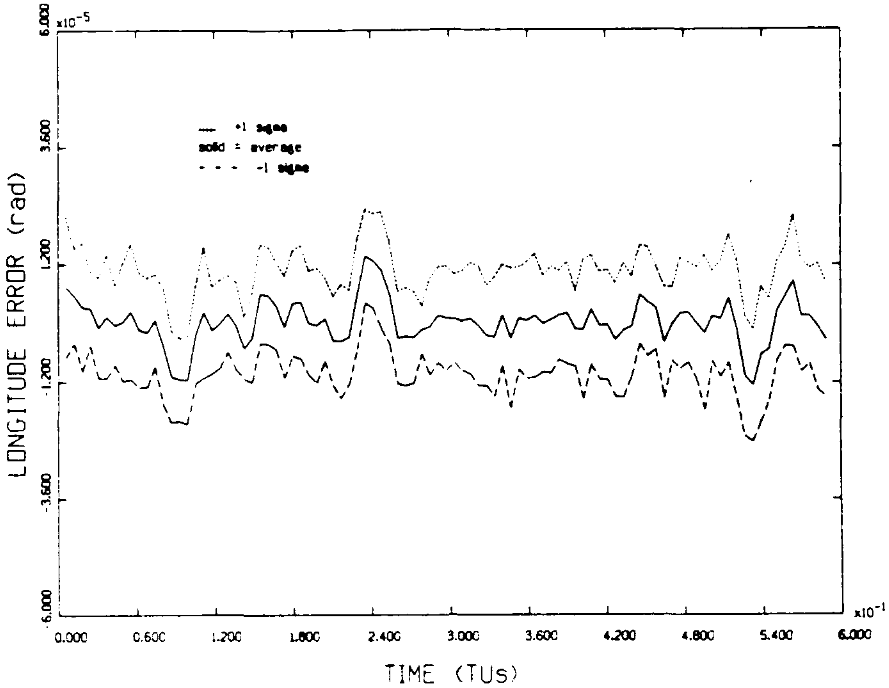

Figure C.1. Monte Carlo Longitude Error Statistics, 1 G,

1 Second Data Interval, Six State Filter

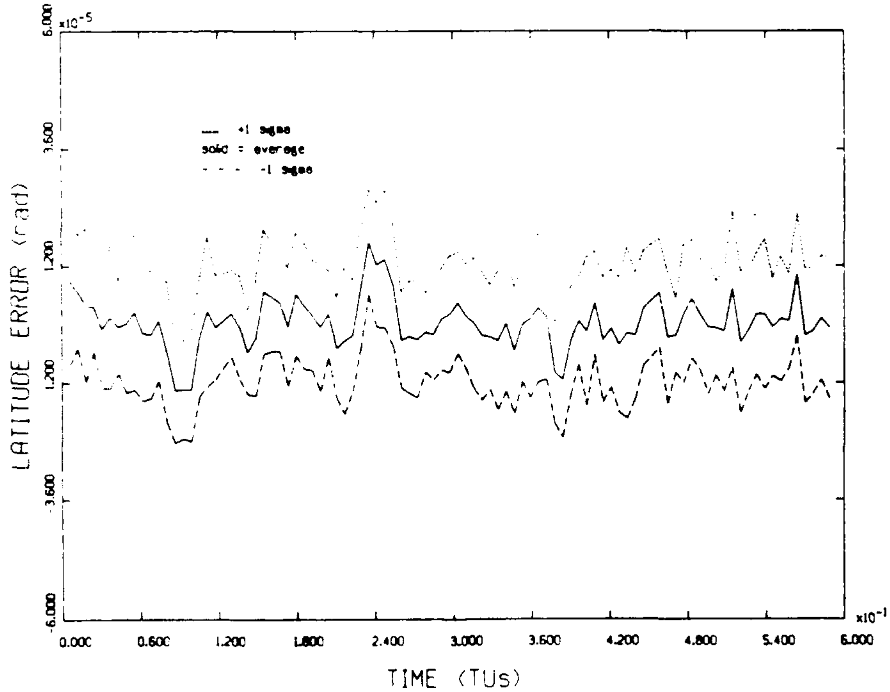

Figure C.2. Monte Carlo Latitude Error Statistics, 1 G,

1 Second Data Interval, Six State Filter

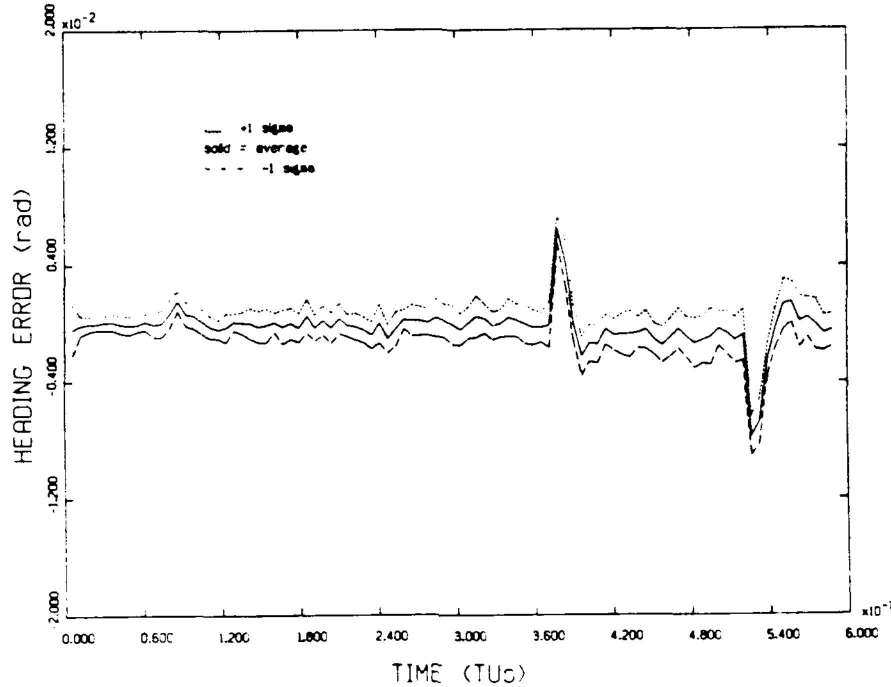

Figure C.3. Monte Carlo Heading Error Statistics, 1 G, 1 Second Data Interval, Six State Filter

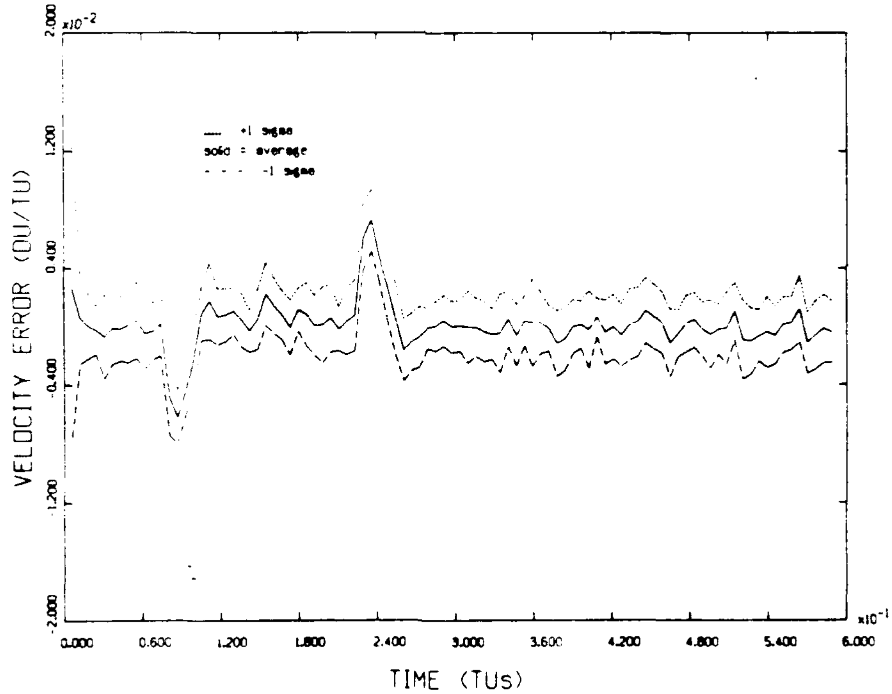

Figure C.4. Monte Carlo Velocity Error Statistics, 1 G, 1 Second Data Interval, Six State Filter

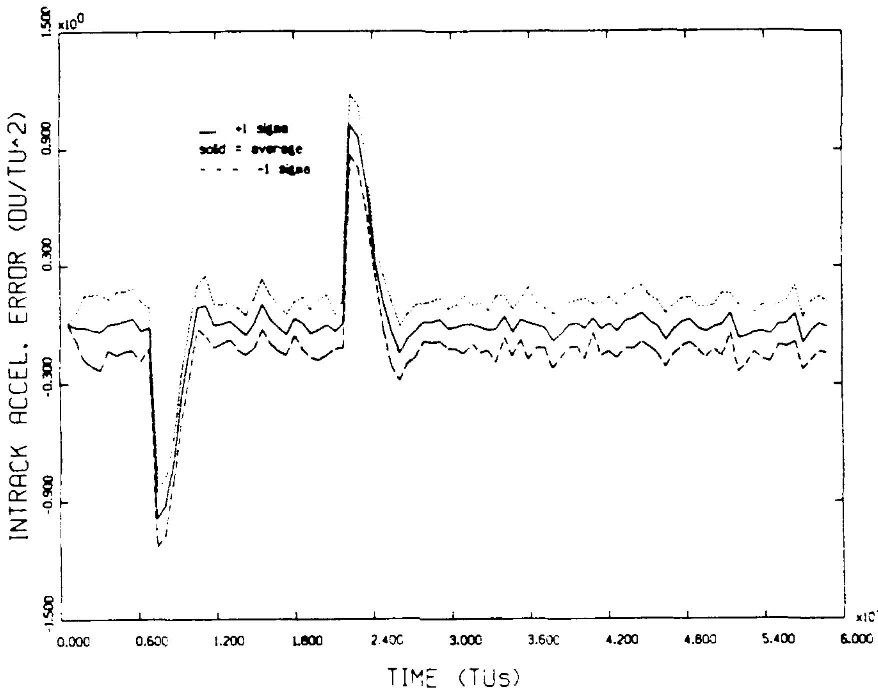

Figure C.5. Monte Carlo a_I Error Statistics, 1 G, 1 Second Data Interval, Six State Filter

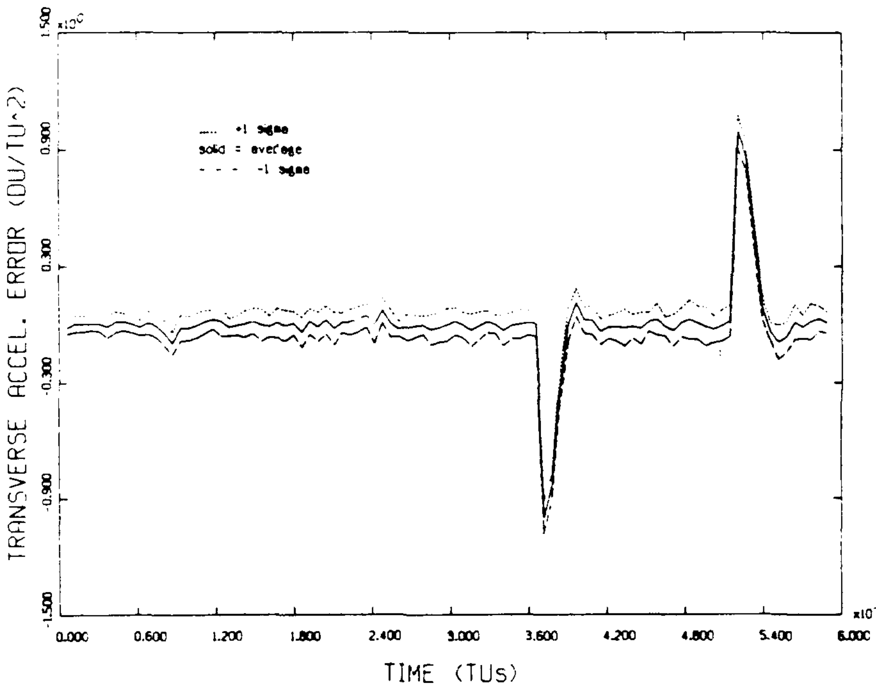

Figure C.6. Monte Carlo a_T Error Statistics, 1 G, 1 Second Data Interval, Six State Filter

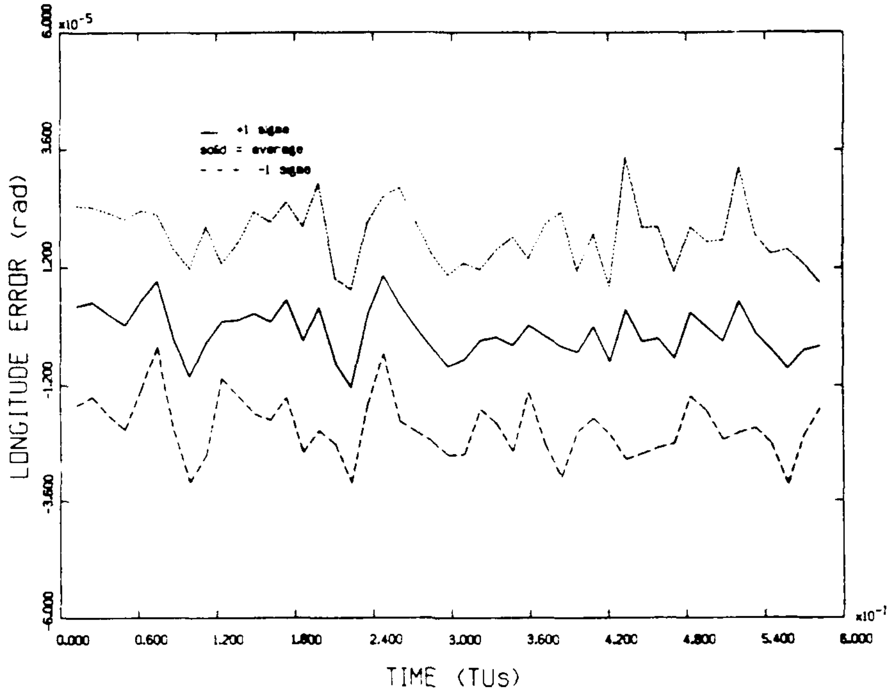

Figure C.7. Monte Carlo Longitude Error Statistics, 1 G, 10 Second Data Interval, Six State Filter

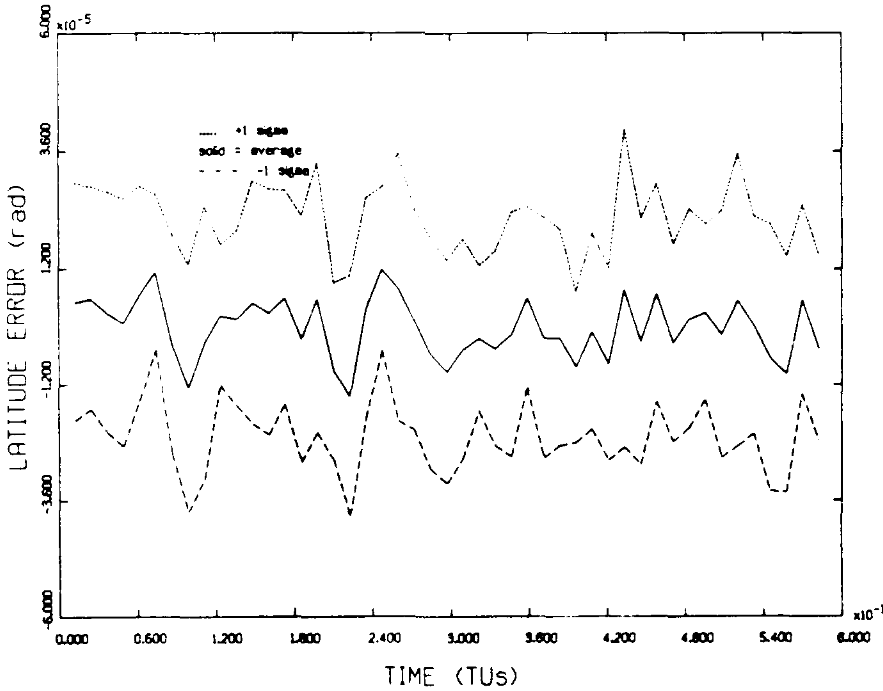

Figure C.8. Monte Carlo Latitude Error Statistics, 1 G, 10 Second Data Interval, Six State Filter

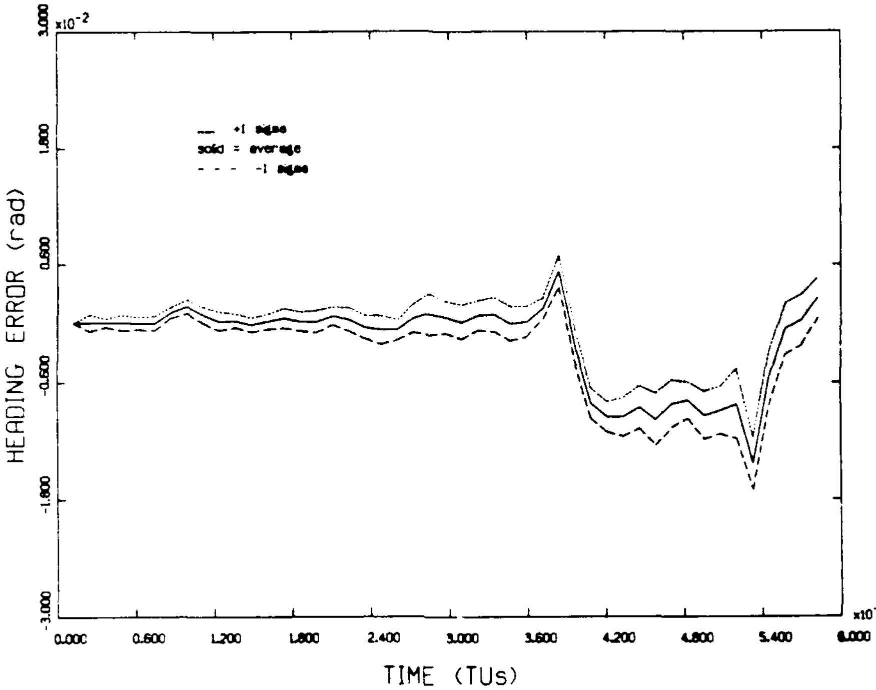

Figure C.9. Monte Carlo Heading Error Statistics, 1 G, 10 Second Data Interval, Six State Filter

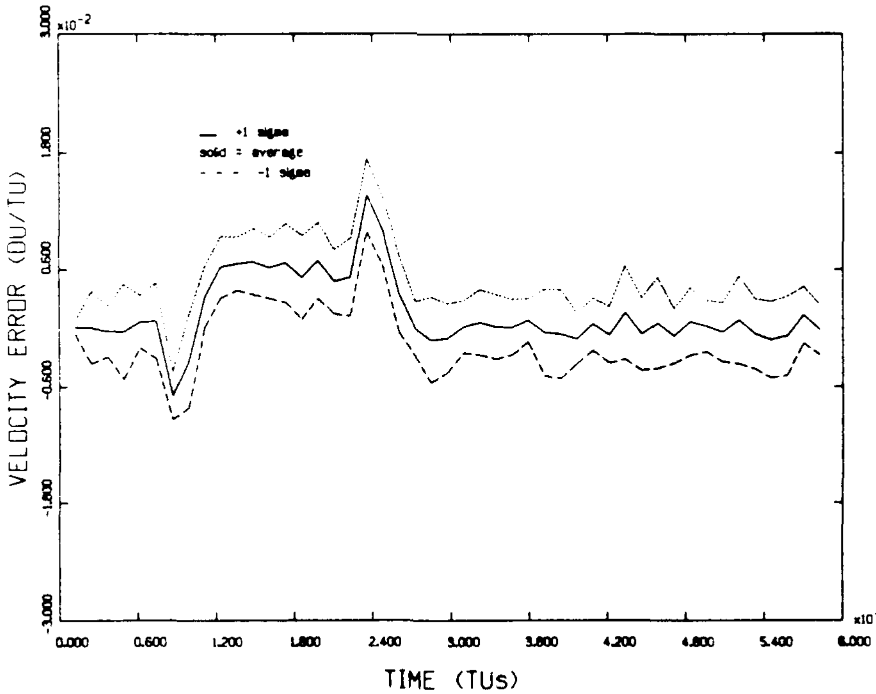

Figure C.10. Monte Carlo Velocity Error Statistics, 1 G, 10 Second Data Interval, Six State Filter

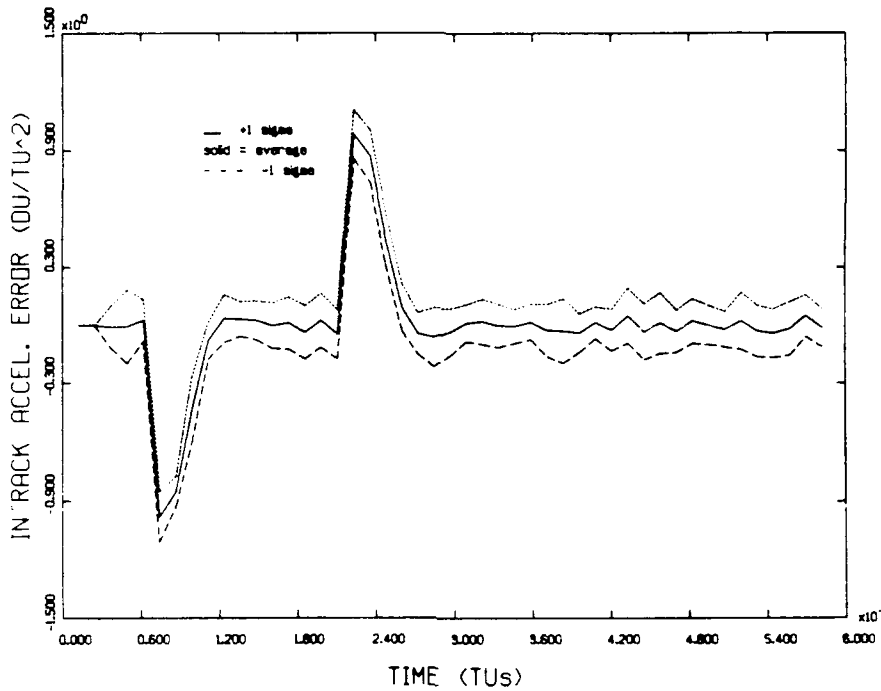

Figure C.11. Monte Carlo a_I Error Statistics, 1 G, 10 Second Data Interval, Six State Filter

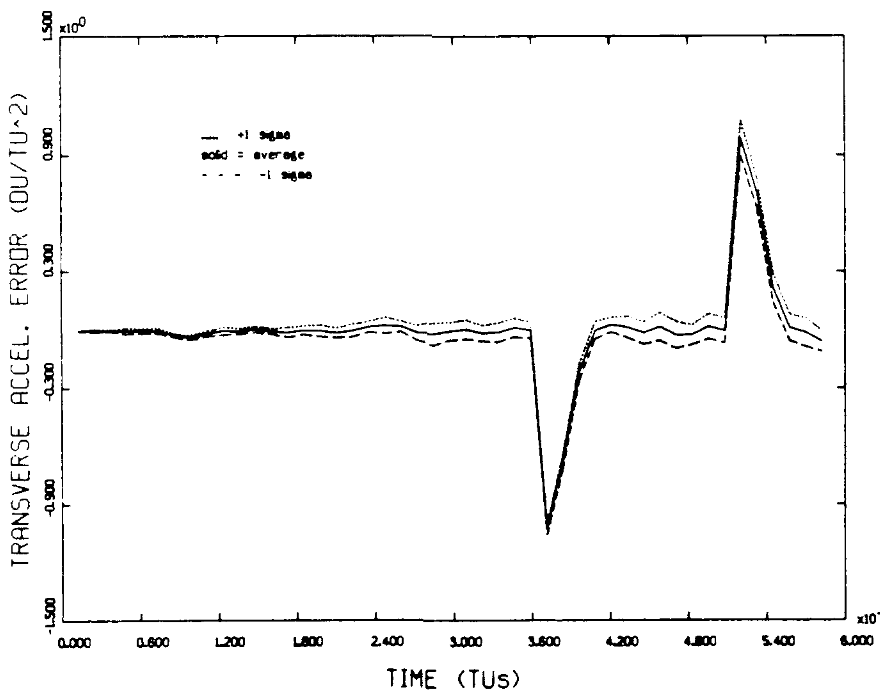

Figure C.12. Monte Carlo a_T Error Statistics, 1 G, 10 Second Data Interval, Six State Filter

Appendix D: Comparison of Errors, Central Trajectory

Chapter 8 compared the six state Kalman filter, the probability weighting adaptive filter, and the smoother via plots of the average magnitude of their errors. All of the error comparison plots for the one and ten second data interval estimators are presented below.

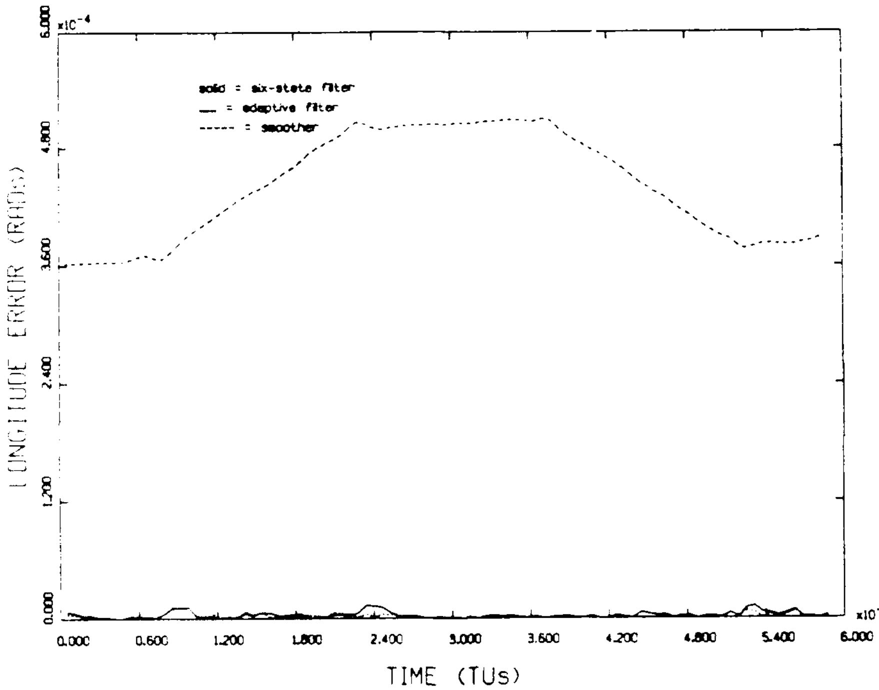

Figure D.1. Longitude Error Comparison, 1 Second Interval

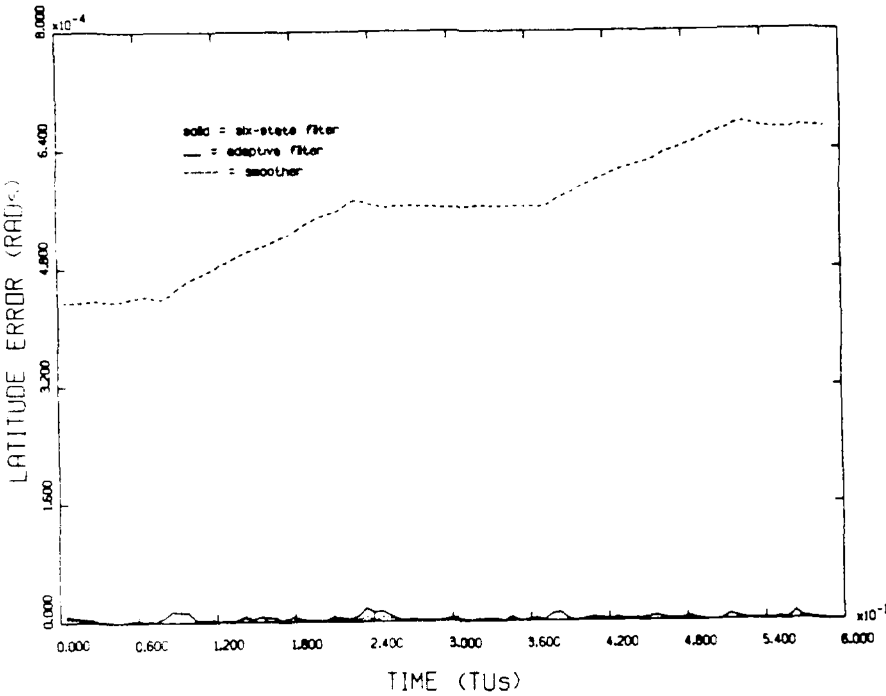

Figure D.2. Latitude Error Comparison, 1 Second Interval

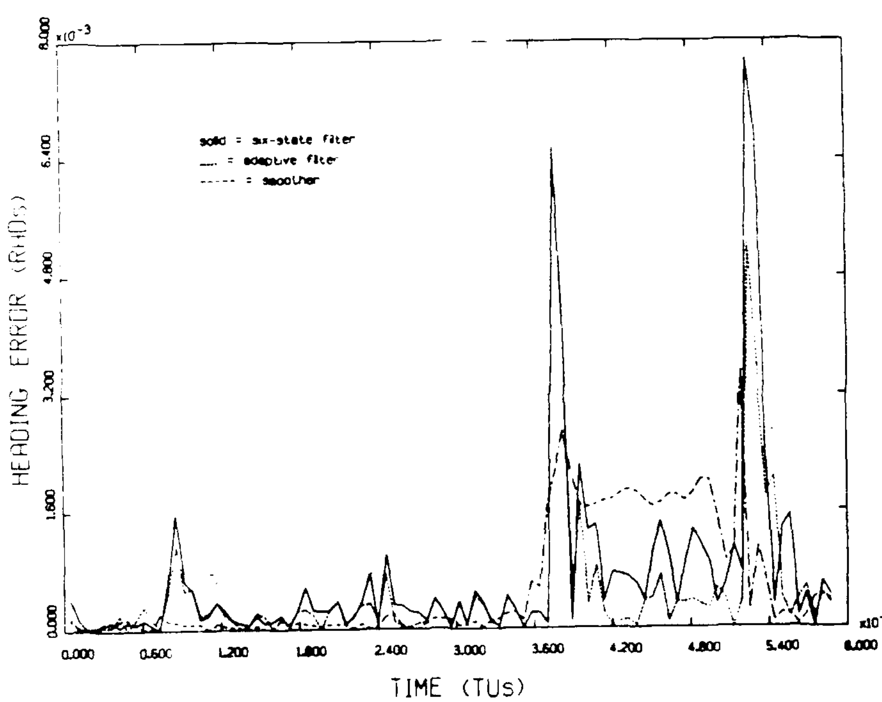

Figure D.3. Heading Error Comparison, 1 Second Interval

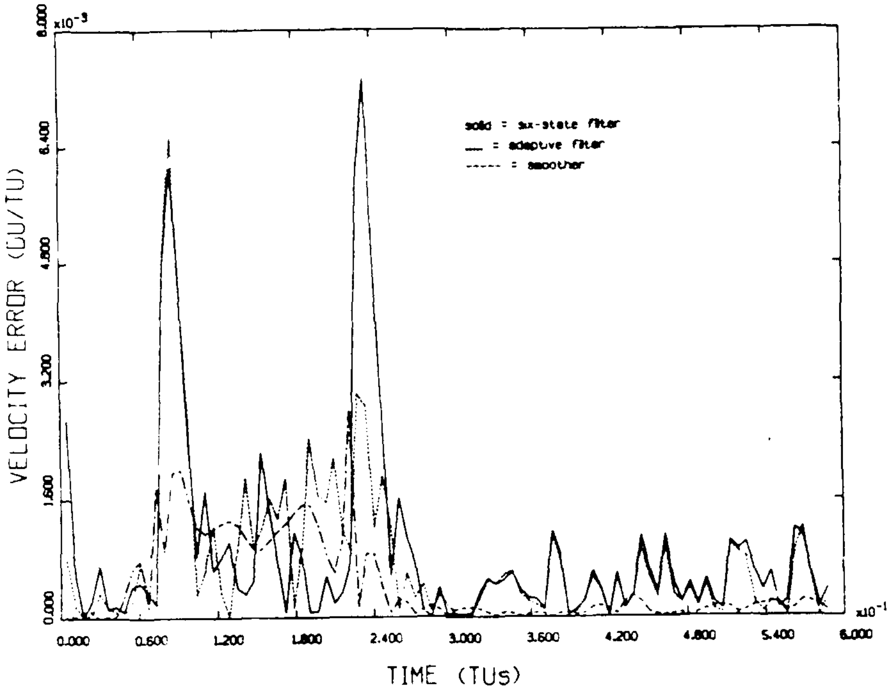

Figure D.4. Velocity Error Comparison, 1 Second Interval

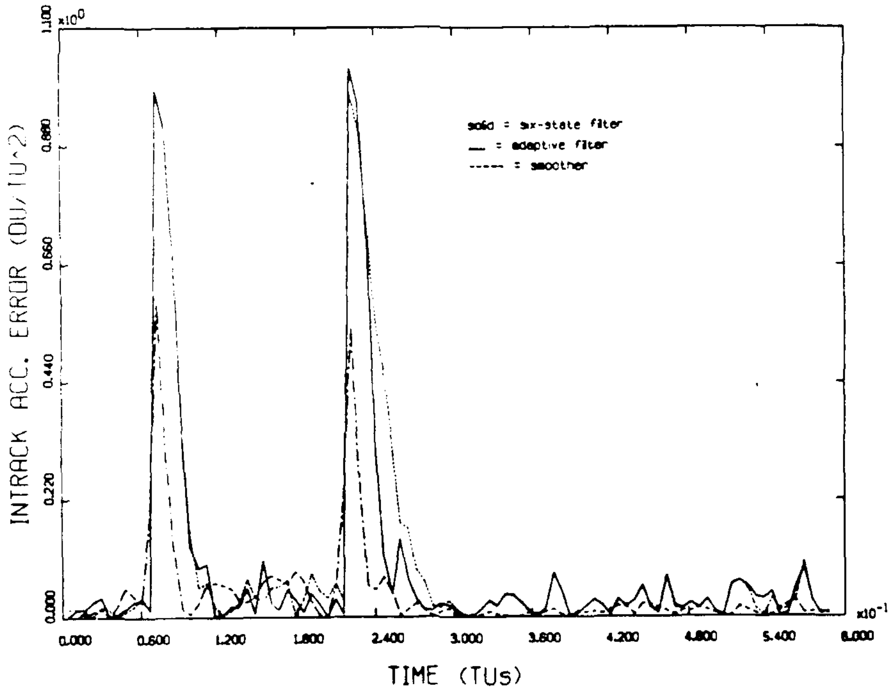

Figure D.5. a_I Error Comparison, 1 Second Interval

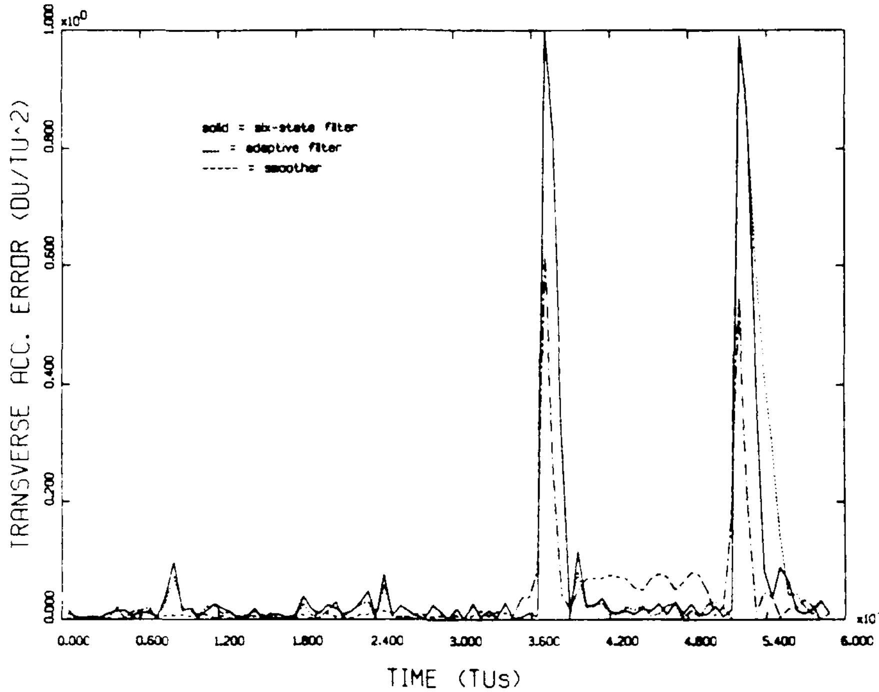

Figure D.6. a_T Error Comparison, 1 Second Interval

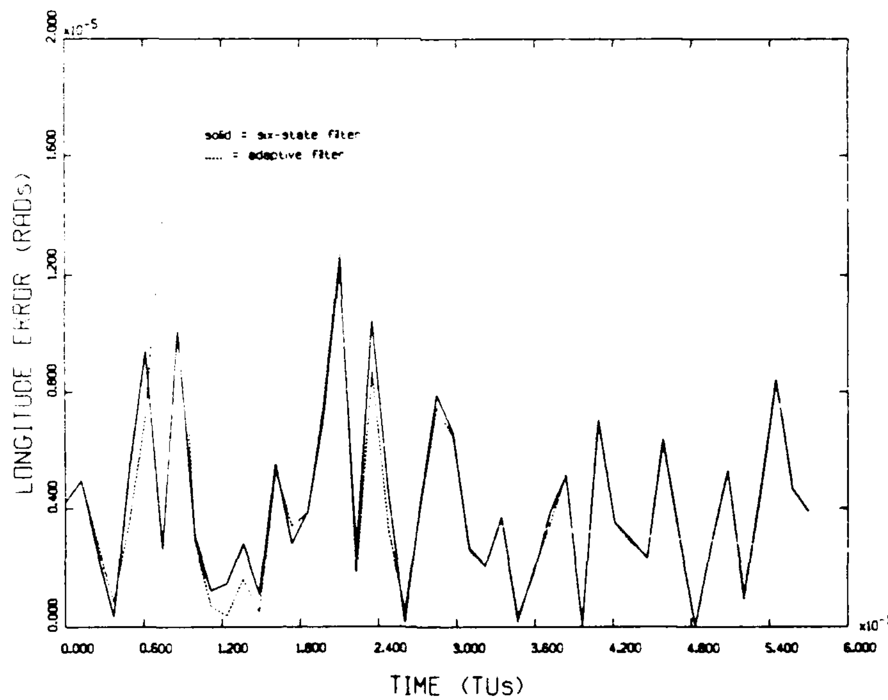

Figure D.7. Longitude Error Comparison, 10 Second Interval

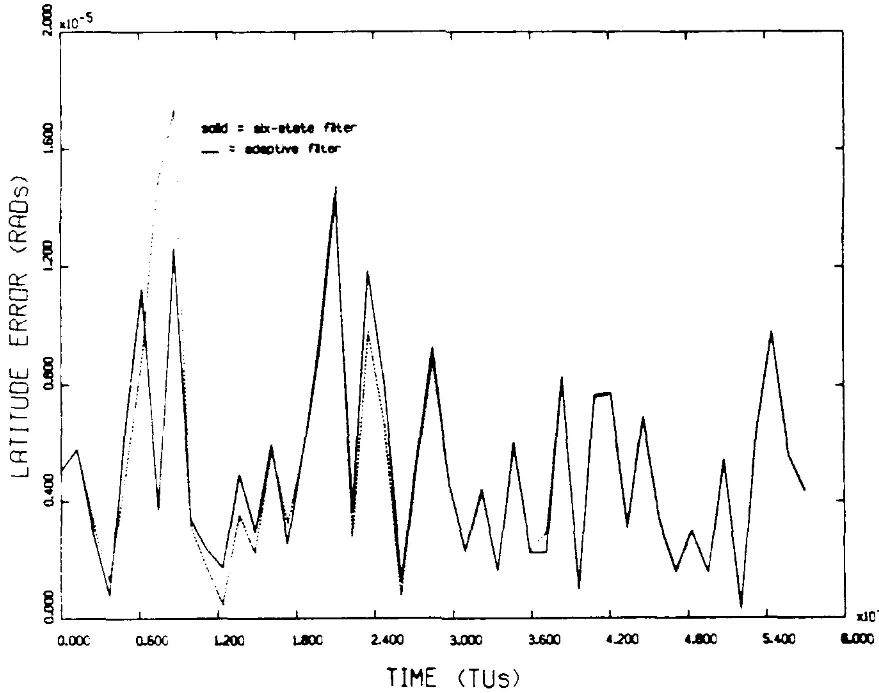

Figure D.8. Latitude Error Comparison, 10 Second Interval

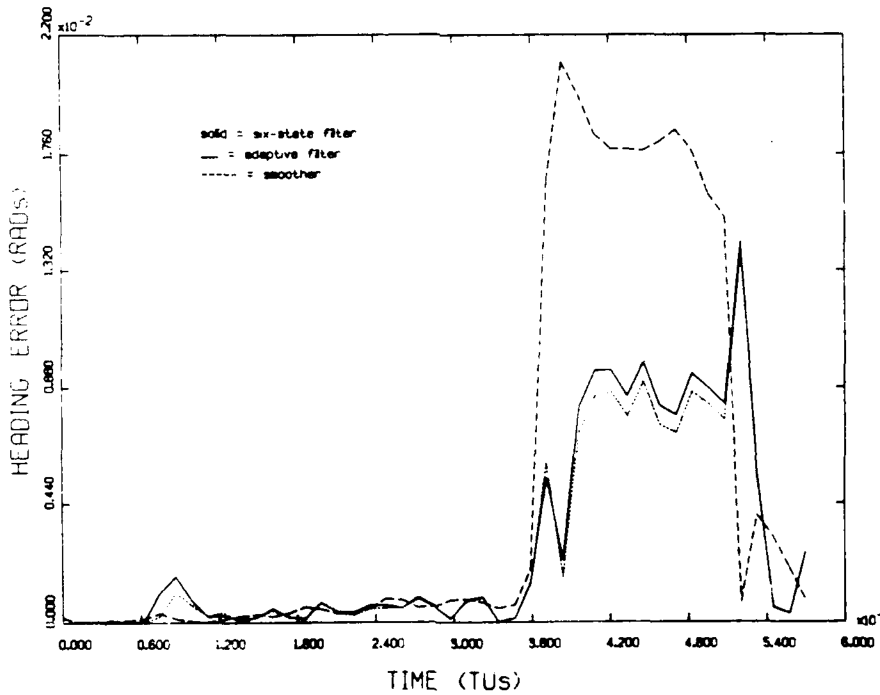

Figure D.9. Heading Error Comparison, 10 Second Interval

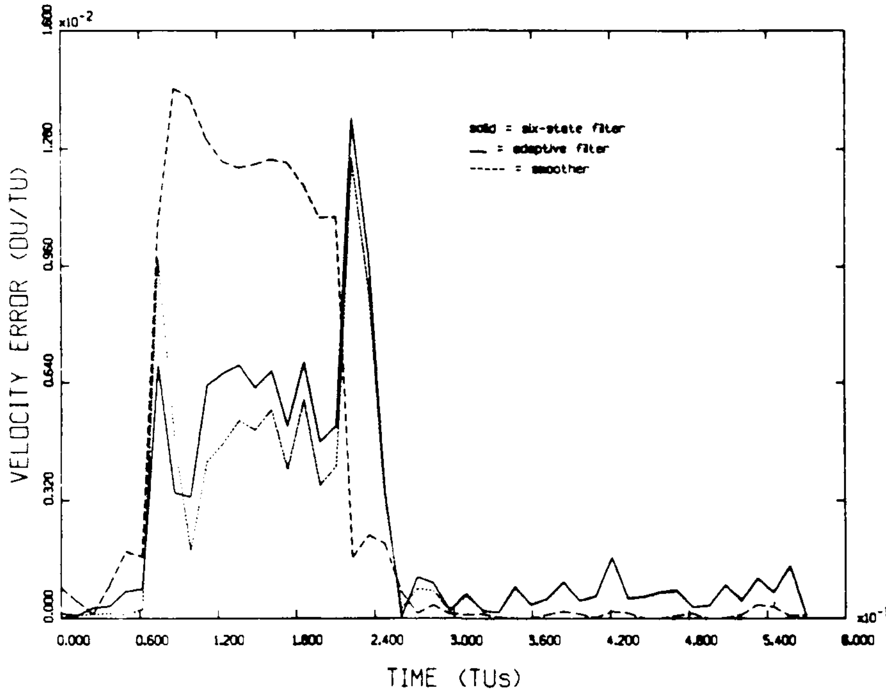

Figure D.10. Velocity Error Comparison, 10 Second Interval

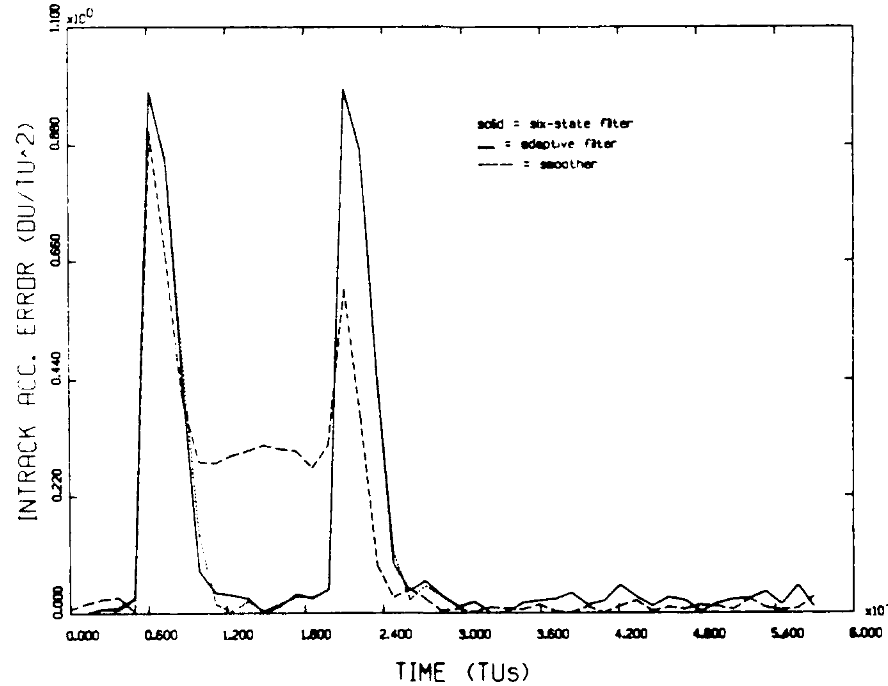

Figure D.11. a_I Error Comparison, 10 Second Interval

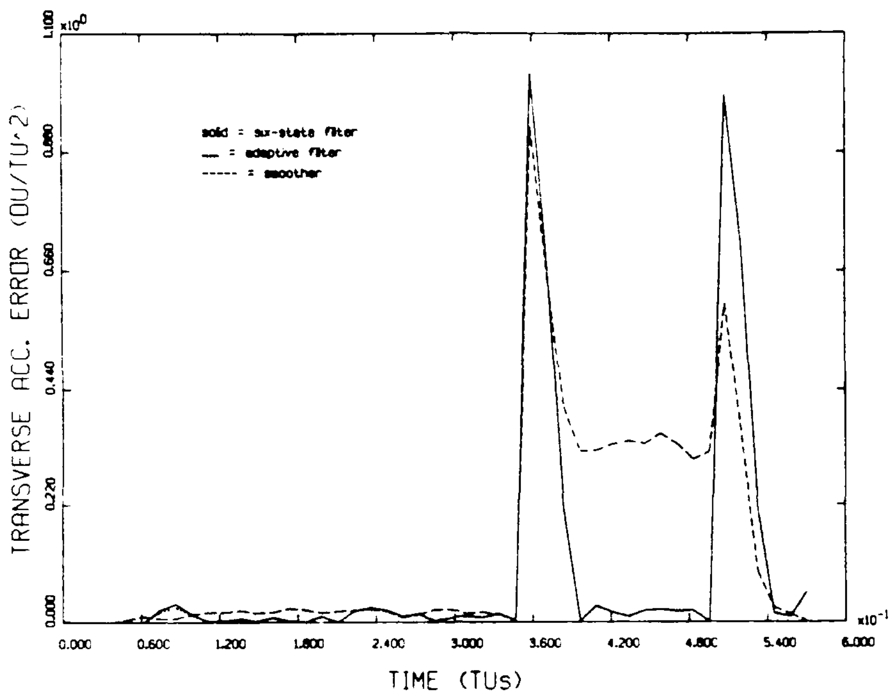

Figure D.12. a_T Error Comparison, 10 Second Interval

Bibliography

1. Maybeck, Peter S. in private conversations, Sep 90.

2. Maybeck, Peter S. Stochastic Models, Estimation, and Control (Volume 1), San Diego: Academic Press, Inc., 1979.

3. Maybeck, Peter S. Stochastic Models, Estimation, and Control (Volume 2), New York: Academic Press, Inc., 1982.

4. Osedacz, Capt Richard M. Orbit Determination of Sunlight Illuminated Objects Detected by Overhead Platforms. MS Thesis, AFIT/GA/ENY/89J-3. School of Engineering, Air Force Institute of Technology (AU), Wright-Patterson AFB OH, June 1989.

5. Wiesel, William E. Lecture Notes for MC 7.31, Modern Methods of Orbit Determination. School of Engineering, Air Force Institute of Technology (AU), Wright-Patterson AFB OH, 1990.

6. Ziegler, Capt David W. Tracking a Hypersonic Aircraft from a Space Platform. MS Thesis, AFIT/GA/ENY/89D-7. School of Engineering, Air Force Institute of Technology (AU), Wright-Patterson AFB OH, December 1989.

Vita

Captain Kenneth A. Gotski [redacted] He graduated from Riverside-Brookfield Township High School in Riverside, Illinois in 1982 and attended the U.S. Air Force Academy, graduating in May 1986 with a Bachelor of Science in Astronautical Engineering. He was assigned to the Upper Stages Program Office, Los Angeles Air Force Base, California, as a software engineer for the Inertial Upper Stage (IUS). Initially he managed the independent verification and validation of IUS flight software. He was chosen to help write the requirements for the development of an IUS interplanetary capability , and was later selected as the overall software manager for flight related software production and testing on all DoD and National Aeronautics and Space Administration missions. In May 1989 he entered the school of Engineering, Air Force Institute of Technology.

[redacted]

[redacted]

REPORT DOCUMENTATION PAGE

Form Approved
OMB No. 0704-0188

1. AGENCY USE ONLY (Leave blank)	2. REPORT DATE December 1990	3. REPORT TYPE AND DATES COVERED Master's Thesis

4. TITLE AND SUBTITLE ADAPTIVE FILTERING AND SMOOTHING FOR TRACKING A HYPERSONIC AIRCRAFT FROM A SPACE PLATFORM	5. FUNDING NUMBERS
6. AUTHOR(S) Kenneth A. Gotski, Captain, USAF	
7. PERFORMING ORGANIZATION NAME(S) AND ADDRESS(ES) Air Force Institute of Technology, WPAFB OH 45433-6583	8. PERFORMING ORGANIZATION REPORT NUMBER AFIT/GA/ENY/90D-6
9. SPONSORING/MONITORING AGENCY NAME(S) AND ADDRESS(ES)	10. SPONSORING/MONITORING AGENCY REPORT NUMBER
11. SUPPLEMENTARY NOTES	
12a. DISTRIBUTION/AVAILABILITY STATEMENT Approved for public release; distribution unlimited	12b. DISTRIBUTION CODE

13. ABSTRACT (Maximum 200 words)

This study took a previously developed six state Kalman filter (designed for space-based tracking of a hypersonic transatmospheric vehicle), tuned it, and performed a Monte Carlo analysis. Three multiple model adaptive filters were then developed, with sub-filters designed for quiescent periods and periods with apparent acceleration. Next, a smoother was developed using the six state filter as the forward filter and a form of that same filter as the backward filter. The smoother and all of the above filters were compared for their ability to most accurately estimate the transatmospheric vehicle's state, with special emphasis on the acceleration states. This emphasis was motivated by a desire to evaluate the Kalman filter's usefulness as a real-time intelligence gathering tool. From the data generated, it was concluded that neither the adaptive filters nor the smoother improved upon the performance of the six state Kalman filter.

14. SUBJECT TERMS Kalman Filtering, Tracking, Adaptive Filters, Smoothing Data	15. NUMBER OF PAGES 129
	16. PRICE CODE

17. SECURITY CLASSIFICATION OF REPORT	18. SECURITY CLASSIFICATION OF THIS PAGE	19. SECURITY CLASSIFICATION OF ABSTRACT	20. LIMITATION OF ABSTRACT
Unclassified	Unclassified	Unclassified	UL

GENERAL INSTRUCTIONS FOR COMPLETING SF 298

The Report Documentation Page (RDP) is used in announcing and cataloging reports. It is important that this information be consistent with the rest of the report, particularly the cover and title page. Instructions for filling in each block of the form follow. It is important to **stay within the lines to meet optical scanning requirements.**

Block 1. Agency Use Only (Leave Blank)

Block 2. Report Date. Full publication date including day, month, and year, if available (e.g. 1 Jan 88). Must cite at least the year.

Block 3. Type of Report and Dates Covered. State whether report is interim, final, etc. If applicable, enter inclusive report dates (e.g. 10 Jun 87 - 30 Jun 88).

Block 4. Title and Subtitle. A title is taken from the part of the report that provides the most meaningful and complete information. When a report is prepared in more than one volume, repeat the primary title, add volume number, and include subtitle for the specific volume. On classified documents enter the title classification in parentheses.

Block 5. Funding Numbers. To include contract and grant numbers; may include program element number(s), project number(s), task number(s), and work unit number(s). Use the following labels:

C - Contract	**PR** - Project
G - Grant	**TA** - Task
PE - Program Element	**WU** - Work Unit Accession No.

Block 6. Author(s). Name(s) of person(s) responsible for writing the report, performing the research, or credited with the content of the report. If editor or compiler, this should follow the name(s).

Block 7. Performing Organization Name(s) and Address(es). Self-explanatory.

Block 8. Performing Organization Report Number. Enter the unique alphanumeric report number(s) assigned by the organization performing the report.

Block 9. Sponsoring/Monitoring Agency Names(s) and Address(es). Self-explanatory.

Block 10. Sponsoring/Monitoring Agency. Report Number. (If known)

Block 11. Supplementary Notes. Enter information not included elsewhere such as: Prepared in cooperation with...; Trans. of ..., To be published in .... When a report is revised, include a statement whether the new report supersedes or supplements the older report.

Block 12a. Distribution/Availablity Statement. Denote public availability or limitation. Cite any availability to the public. Enter additional limitations or special markings in all capitals (e.g. NOFORN, REL, ITAR)

DOD - See DoDD 5230.24, "Distribution Statements on Technical Documents."
DOE - See authorities
NASA - See Handbook NHB 2200.2.
NTIS - Leave blank.

Block 12b. Distribution Code.

DOD - DOD - Leave blank
DOE - DOE - Enter DOE distribution categories from the Standard Distribution for Unclassified Scientific and Technical Reports
NASA - NASA - Leave blank
NTIS - NTIS - Leave blank.

Block 13. Abstract. Include a brief (Maximum 200 words) factual summary of the most significant information contained in the report.

Block 14. Subject Terms. Keywords or phrases identifying major subjects in the report.

Block 15. Number of Pages. Enter the total number of pages.

Block 16. Price Code. Enter appropriate price code (NTIS only).

Blocks 17. - 19. Security Classifications. Self-explanatory. Enter U.S. Security Classification in accordance with U.S. Security Regulations (i.e., UNCLASSIFIED). If form contains classified information, stamp classification on the top and bottom of the page.

Block 20. Limitation of Abstract. This block must be completed to assign a limitation to the abstract. Enter either UL (unlimited) or SAR (same as report). An entry in this block is necessary if the abstract is to be limited. If blank, the abstract is assumed to be unlimited.